Abdalla Almukashfi, BSc

Comparison of Different Constitutive Models for Deep Excavation Analysis

Master's Thesis

Submitted in fulfillment of the requirements for the degree of

Diplom-Ingenieur / Diplom-Ingenieurin

Master's programme Civil Engineering, Geotechnics and Hydraulics

at

Graz University of Technology

Supervisor

Ao.Univ.-Prof. Dipl.-Ing. Dr.techn. M.Sc. Helmut Schweiger

Institute of Soil Mechanics, Foundation Engineering and Computational Geotechnics
Graz University of Technology

Graz, October 2018

EIDESSTATTLICHE ERKLÄRUNG

Ich erkläre an Eides statt, dass ich die vorliegende Arbeit selbstständig verfasst, andere als die angegebenen Quellen/Hilfsmittel nicht benutzt, und die den benutzten Quellen wörtlich und inhaltlich entnommenen Stellen als solche kenntlich gemacht habe. Das in TUGRAZonline hochgeladene Textdokument ist mit der vorliegenden Masterarbeit identisch.

Datum / Date

Unterschrift / Signature

AFFIDAVIT

I declare that I have authored this thesis independently, that I have not used other than the declared sources/resources, and that I have explicitly marked all material which has been quoted either literally or by content from the used sources. The text document uploaded to TUGRAZonline is identical to the present master‘s thesis.

Datum / Date

Unterschrift / Signature

Acknowledgements

First and foremost, I would like to thank God Almighty for giving me the strength, knowledge, ability and opportunity to undertake this research study and to persevere and complete it satisfactorily. Without his blessings, this achievement would not have been possible.

There are many people who contributed to the success of my studies and finally this master thesis and I want to express my gratitude to all of them.

I want to thank Ao.Univ.-Prof. Dipl.-Ing. Dr.techn. M.Sc. Helmut Schweiger who offered an excellent supervision of this thesis. Also for giving me his full support throughout the course of this work and his sincere dedication to answer all my questions and sharing his knowledge.

Thanks to my friends and colleagues. You all made every single moment of my studies to what they were – an interesting, diversified, and of course informative but most of all an amazing and joyful chapter of my life.

Very special thank goes to Amra Prses and Adnan Kamenica for their support while I was writing my master thesis. Without them this accomplishment would not have been possible.

I must gratefully acknowledge other close personal friends, like Tobias Schlager, and many more, for the great times and memorable moments we had.

Finally, I must express my very profound gratitude to my parents and to my brothers for providing me with unfailing support, financial support and continuous encouragement through my years of study and through the process of researching writing this thesis.

This accomplishment would not have been possible without them. Thank you.

Abstract

Finite element programs usually offer a wide range of constitutive models to simulate the mechanical behaviour of soils. The linear elastic-perfectly plastic Mohr-Coulomb model is still widely used by engineers due its simplicity. However, this model is not appropriate for most practical applications and therefore more advanced constitutive models are required. In this thesis, three advanced models (Hardening Soil Model, The Hardening Soil small model and The Generalized Hardening Soil model) are used to analyse the geotechnical problems that arise, i.e. deep excavations, embankments and tunnels. From the results it can be concluded that the GHS model represents the soil behaviour in a more appropriate way compared to HS and HSS models. This is due to the fact that the pre-consolidation stress and the mean effective stresses are used to calculate soil stiffness rather than the minimal principal stress as in the standard HS model.

Kurzfassung

FE – Programme bieten mehrere Konstitutivgesetze zur Beschreibung des mechanischen Verhaltens vom Boden. Das linear-elastisch, perfekt-plastische Mohr-Coulomb-Modell findet wegen seiner Einfachheit immer noch weltweite Verwendung. Für die meisten praktischen Anwendungen eignet sich jedoch dieses Modell nicht, so dass fortgeschrittene Konstitutivgesetze erforderlich sind. In dieser Arbeit wurden drei fortgeschrittene Modelle (Hardening Soil Modell, Hardening Soil Small Modell und das Generalized Hardening Soil Modell) zur Analyse von geotechnischen Problemen, wie z.B. tiefe Baugruben, Böschungen und Tunnel untersucht. Vorläufige Ergebnisse zeigen, dass das GHS-Modell im Vergleich zu HS- und HSS-Modell das Bodenverhalten besser beschreiben kann. Dies liegt daran, dass die Vorkonsolidierung und die mittleren effektiven Spannungen, anstatt der minimalen Hauptspannung wie im HS-Modell, zur Berechnung der Bodensteifigkeit verwendet werden.

Table of contents

List of figures

List of tables

List of symbols and abbreviations

Capital letters

C_{inter}	Shear strength within the interface in PLAXIS	$[\mathrm{N/m^2}]$
E	Young's modulus	$[\mathrm{N/m^2}]$
E_u	Undrained Young's modulus	$[\mathrm{N/m^2}]$
E'	Effective Young's modulus	$[\mathrm{N/m^2}]$
E_{50}	secant stiffness	$[\mathrm{N/m^2}]$
E_{ur}	Unloading-reloading stiffness	$[\mathrm{N/m^2}]$
E_{50}^{ref}	Reference secant modulus	$[\mathrm{N/m^2}]$
E_{oed}^{ref}	Reference tangent modulus	$[\mathrm{N/m^2}]$
E_{ur}^{ref}	Reference unloading/reloading stiffness	$[\mathrm{N/m^2}]$
G	Shear modulus	$[\mathrm{N/m^2}]$
G_0	Shear modulus at very small strain	$[\mathrm{N/m^2}]$
G_0^{ref}	Reference shear modulus at very small strain	$[\mathrm{N/m^2}]$
G_{ur}^{ref}	Reference shear modulus at unloading and reloading	$[\mathrm{N/m^2}]$
K_0	Coefficient of lateral earth pressure	[-]
K_0^{nc}	Coefficient of lateral earth pressure at normally consolidated state	[-]
M	Bending moment	$[\mathrm{Nm/m}]$
N	Normal force	[N]
I	Moment of inertia	$[\mathrm{m^4}]$
R_{inter}	Strength reduction factor for interface	[-]
R_f	Failure ratio	[-]

U_y	Maximum surface settlement	[m]
Q	Shear force	[N]

Small letters

c	Cohesion	$[\mathrm{N/m^2}]$
c^{ref}	Reference cohesion of the interface	$[\mathrm{N/m^2}]$
p_c	Pre-consolidation pressure	$[\mathrm{N/m^2}]$
m	Power for stress-level dependency of stiffness	[-]
p	Mean stress	$[\mathrm{N/m^2}]$
p_w	Pore water pressure	$[\mathrm{N/m^2}]$
p_{excess}	Excess pore pressure in Plaxis 2D	$[\mathrm{N/m^2}]$
p_{water}	Pore water pressure in Plaxis 2D	$[\mathrm{N/m^2}]$
u	Displacements	[m]

Greek letters

γ	Soil weight	$[\mathrm{N/m^3}]$
γ_w	Unit weight of water	$[\mathrm{N/m^3}]$
γ_{sat}	Saturated soil unit weight	$[\mathrm{N/m^3}]$
γ_{unsat}	Unsaturated unit weight	$[\mathrm{N/m^3}]$
$\gamma_{0.7}$	Shear strain level where G = 0.722 G_0	[-]
γ_s	Shear strain	[-]
ε_1	Axial strain	[-]
ε_q	Deviatoric strain	[-]

ε_v	Volumetric strain	[-]
υ	Poisson's ratio	[-]
υ_u	Undrained Poisson's ratio	[-]
υ_{ur}	Poisson's ratio for unloading-reloading	[-]
υ'	Effective Poisson's ratio	[-]
φ'	Angle of internal friction	[°]
φ_{inter}	Friction angle of interface (PLAXIS)	[°]
Ψ	Dilatancy angle	[°]
σ'	Effective stress	$[\mathrm{N/m^2}]$
σ_1'	Effective major principal stress	$[\mathrm{N/m^2}]$
σ_3'	Effective minor principal stress	$[\mathrm{N/m^2}]$
β	Pre-relaxation factor	[-]

ABBREVIATIONS

FE	Finite element
HS	Hardening Soil
HSS	Hardening Soil with small strain stiffness
GHS	Generalized hardening soil model
MC	Mohr-Coulomb
OCR	Over-consolidation Ratio
OC	Over-consolidated
NC	Normally-consolidated
PWP	Pore Water Pressure
POP	Pre-overburden pressure
SD	Stress dependency

1 Introduction

The use of a numerical method such as finite element analysis (FEA) has become a standard practice in solving geotechnical problems. However the quality of any prediction depends on the adopted modeling tools and the adequate model.

Nowadays, some FEM codes are especially designed for geotechnical problems and more specifically, to analyse the stability and ground movement due to excavation. Different constitutive models, from simple elastic model to mathematically complex non-linear elasto-plastic models have been established to describe the strength and deformation behaviour of soils. However, there are still problems in the prediction of ground movements in and around an excavation with the numerical tools. The results of the numerical analysis are influenced by many factors such as simplified geometry and boundary conditions, mesh configuration, initial input parameters of ground conditions and significantly the constitutive model chosen to simulate the soil behaviour.

Therefore, the selection of suitable soil constitutive models in engineering problems is an essential part of the modelling process. It should be mentioned that any soil constitutive model, even the most complex, is a simplification of real soil behaviour and it includes numbers of limitations [2].

This research aims to present a simplified two-dimensional finite element study on deep excavations, embankments, and tunnels. The Finite Element Code PLAXIS is selected as a numerical tool. This study will focus on the effects of taking into account the mean effective stress and pre-consolidation stress to calculate the stiffness of the soils rather than the standard HS model.

1.1 The aim of the Thesis

The main objective of the thesis is to study the differences between the three soil models e.g., the hardening soil model (HS), the hardening soil with small strain model (HSS) and the generalized hardening soil model (GHS) for different geotechnical problems, i.e. deep excavations, embankments and tunnels.

The soil stiffness for HS model and HSS model is based on the minimum principle effective stress. Therefore, the substantial benefits of the so-called GHS model is that the soil stiffness formula in GHS model considers for the pre-consolidation stress as well as the mean effective stress instead of a stress component.

The generalized hardening soil model (GHS) is a user-defined soil model (USDM), and can be considered as an updated version of the hardening soil small model (HSS). The GHS allows the users to use different configurations of the stress and strain dependency [2].

2 Soil Modelling

The following contents in this chapter are based on [1], [2], [4].

Plaxis 2016 provides a certain range of different constitutive models, which can be utilized according to the soil conditions and soil input parameters. The three material models which are used in this parametric study are the Hardening Soil, Hardening Soil with small-strain stiffness and the Generalized Hardening soil material models.
In this thesis all constitutive models used for simulation and modeling, i.e. the deep excavations, tunnel and embankment in Plaxis 2D are explained below briefly. All input parameters and equations, which are essential to describe the selected material models are based on [1], [4],[5].

2.1 The Hardening Soil (HS)

The Hardening Soil material model (HS) is one of the advanced material models presented by Plaxis [1] and introduced by [4]. The difference between the Mohr-Coulomb model and the HS material model is that the HS model accounts for stress-dependency of the stiffness. Furthermore, the HS material model uses a hyperbolic stress-strain curve (Figure 2) [4]. In contrast the Mohr-Coulomb model uses a bi-linear curve [1].

2.2 The Hardening Soil Small Model (HSS)

The Hardening Soil material model with small-strain stiffness is an advanced constitutive law which is an extended version of the HS model.
The concept of HS small model is to consider small strain properties by introducing a threshold shear strain,$\gamma_{0.7}$, which is the shear strain when the secant shear modulus, G_s is reduced to about 70% of G_0[8].
The HS small material model uses stiffness reduction curve to show the behaviour at very small strains levels (“S-curve”, Figure 6) [1].

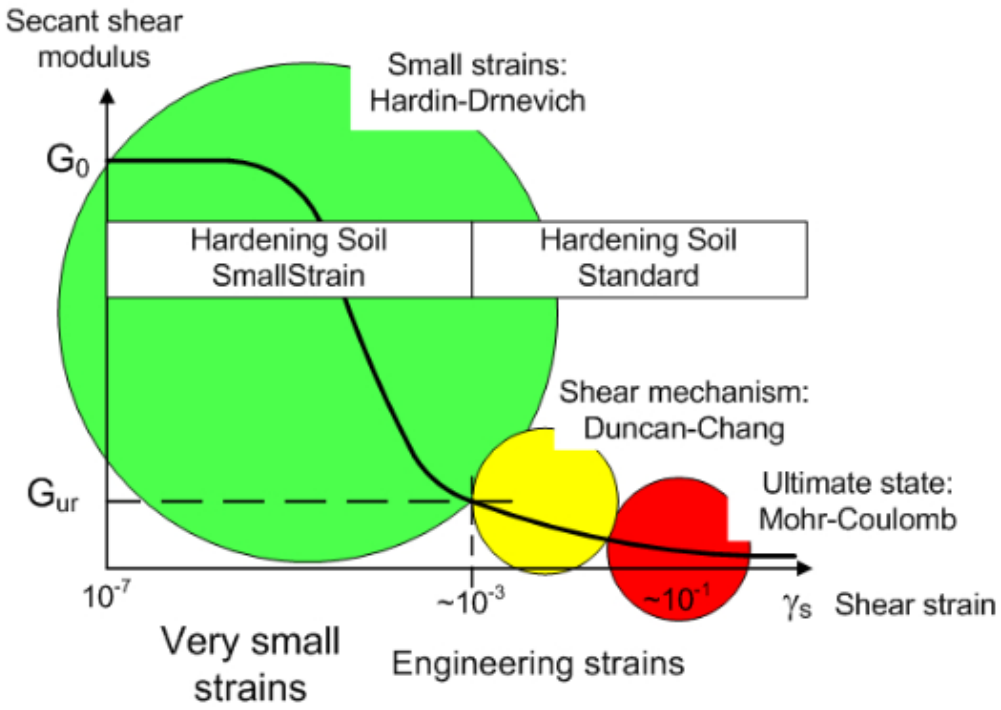

Figure 1: Schematic depiction of the HS model and HS small model [10].

2.3 Generalized Hardening Soil Model (HSS)

The Generalized hardening soil model is a user-defined model which is a modified version of the HSS model. Plaxis 2016 has implemented this model in order to account for different strain dependency as well as various stress dependency [2].

3 Hardening Soil Model (HS)

The following contents in this chapter are based on [1],[4]

The Hardening Soil (HS) model is an enhanced constitutive model for describing the behaviour of various types of soils. The HS model was implemented and calibrated by [4]. The Hardening soil model (HS) is derived from the hyperbolic model of [3] however, formulated in an elastoplastic framework of [4].

The Hardening Soil model is an isotropic hardening model. The yield surface expands with plastic strain. Hence, two types of hardening can be defined. Deviatoric hardening due to shear loading is governed by the secant stiffness E_{50} at 50 % of strength in the triaxial test. Volumetric hardening due to compression loading is governed by the oedometric stiffness E_{oed} [4].

The soil behaves elastically if the yield surface is inactive. The stress path at the unloading and reloading stage is modelled as elastic using the unloading and reloading stiffness E_{ur} [1], [4].

In Figure 2, the shear yield stress surface is moving in p-q space. Therefore, the yield stress surface can change from the initial yield stress to the failure stress surface [5]. The soil is considered elastic within the area limited by the two yield surfaces (Figure 2) [1].

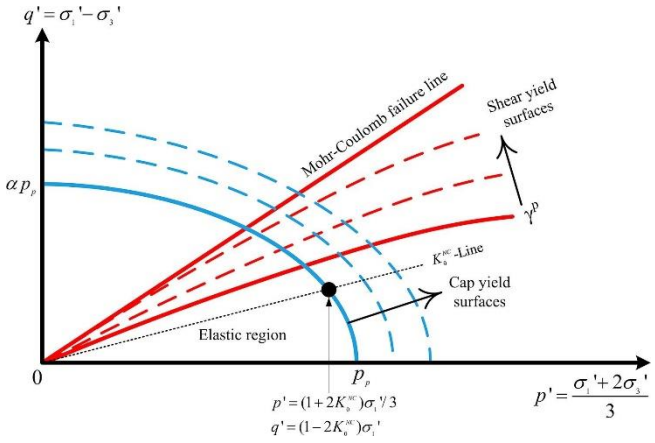

Figure 2: Shear yield surface and cap yield surface in the Hardening Soil model adopted from [1], [11].

3.1 Deviatoric Hardening

In Figure 3, the non-linear stress-strain relation curve for primary loading is shown, the stress strain curve is described by a hyperbolic function derived by [3]. The location of the deviatoric hardening surface is associated with the mobilized friction and governed by E_{50} [1].

During the un-/reloading phases, the soil behaves elastic and the responses are considerably stiffer. The failure line at q_f corresponds to the MC failure criterion (Figure 3).

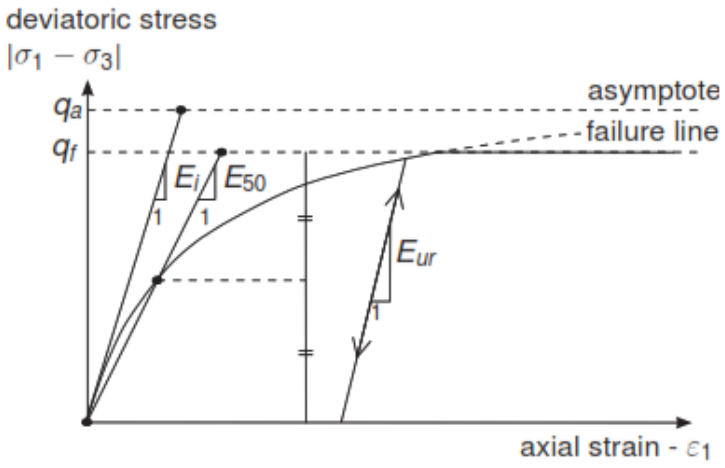

Figure 3: Deviatoric stress- axial strain relationship [4].

R_f	[-]	$R_f = q_f/q_a$ – by default 0.9.
E_{50}	$[kN/m^2]$	Stiffness modulus at 50% of strength for primary loading – equation (1)
E_{ur}	$[kN/m^2]$	Elastic modulus for unloading/reloading – equation (2)

In order to achieve the so-called hyperbolic function, the stiffness modulus at 50 % of strength for primary loading E_{50} as well as the stiffness during un-/reloading phase E_{ur} are essential. Plaxis 2016 requires the reference stiffness parameters E_{50}^{ref}, E_{oed}^{ref} and E_{ur}^{ref} for the HS model as well as HS small model.

Stress dependency is defined by the following formulas:

- The triaxial unloading/reloading stiffness E_{ur} is given as below:

$$E_{ur} = E_{ur}^{ref} \left(\frac{c' \cos \varphi' - \sigma_3' \sin \varphi'}{c' \cos \varphi' + p^{ref} \sin \varphi'} \right)^m \quad (1)$$

- In a drained triaxial test the formula for the primary loading stiffness E_{50} is:

$$E_{50} = E_{50}^{ref} \left(\frac{c' \cos \varphi' - \sigma_3' \sin \varphi'}{c' \cos \varphi' + \sigma_3'^{ref} \sin \varphi'} \right)^m \quad (2)$$

E_{50}^{ref} $[kN/m^2]$ Reference secant modulus from triaxial testing.

E_{ur}^{ref} $[kN/m^2]$ Reference modulus for unloading/reloading.

p^{ref} $[kN/m^2]$ Reference stress corresponds to $\sigma_3'^{ref}$.

Failure Ratio for HS model:

The failure ratio R_f defines the relationship between the ultimate deviator stresses q_f derived from the Mohr-Coulomb failure criterion, and the quantity asymptote of stress q_a. Thus R_f limits the strain at failure [4].

$$R_f = 0.9$$

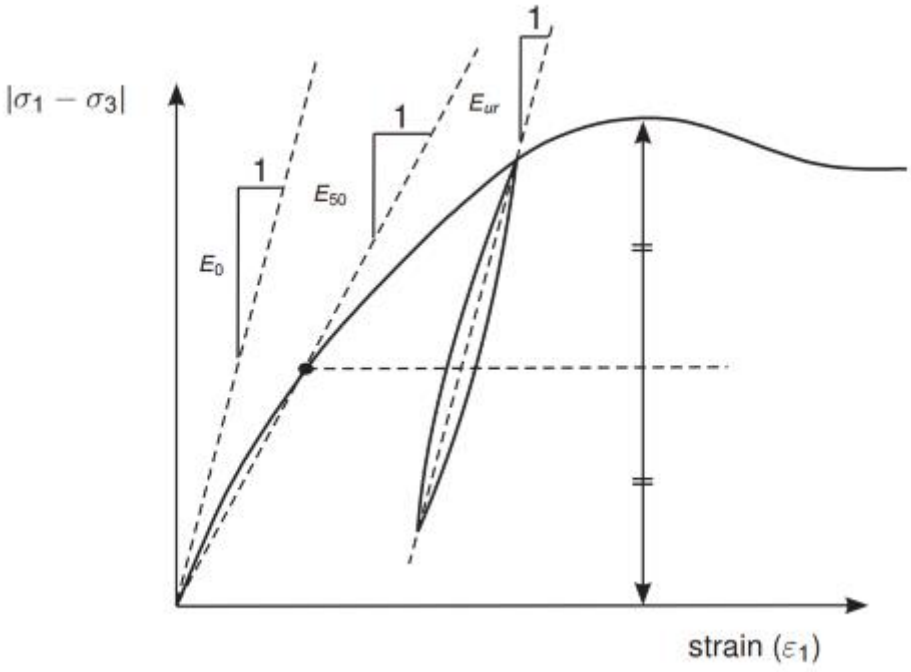

Figure 4: Stiffness E_0 ,E_{50}, and E_{ur} for triaxial test [1].

3.2 Volumetric Hardening

The volumetric yield surface f_c is given by an ellipse in the $p - q'\ plane$. The size of the volumetric yield surface is controlled by the isotropic pre-consolidation pressure p_c on the $p - axis$. p_c is based on OCR or POP (pre-overburden pressure) [1].
The stress-dependent loading stiffness E_{oed} can be described with the following formula:

$$E_{oed} = E_{oed}^{ref} \left(\frac{c' \cos\varphi' - \sigma_1' \sin\varphi'}{c' \cos\varphi' + p^{ref} \sin\varphi'} \right)^m \tag{3}$$

E_{oed}	$[kN/m^2]$	Tangential stiffness from oedometer test – derived from (3).
P^{ref}	$[kN/m^2]$	Reference stress based on $\sigma_1^{'ref}$.
m	[-]	Power for stress dependency of stiffness (relies on the soil).

Figure 5 shows the yield surface in principle stress space.

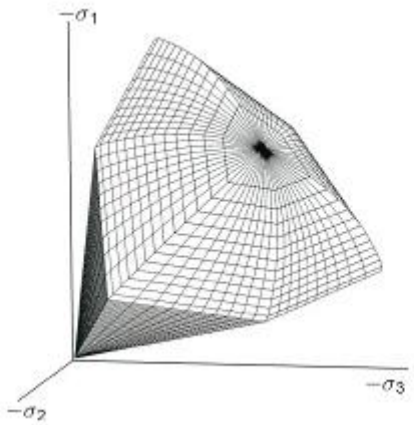

Figure 5: Depiction of the yield surface of the HS-model in principle stress space [1].

3.3 Failure Criterion

The failure criterion for the HS model is defined by the MC criterion, hence the following parameters are essential:

$[\varphi']$	[°]	Effective friction angle.
$[c']$	$[kN/m^2]$	Effective cohesion.
$[\Psi]$	[°]	Dilatancy angle.
$[\sigma_t]$	$[kN/m^2]$	Tensile strength.

3.4 Over-consolidation

In Plaxis 2016, over-consolidation is defined by the over-consolidated ratio (OCR) or pre-overburden pressure (POP). POP or OCR defines the initial yield surface as well as the initial stress state [1].

3.5 Model limitations

The main advantage of the HS model is that it can describe realistically the non-linear behaviour of the soil. As other models, it also has some limitations, so it is not able to reproduce softening effects. Furthermore, the standard HS model does not account for the higher soil stiffness at small strain levels.

4 Hardening Soil Small Model (HSS)

The HS small model is an enhanced version of the HS-Standard. The Hardening Soil Small model (HS-Small Strain) was formulated in [5] in order to describe the variation of the stiffness with increasing shear strain at very small strains [1].

Figure 6 shows that the shear modulus of soil is based on the level of shear strain.

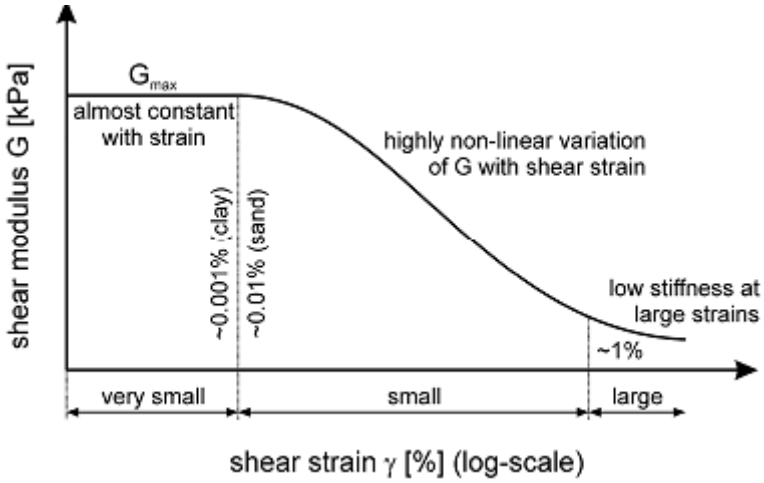

Figure 6: Shear modulus with increasing shear strains [6].

In Figure 6, at very small strain rates, soil shows a linear elastic behavior and responds with a very high stiffness compared to higher strain rates.

4.1 Small Strain Parameters

The HS small model HSS is based on the hardening soil model HS and uses the same parameters. To describe the variation of the small strain-stiffness two additional stiffness parameters are required [1], [5].

G_0^{ref} $[kN/m^2]$ Reference shear modulus at very small strains – equation from (4).

$\gamma_{0.7}$ $[kN/m^2]$ Shear strains at $G_s = 0.722\ G_0$

According to the stress-strain relationship in the HS-small model the secant shear modulus is given as:

$$\frac{G_s}{G_0} = \frac{1}{1 + a \,.\left|\frac{\gamma}{\gamma_r}\right|} \tag{4}$$

Whereas the threshold shear strain γ_r is given as follow:

$$\gamma_r = \frac{\tau_{max}}{G_0} \tag{5}$$

τ_{max} is the shear stress at failure. It is recommended by [8] to use $\gamma_r = \gamma_{0.7}$ at which the secant modulus G_s is reduced to about 70% of its initial value.

Eq. (4) can now be rewritten as follow:

$$\frac{G_s}{G_0} = \frac{1}{1 + a \,.\left|\frac{\gamma}{\gamma_{0.7}}\right|}, \qquad where\ a = 0.385 \tag{6}$$

Using $a = 0.385$ and $\gamma_r = \gamma_{0.7}$, gives $G_s/G_0 = 0.722$, thus the formulation ‘’about 70’’ should be interpreted accurately as 72.2%.

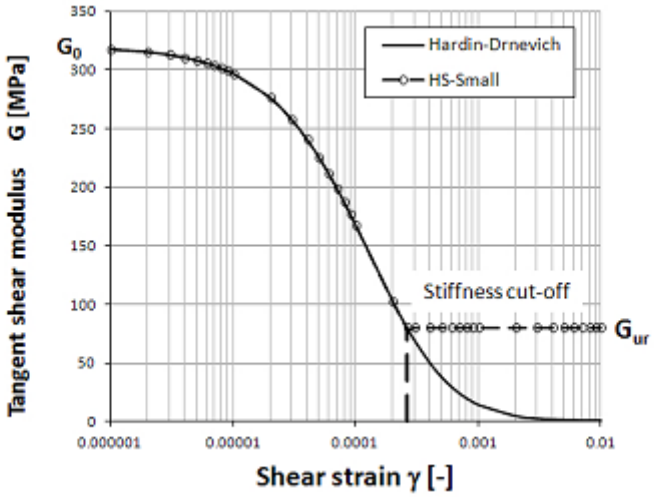

Figure 7: Small-strain stiffness degradation curve in the HS small model based on [9].

Figure 7 explains that the HS small model changes to hardening plasticity of the HS model, if the tangent shear modulus G_t is lower than the un-/reloading stiffness G_{ur}[5].

Within the HS small model, with respect to the stress strain relationship the tangent shear modulus is given by:

$$G_t = \frac{G_0}{\left(1 + 0.385 \,.\frac{\gamma}{\gamma_{0.7}}\right)^2} \tag{7}$$

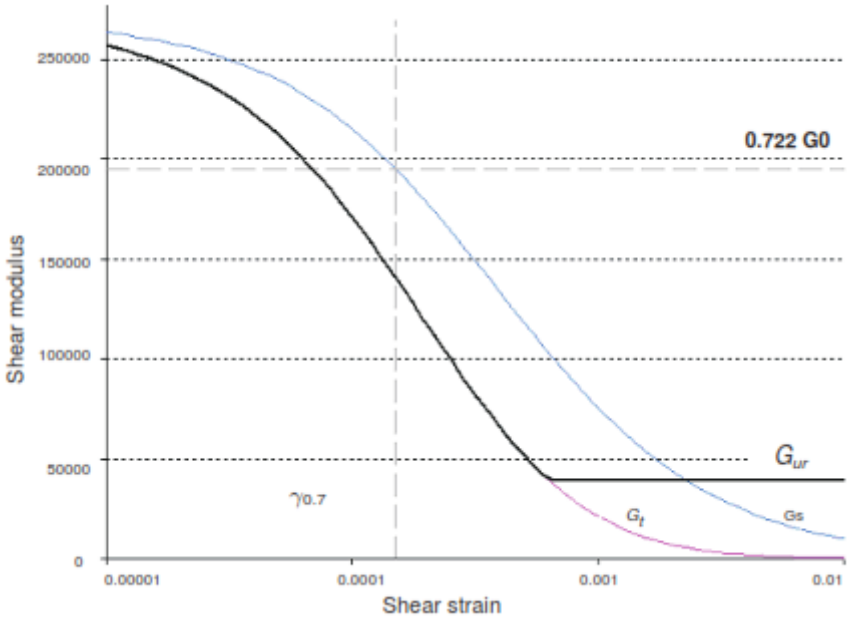

Figure 8: Tangent and secant reduction curve [1].

In the HS-small model stress dependency of the shear modulus is taken into account by [1]

$$G_0 = G_0^{ref}\left(\frac{(-\sigma_3' + c\cos\varphi)}{(p^{ref} + c\cos\varphi)}\right)^m \tag{8}$$

The knowledge of the material's initial void ratio can be very advantageous in deriving its shear stiffness at very small strain G_0. Many correlation are presented in the literature [5]. For example the relation given by [7]:

$$G_0^{ref} = 33.\frac{[2.97 - e]^2}{1 + e}\ [MPa] \tag{9}$$

For $p^{ref} = 100\ [kPa]$

According to [6] a realistic order of magnitude is:

$$G_0^{ref} = (2.5 - 10) \quad G_{\text{ur}}^{ref} \tag{10}$$

Whereas:

$$G_{\text{ur}}^{ref} = \frac{E_{\text{ur}}^{ref}}{2(1 + \upsilon_{ur})} \tag{11}$$

G_{ur}^{ref} $[kN/m^2]$ Unloading-reloading shear modulus at reference stress level – equation from (11).

5 Generalized Hardening Soil Model USDM

The following chapter is based on the [1], [2].

5.1 User-Defined Soil Models

PLAXIS allows users to modify the stress-strain relationship and this is usually done by implementing the new FE code in FORTRAN or any other programing language as example Python. The input parameters for UD can be added in the material window of the PLAXIS input program [1].

5.2 The Generalized Hardening Soil Model

The Generalized Hardening Soil model (GHS) is a user-defined model introduced by [1]. The Generalized HS model is based on the HS small model. The purpose of implementing the GHS model is to allow the users to change between different options. The options that can be activated and deactivated in this model are in particular the “Stress Dependent Stiffness”, the “Strain Dependent Stiffness” as well as different parts of the plasticity model.

5.3 Structure of the GHS Model:

According to [2] there are two main modifications implemented in the source code of the HS-Small UD subroutine. One accounts for the formulation of the Elastic Effective Stiffness Matrix and one is in the subroutine which is correcting the trial stress for plasticity.

5.3.1 Strain Dependency

There are two options for the strain dependency. The strain dependent stiffness is deactivated if the strain dependency option value is assigned to 0, which is the case of the HS model; setting the value to 1 means the strain dependent stiffness is activated, which is the case of the HS small model.

5.3.2 Stress Dependency

There are two options of the stress dependency formulations in the GHS model, which are the "Stress Dependent Stiffness" and the "Stress Dependent Formula". The "Stress Dependent Stiffness "governs whether the stress dependent stiffness is used; the "Stress Dependent Formula "defines which stress dependency formula is applied.

In summary, there are three switchers for the "Stress Dependent Stiffness", namely:

I. Option [0]

The soil stiffness E_{ur} is constant during the calculations steps, this case is the same as $m = 0$.

II. Option [1]

The soil stiffness E_{ur} is updated for each calculation phase and is determined by the ''Stress Dependent Formula''.

III. Option [2]

The soil stiffness E_{ur} is updated for each calculation step based on the stress dependency formula determined by the "Stress Dependent Formula" switch, referred to the mean effective stresses at the beginning of each calculation step.

To be more detailed, there are also three possibilities for the "Stress Dependent Formula" option, namely:

1. Option [0]:

The stress dependency depends on σ_3 and strength parameters, which is given by:

$$E_{ur} = E_{ur}^{ref} \left(\frac{(\sigma_3' + c' cot\varphi')}{(\sigma^{ref} + c' cot\varphi')} \right)^m \tag{5}$$

Thus, this is the same formula as used in HS Standard model.

2. Option [1]:

The stress dependency is referred to σ_3 and the pre-consolidation parameters p_c, which is given by:

$$E_{ur} = E_{ur}^{ref}\left(\frac{(\sigma_3' + p_c)/2}{(p^{ref})}\right)^m \tag{6}$$

3. Option [2]:

The stress dependency is based on the mean effective stress p' and the pre-consolidation parameters p_c, which is given by:

$$E_{ur} = E_{ur}^{ref}\left(\frac{(p' + p_c)/2}{(p^{ref})}\right)^m \tag{7}$$

In the case of Option 1 or 2, a minimum value of the numerator of $p^{ref}/100$ is utilized.

A Summary of the combinations of the stress dependent stiffness switches is given in Table 1.

Table 1: The function of the stress dependency stiffness.

SD Formula / SD Stiffness	0	1	2
	Stress dependency based on the original formula of the HS model	The stress dependency is based on σ_3' and the pre-consolidation parameters p_c	The stress dependency is based on p' and the pre-consolidation parameters p_c
Constant E_{ur} being equal to the input value [0].	E_{ur}	E_{ur}	E_{ur}
Stiffness updates within each calculation phase [1].	$E_{ur} = E_{ur}^{ref}\left(\frac{(\sigma_3' + c'cot\varphi')}{(\sigma^{ref} + c'cot\varphi')}\right)^m$	$E_{ur} = E_{ur}^{ref}\left(\frac{(\sigma_3' + p_c)/2}{(p^{ref})}\right)^m$	$E_{ur} = E_{ur}^{ref}\left(\frac{(p' + p_c)/2}{(p^{ref})}\right)^m$
Stiffness updates within each calculation phase [2].	$E_{ur} = E_{ur}^{ref}\left(\frac{(\sigma_3' + c'cot\varphi')}{(\sigma^{ref} + c'cot\varphi')}\right)^m$	$E_{ur} = E_{ur}^{ref}\left(\frac{(\sigma_3' + p_c)/2}{(p^{ref})}\right)^m$	$E_{ur} = E_{ur}^{ref}\left(\frac{(p' + p_c)/2}{(p^{ref})}\right)^m$

Note that the other soil stiffnesses which are E_{50}, E_{oed} and G_0, follow the same stress-dependency rule as E_{ur}.

5.3.3 Plasticity Model

The options of the "Plasticity Model" is introduced to control between different yield functions. The description of the switcher options are listed in Table 2.
For example the HS Standard model is obtained if the value of the plastic model function is set to 4.

Table 2: Plastic yield functions for the GHS

Options	Plastic Yield Function
1	Mohr Coulomb Model
2	Shear hardening + MC failure criterion
3	Cap hardening + MC failure criterion
4	Shear hardening + Cap hardening + MC failure criterion

5.3.4 GHS switcher in this thesis

For this thesis, the comparison is between the original HS model, HS small model and the GHS model. The input material parameters for the two models are identical except for the "stress dependency formula". Table 3 shows the switch modes for the GHS model.

Table 3: Implementation of GHS switches modes in Plaxis

Options	GHS Switches Mode
1	Stain Dependent Stiffness
2	Stress Dependent Stiffness
2	Stress Dependency Formula
4	Plasticity model

6 GHS in PLAXIS 2016

The following chapter is based on the [1],[2].

6.1 Input Parameters in UDSM-GHS

Table 4: Input parameters for the GHS

Identification	Units	Definition
E_{50}^{ref}	$[kN/m^2]$	Reference secant stiffness
E_{oed}^{ref}	$[kN/m^2]$	Reference tangent stiffness
E_{ur}^{ref}	$[kN/m^2]$	Reference unloading/reloading stiffness
m	[-]	Power for stress-level dependency of stiffness
φ	[°]	Friction angle
Ψ	[°]	Dilatancy angle
c	$[kN/m^2]$	Cohesion
$\gamma_{0.7}$	$[kN/m^3]$	Shear strain at which $G_s = 0.722\ G_0$
G_0^{ref}	$[kN/m^2]$	Reference shear modulus at very small strains
v_{ur}	[-]	Poisson's ratio for unloading and reloading
p^{ref}	$[kN/m^2]$	Reference stress
R_f	[-]	Failure ratio
σ_t	$[kN/m^2]$	Tensile strength
Failure mode (0:MC or 1:MN)	[-]	Options for failure criteria (Mohr-Coulomb or Matsouka-Nakai), only MC is used.
OCR	[-]	Over-consolidation ratio
POP	[-]	Pre-consolidation Pressure

Identification	Units	Definition
k_0^{NC}	[-]	For normal consolidation pressure
v_u	[-]	Undrained passion ratio, if the value is 0 the default value 0.495 is assigned automatically
M k_s/k_c (internal) G_{50}^{ref} (internal)	[-] [-] $[kN/m^2]$	These values are automatically calculated by the ‘’hscapitr.exe’’ when 0 are applied.
Stress dependent stiffness Strain dependent stiffness Plasticity Model Stress Dependency Formula	[-] [-] [-] [-]	See Table 1 and Table 2
E_{oed}^{ref}	$[kN/m^2]$	Reference tangent stiffness for the interface.
φ	[°]	Friction angle of the interface
Ψ	[°]	Dilatancy angle of the interface
c^{ref}	$[kN/m^2]$	Reference cohesion of the interface
UD-Power	[-]	User-defined power stress dependency of stiffness of the interface
UD $- P^{ref}$	$[kN/m^2]$	User defined reference stress of interface
$k_0 -$ determination	[-]	Value for the initial phase

7 Benchmarks

The geotechnical models in this chapter including geometry, dimensions and boundary conditions as well as the soil profile and input parameters, are given.
There are numerous combinations of the switchers to change with for different purposes. In this thesis, the application of using pre-consolidation as well as mean effective stresses in the stress dependency formula is examined, the aim is to achieve more realistic unloading/reloading stiffness in excavation projects.

7.1 Excavation of building pit

This case study validates the importance of modelling excavation problems with the use of the Generalized Hardening Soil model. The study presents an analysis of main differences between HS Standard, HS-Small and the Generalised Hardening soil models.

7.1.1 Problem definition

The excavation pit is 30 m wide and 15 m deep. The excavated pit was retained by a 0.60-m-thick and 25-m-deep diaphragm wall. The wall is supported by two rows of pre-stressed ground anchors.

7.1.2 Material Parameters

The soil properties for each model are presented in Table 5. The input material parameters for the HS small model and the GHS model are identical except for the “Stress dependency formula”. The upper 40.0 m of the subsoil consist of a homogeneous layer of medium dense fine sand with unit weight of 18.0 [kN/m^2]. Underneath, there is a layer of “deep sand 1” with a thickness of 10.0 m, followed by a layer of “deep sand 2” with a thickness of 10.0 m (see Figure 9).

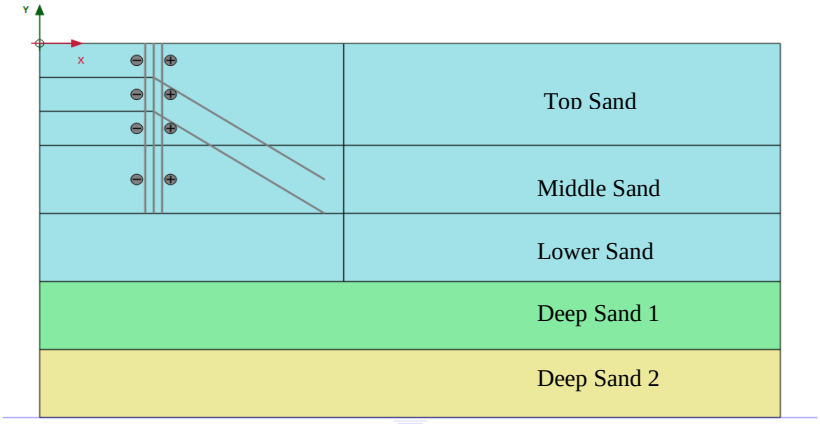

Figure 9: Excavation pit geometry

Table 5: Excavation pit: material properties for soil layers.

Symbol	Top/Middle/Lower Sand	Deep Sand 1	Deep Sand 2	Unit
Material Model	HSS and HS model	HS model	HS model	
Type of Behaviour	Drained	Drained	Drained	
γ_{sat}	18	18	18	$[kN/m^3]$
γ_{unsat}	18	18	18	$[kN/m^3]$
${E_{oed}}^{ref}$	20000	40000	60000	$[kN/m^2]$
${E_{50}}^{ref}$	20000	40000	60000	$[kN/m^2]$
${E_{ur}}^{ref}$	80000	160000	240000	$[kN/m^2]$
m	0.5	0.5	0.5	[-]
ν_{ur}	0.2	0.2	0.2	[-]
c′	1.0	1.0	1.0	$[kN/m^2]$
φ′	35	35	35	[°]
ψ	5.0	5.0	5.0	[°]
p^{ref}	100	100	100	$[kN/m^2]$
${K_0}^{NC}$	0.426	0.426	0.426	[-]
R_f	0.6	1.0	1.0	[-]
G_0^{ref}	100000	-	-	$[kN/m^2]$
$\gamma_{0.7}$	0.0001	-	-	$[kN/m^3]$

7.1.3 Excavation stages

Initial phase: generating an initial stress state, k_0- procedure.

Phase 1: excavation step 1 (to level - 5.0 m) and activation of the diaphragm wall.

Phase 2: activation of the anchor and geotextile, pre-stressing of the anchor to a value of 300 $[kN/m]$.

Phase 3: excavation step 2 (to level - 10.0 m).

Phase 4: activation of the second anchor and geotextile, pre-stressing of the anchor to a value of 300 $[kN/m]$.

Phase 5: excavation step 3 (to level - 15.0 m).

7.1.4 General assumptions postulated:

I. Interface elements between wall and soil.

II. For the case of the HS small model and the GHS model, the top/middle/lower sand has been applied to the whole model, whereas the deep sand 1 and 2 has been neglected.

7.1.5 Mesh discretisation

Due to symmetry, only half of the excavation is analysed in this example. The finite element model and the mesh generation are shown in Figure 10. The model has a dimension of 97.0 m in width and 55.0 m in depth. A plane-strain model with 15 nodded-elements is used. In mesh mode, additional refinement was made around the wall, and the mesh option 'Medium' is used.

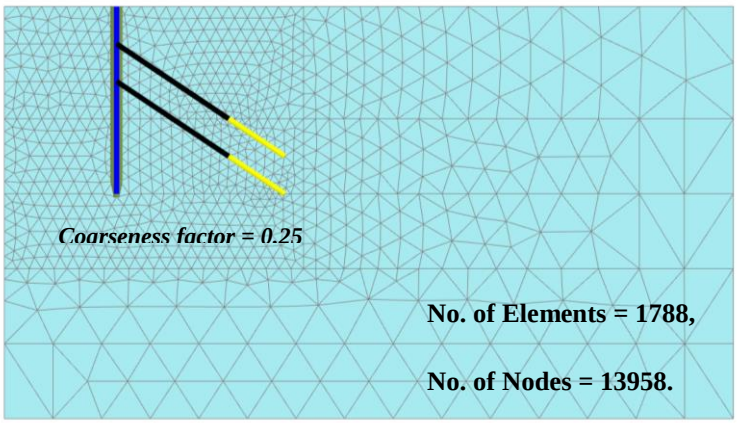

Figure 10: Excavation pit: 2D mesh

7.1.6 Results

1. In Figure 11 (A) and (B), the bending moment and the wall deflection are displayed. The highest bending moments are obtained by HS-Standard model. The shape of the bending moment diagrams as well as the lateral deflection is similar for all models.

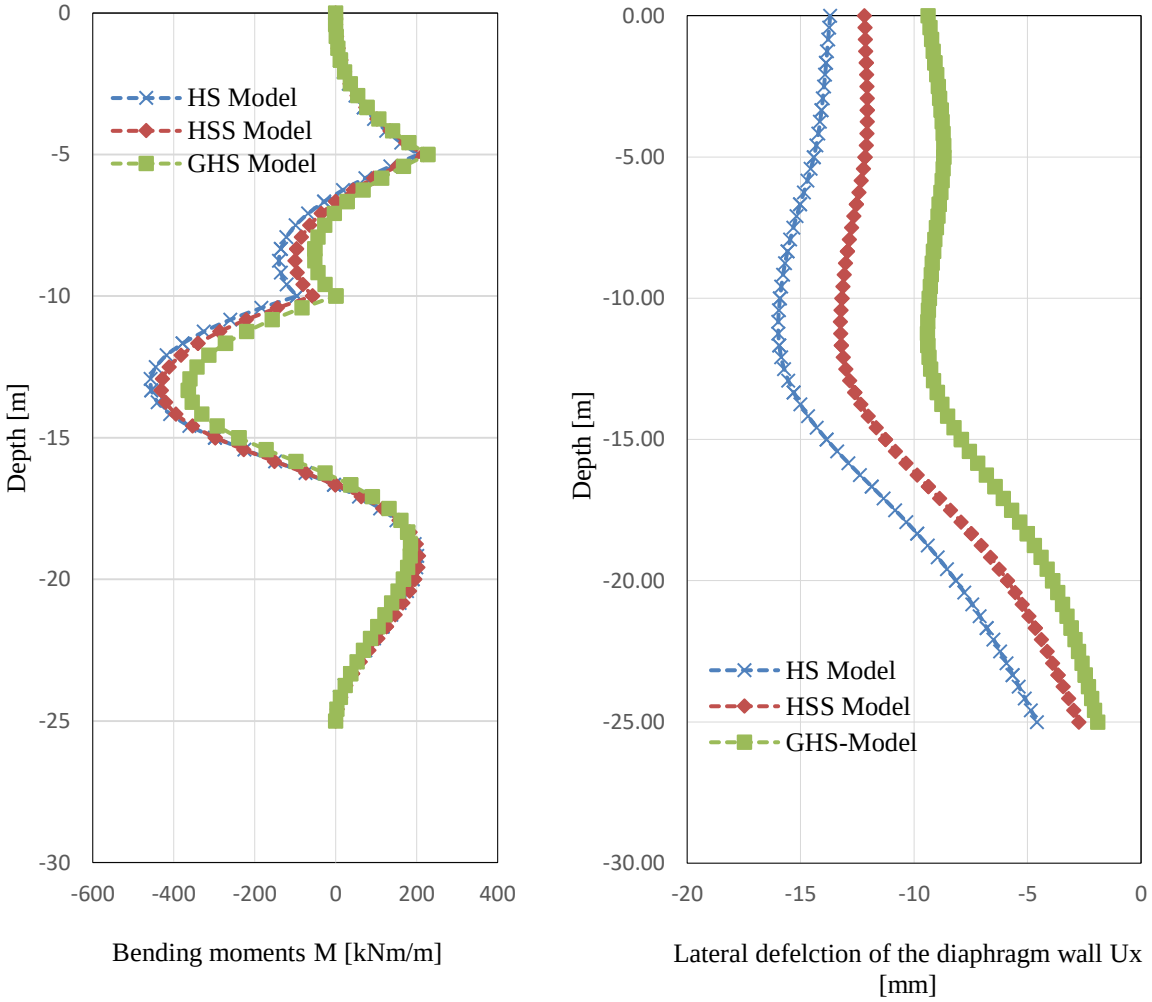

(A) (B)

Figure 11: Bending moment and Horizontal displacement of the sheet pile wall at the last excavation step.

Figure 11 (B) shows the deflection curve of the diaphragm wall for the final excavation stage for all solutions submitted. The horizontal displacement of the top of the wall varies between -13 mm and -9 mm (-ve sign means displacement towards the excavation).

2. Vertical heaving generated by GHS-model is significantly reduced compared to results which are generated by HS small model.

Figure 12 shows the heave of the excavation pit for the final excavation stage. The displacements have the same shape but have a maximum difference of 17.0 mm, the heave predicted by the GHS is approximately 27.0% smaller.

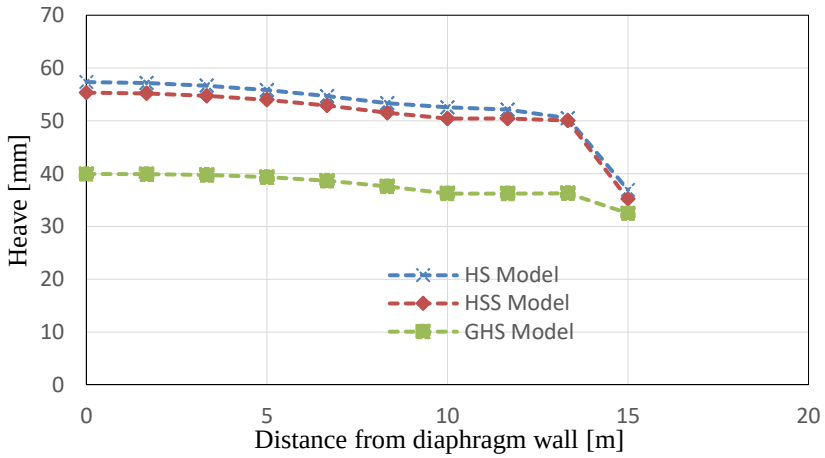

Figure 12: Heave of the bottom of the excavation

Figure 13 shows the settlement behaviour of the top ground surface behind the wall. The maximum settlement calculated by the GHS at the wall shows a similar value to the one obtained by the HS model, however the settlement trough is different.

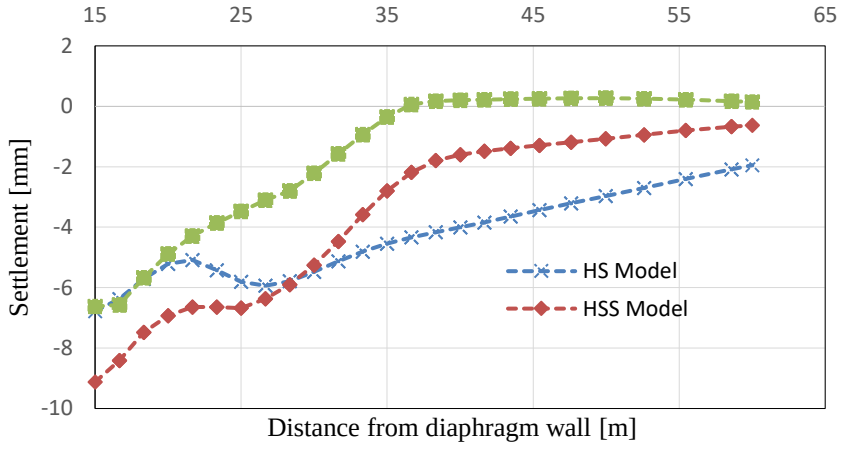

Figure 13: Surface settlement behind the diaphragm wall

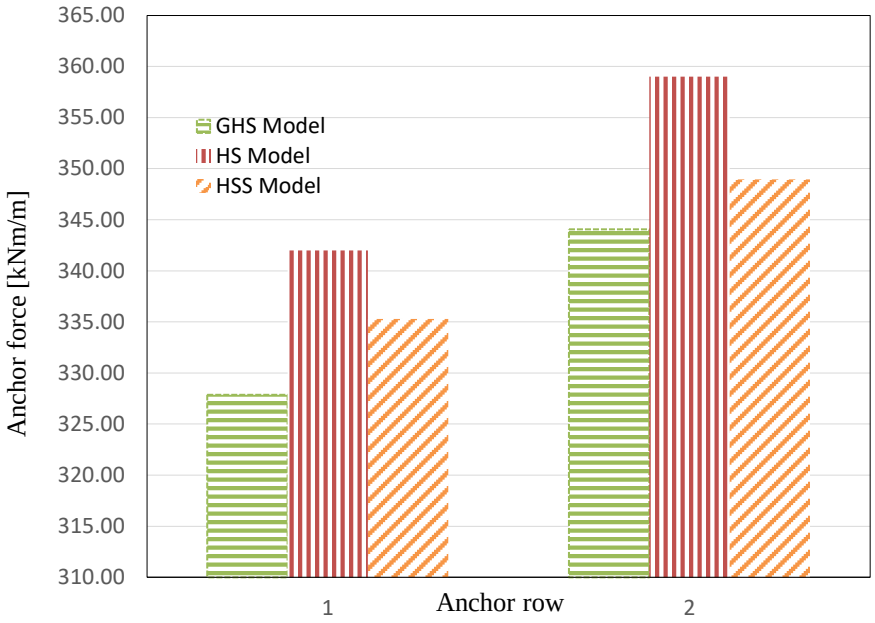

Figure 14: Anchor force at the final construction stage for all two anchor rows

Figure 14 shows the development of anchor forces in the first row of anchors with progressing excavation. The anchor forces of the first row and the second row obtained by using the GHS model are smaller than calculated using HS standard and HS small model.

Table 6: Summary of the FE results

	Symbol	HS	HSS	GHS	Units
Maximum heave	Uy	57	55	39	mm
Maximum lateral deflection	Ux	-16	-13	-9	mm
Maximum surface settlement	Uy	-7	-9	-6	mm
Maximum bending moment	My	-457	-428	-359	kNm/m

7.2 NATM Tunnel Construction

This case study shows the importance of modelling NATM tunnel problems with the use of advanced constitutive models such as HS small and GHS models. The example shows the differences in predictions of subsurface displacements during tunnel excavation as well as the lining forces under drained conditions.

The problem statement, i.e. tunnel geometry and the soil profile is shown in Figure 16.

7.2.1 Soil profile

The area of interest consists of four main strata, and for the numerical model soil layering has been simplified to horizontal soil stratification.
The top layer is called Q1 and is 2.0 m thick, this layer consists of soils mostly composed of sandy clays, with medium plasticity clays. Underneath there is a thin soil layer is specified as Q5 and is located between GL -2.0 m and GL -13.0 m, followed by thick N1, this layer is defined as sandy clays and clay with low-plasticity, and this layer is located between GL -13.0 m to -23.0 m.
The last layer N5 consist of sandy soils composed of clayey sand, mostly compacted, starts at GL -23.00 m and reaches the bottom model boundary at GL -50.0 m. Furthermore, the groundwater table is assumed at about GL -5.45 m below the surface.

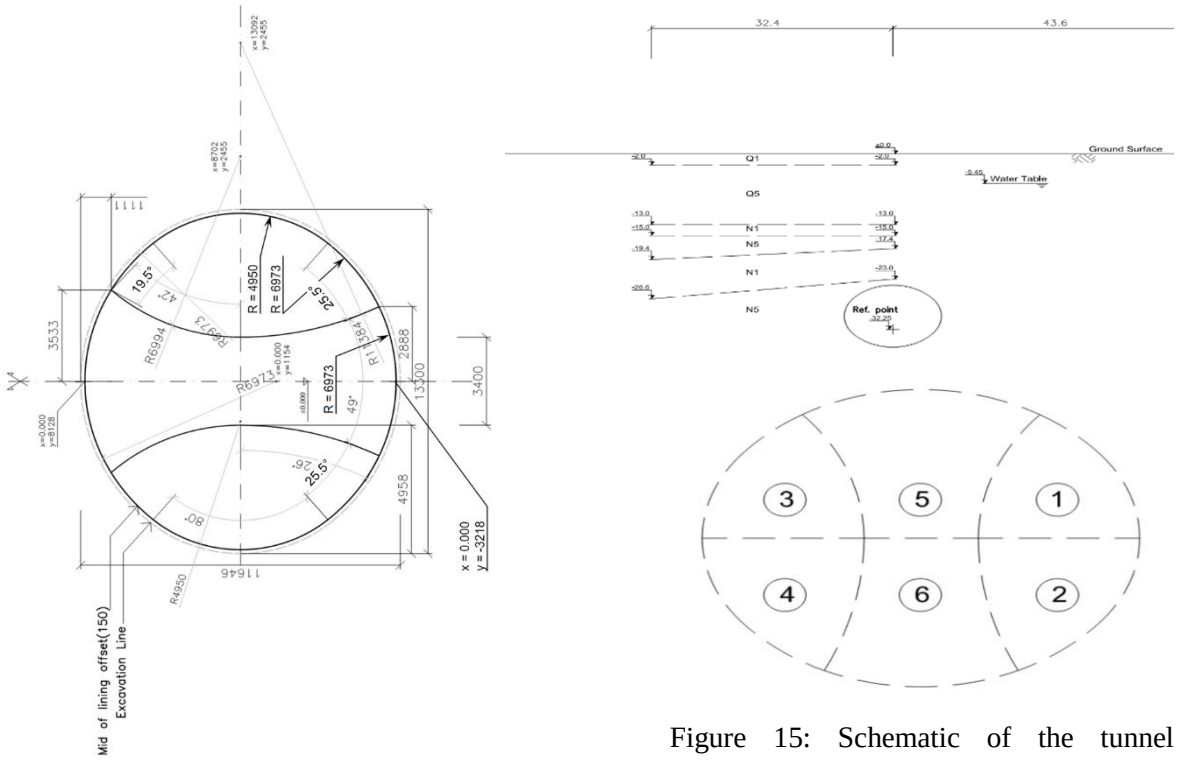

Figure 15: Schematic of the tunnel excavation

Figure 16: Tunnel geometry and soil profile layout, Dimension in [mm].

7.2.2 Material parameters

The mechanical properties of the above mentioned soil layers assuming the HS and HS small model are given in Table 7. The primary shotcrete lining is 30.0 cm thick and the side drift lining is 25 cm thick.

Table 7: NATM tunnel: Material parameters for HS and HS small model

Symbol	Q1	Q5	N1	N5	Units
Material Model	HSS and HS model	HS model	HSS and HS model	Model	
Type of Behaviour	Drained	Drained	Drained	Drained	
γ_{sat}	20	20	20	20	$[kN/m^3]$
γ_{unsat}	20	20	20	20	$[kN/m^3]$
${E_{oed}}^{ref}$	10000	98000	25000	39000	$[kN/m^2]$
${E_{50}}^{ref}$	10000	98000	25000	39000	$[kN/m^2]$

Symbol	Q1	Q5	N1	N5	Unit
Material Model	HSS and HS model	HSS and HS model	HSS and HS model	HSS and HS model	
Type of behaviour	Drained	Drained	Drained	Drained	
$E_{ur}{}^{ref}$	30000	294000	75000	117000	$[kN/m^2]$
m	0.8	0.8	0.8	0.6	[-]
c'	16	0	21	5.0	$[kN/m^2]$
φ'	20	34	25.5	27	[°]
ψ	0.0	0.0	0.0	0.0	[°]
ν_{ur}	0.2	0.2	0.2	0.2	[-]
p^{ref}	100	100	100	100	$[kN/m^2]$
K_0	0.66	0.44	0.57	0.55	[-]
R_f	1.0	1.0	1.0	1.0	[-]
G_0^{ref}	37500	367500	93750	146250	$[kN/m^2]$
$\gamma_{0.7}$	0.0002	0.0002	0.0002	0.0002	$[kN/m^3]$

7.2.3 Excavation/Construction stages

1- Initial stress state (K_0-procedure, normally consolidated)
2- Dewatering
3- Stress release of the top right part– Mstage 15%, β = 0.85.
4- Excavation of the top right part – Mstage 50% – lining installation (shotcrete modulus 5 GPa)
5- Stress release of the bottom right part – Mstage 15%, β = 0.85.
6- Excavation of the bottom right part – Mstage 100% – lining installation (shotcrete modulus 5 GPa) – change shotcrete modulus to 15 GPa in top right part.
7- Harden the bottom right part lining and Stress release of the top left part– Mstage 15%, β = 0.85.
8- Excavation of the top left part – Mstage 50% – lining installation (shotcrete modulus 5 GPa).

9- Stress release of the bottom left part – Mstage 15%, β = 0.85.
10- Excavation of the bottom left part – Mstage 100% – lining installation (shotcrete modulus 5 GPa) – change shotcrete modulus to 15 GPa in top left.
11- Stress release of the centre top heading – 30%, stiffness of the bottom left part 15 GPa.
12- Excavation of the centre top heading – Mstage 80% – Installation of linings, stiffness 5 GPa.
13- Stress release of the centre bench – Mstage 15% – lining of the top heading 15 GPa.
14- Excavation of the centre bench – Mstage 90% – Lining of the invert 5 GPa.
15- Deactivate side drift walls – Mstage 100% – lining of the invert 15 GPa.
16- Reset groundwater conditions around the tunnel.

7.2.4 Model configuration

The finite element model and the mesh generation are shown in Figure 18.
In the Mesh mode, the tunnel and the surrounding zone with 40.0 m x 45.0 m is refined by a coarseness factor of 0.35 and the Mesh option ‘Fine’ is used.

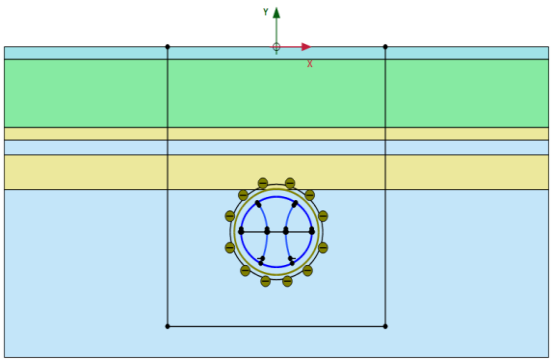

Figure 17: Model configuration of the NATM tunnel

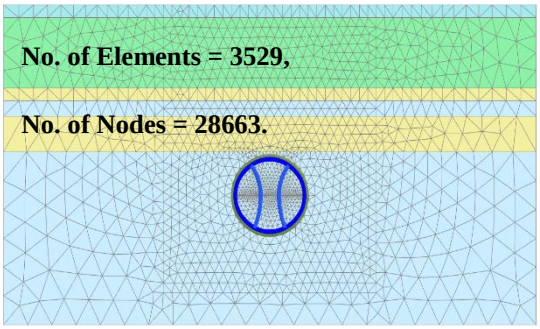

Figure 18: 2D mesh discretisation

7.2.5 Results

1- The consideration of small-strain stiffness results in a significantly shallower vertical settlement profile compared to the standard Hardening Soil model. The displacements from 20 m- offset from the tunnel axis are reduced further away to the boundary sides.

2- In Figure 19, the surface settlements using HS standard, HSS and GHS model are shown. The maximum value of GHS is -31 mm, in contrast, the maximum value of HSS is -40 mm and the maximum value obtained by the HS standard is -51 mm.

3- Due to the influence of the mean effective stress on the "stress-stiffness dependency", the settlement trough of the GHS-model is narrower than the surface settlement trough of the HS-standard and HS small models.

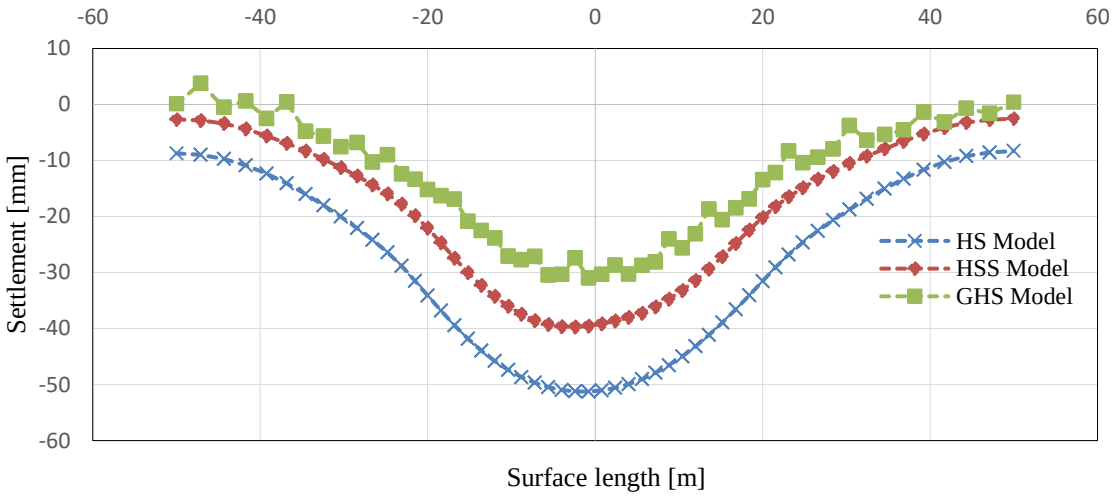

Figure 19: Result NATM tunnel: Ground surface settlement Uy.

Table 8 summarises the maximum values of the axial forces, shear force and bending moments in the lining at the final stage.

Table 8: Summary of the FE results of the lining at the final phase.

	Symbol	HS	HSS	GHS	Units
Maximum surface settlment	Uy	-51	-40	-31	mm
Maximum shear force	Q	114	94	73	kN/m
Maximum axial force	N	-2026	-2080	-2011	kN/m
Maximum bending moment	My	132	114	89	kNm/m

7.3 Case study - Deep excavation in Salzburg I

The geotechnical model is based on a deep excavation in Salzburg. The geometry and the soil parameters are given. The study presents a parametric analysis of main differences between HS Standard, HS-Small and the Generalised Hardening soil models.

7.3.1 Problem definition

An excavation pit was constructed in Salzburg. The pit is 9.9 m deep and 15 m wide. The diaphragm wall is modelled as a continuum element. This wall is supported by two row of struts in a certain depth. The upper 10 m of the subsoil consists of gravel. The next 5.0 m of subsoil consists of “Fine Sand”. The fine sand is bedded on a layer of “Clayey silt”.
Figure 20 shows the geometry of the excavation pit as well as the foundations.

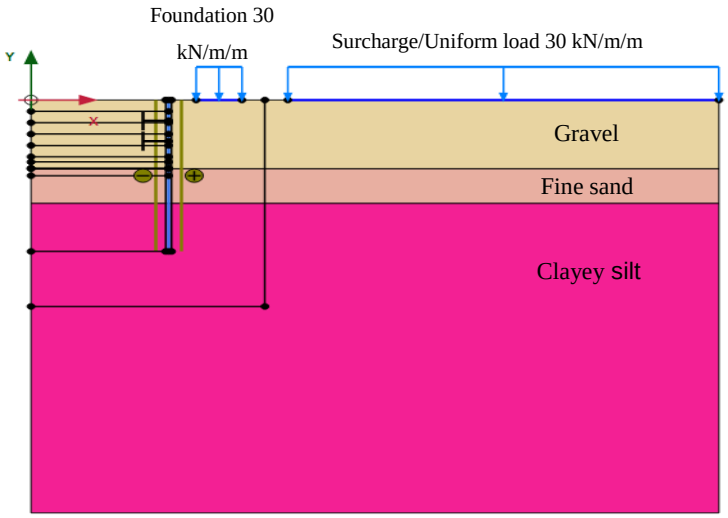

Figure 20: Deep excavation in Salzburg I: Geometry of the model

7.3.2 Material Parameters

The material properties are given in Table 9 and Table 10. The structural elements parameters are illustrated in Table 11.

Table 9: Deep excavation in Salzburg I: Stiffness parameters for the soil layers

Soil layer	Drainage type	level [m]	E_{50}^{ref} $[kN/m^2]$	E_{oed}^{ref} $[kN/m^2]$	E_{ur}^{ref} $[kN/m^2]$	p^{ref} $[kN/m^2]$	m	v_{ur}	G_0^{ref} $[kN/m^2]$	$\gamma_{0.7}$ -
Gravel	Drained	0.0-10.0	52000	52000	208000	100	0	0.2	346666	1.5E-04
Fine Sand	Drained	10.0-15.0	44000	44000	176000	100	0	0.2	422400	1.5E-04
Clayey silt	Undrained	≥15.0	37600	37600	150400	100	0.3	0.2	250666	1.5E-04

Table 10: Deep excavation in Salzburg I: Strength parameters for soil layers.

	γ_{unsat}	γ_{sat}	c′	R_f	R_{inter}	φ′	K_0	k_x/k_y
	$[kN/m^3]$	$[kN/m^3]$	$[kN/m^2]$	[-]	[-]	[°]	[-]	[-]
Gravel	18.95	22.45	2	0.9	0.7	35	0.55	2.59
Fine Sand	21.40	23.90	5	0.9	0.7	28	0.55	1.0
Clayey silt	20.2	24.20	30	0.9	0.7	26	0.55	8.64E-03

Table 11: Deep excavation in Salzburg I: Parameters for structural elements

	EA $[kN/m^2]$	EI $[kN/m^2]$	w $[kNm/m]$
Foundation slab	2.9E7	2.417E6	0.25
Diaphragm wall	2.3E7	1.2E6	0
Strut	1.74E7	$I_{SPACING}$=1.0	-

7.3.3 Mesh configuration

Figure 21 shows the finite element mesh used for analysis, in which the left boundary is the centre of excavation, taking into account the symmetry of the excavation, the right boundary at a distance of 75 m from the excavation centre, which is beyond the excavation influence zone.

The model is meshed with approximately 14329 elements and 115668 nodes. The soil clusters of the brace system as well as the area around the excavation have a coarseness factor equal 0.15. The rest of the model has coarseness factor equal 0.7071. In the Mesh mode the very fine option is used.

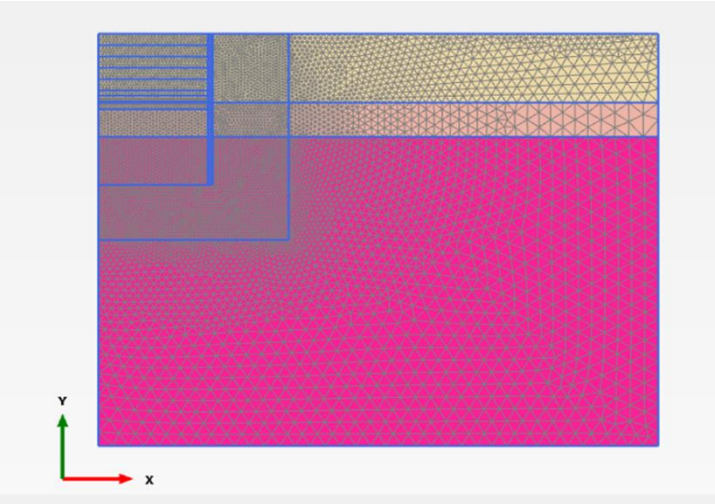

Figure 21: Deep excavation in Salzburg I: connectivity plot

7.3.4 Flow condition

The excavation is done under dry conditions. Therefore, groundwater lowering inside the excavation area is required due to groundwater present at 9.0 m below surface. The excavation is divided into 6 intermediate excavation steps (see Figure 20).

The GW-table lowering takes place in three steps. From 9.0 m to 10.0 m, and from 10.0 m to 11.0 m and the last from 11.0 m to 12.0 m.

In terms of modelling, in order to have equal pore water pressure at the base of the diaphragm wall, it is necessary to interpolate the pore water pressure inside the diaphragm walls.

Hence, interpolation of the pore water pressure inside the wall has been conducted for each lowering phase (see Figure 22, 23 and 24).

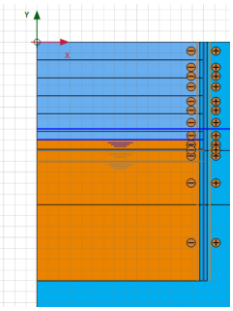

Figure 24: 1st GWT lowering

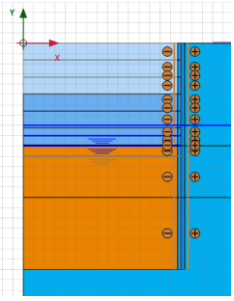

Figure 23: 2nd GWT lowering

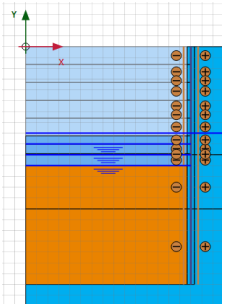

Figure 22: 3rd GWT lowering

Figure 22, Figure 23 and Figure 24 represent the considered flow conditions. As well as the interpolated area.

7.3.5 Construction stages

1- Phase 0: initial phase - K_0-procedure.
2- Phase 1: activation of the diaphragm wall.
3- Phase 2: nil step.
4- Phase 3: first GWT lowering to 9.0 m.
5- Phase 4: excavation up to 1.65 m.
6- Phase 5: excavation up to 3.3 m.
7- Phase 6: activation of the 1st strut.
8- Phase 7: excavation up to 4.95 m.
9- Phase 8: 2nd GWT lowering 10.0 m.
10- Phase 9: excavation up to 6.60 m.
11- Phase 10: activation of the 2nd strut row.
12- Phase 11: excavation 8.25 m.
13- Phase 12: 3rd GWT lowering
14- Phase 13: exaction 9.9 m
15- Phase 14: FoS Analysis $\varphi - c$ reduction method.

7.3.6 Results

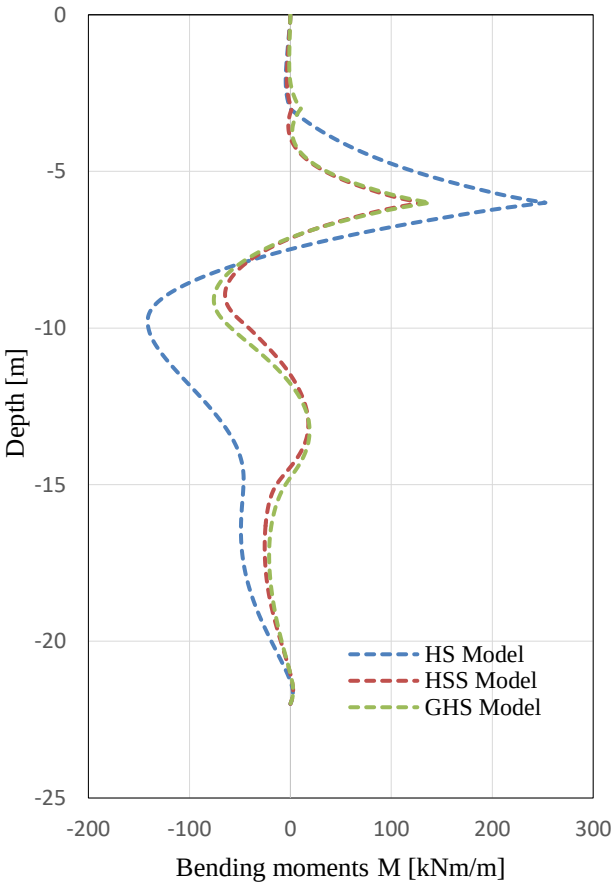

Figure 25: Result deep excavation in Salzburg I: Bending moments M

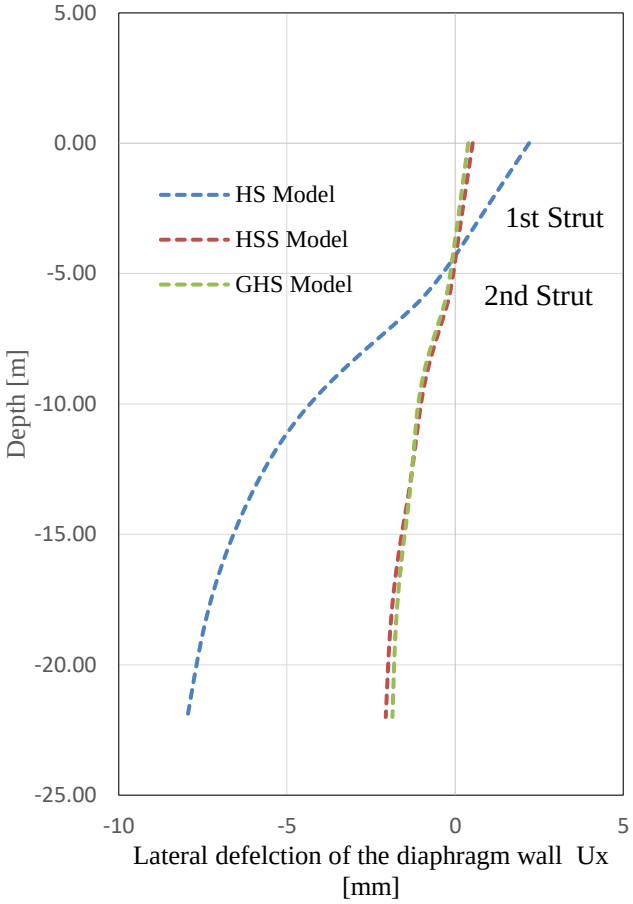

Figure 26: Result deep excavation in Salzburg I: Horizontal deformation of the D wall Ux

Figure 26 shows the lateral displacement of the diaphragm wall for the final excavation stage. The results are calculated by means of a adding a weak plate in the centre line of the diaphragm wall. It is observed that the HS model predicts the highest displacements. HSS and GHS model show similar behaviour but including mean effective stress effects reduces the maximum displacement slightly. For instance, the maximum difference of the wall deflections (using GHS and HS small) approximately is 1.0 mm. A similar trend is observed for bending moments "M" (Figure 25). It should be mentioned the results from the HSS and GHS model may be sensitive on the choice of the parameter $\gamma_{0.7}$.

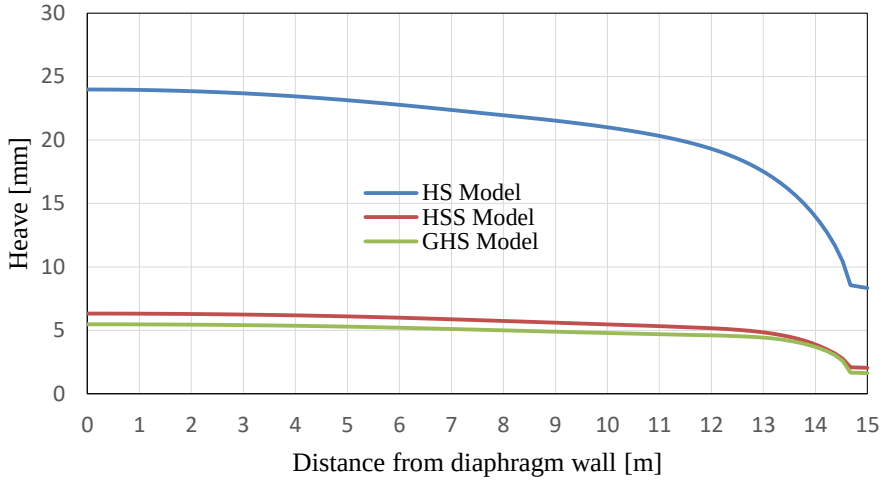

Figure 27: Result deep excavation in Salzburg I: Heave Uy

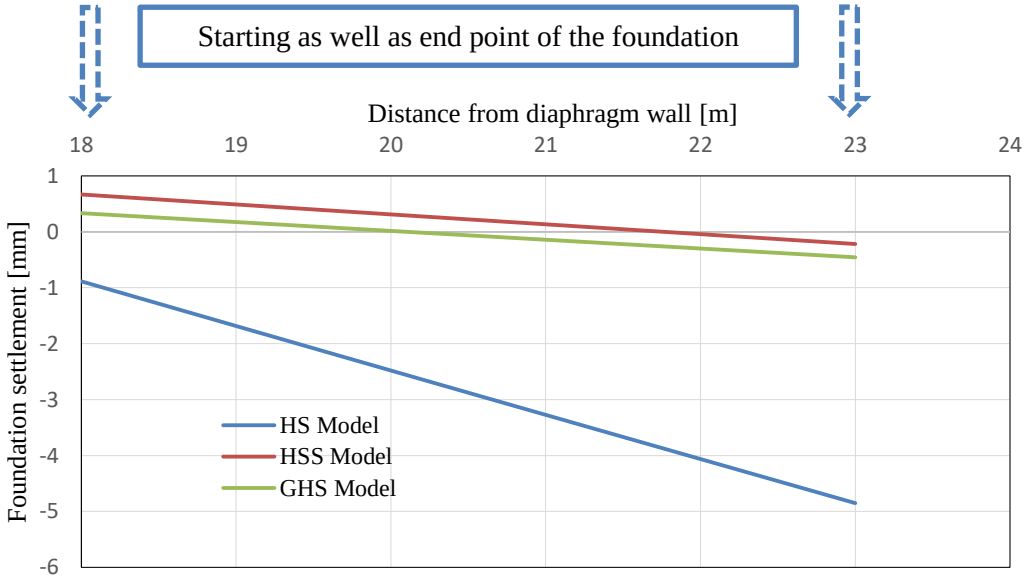

Figure 28: Result deep excavation in Salzburg I: Foundation settlement Uy

In Figure 27 and Figure 28, the heave Uy as well as foundation settlement are presented. The foundation behaves a slight differently at both end sides, the foundation edge near the wall is subjected to heave, and the other side far away from the wall is subjected to settlement. Furthermore, the GHS result shows slightly less heave compared to the HS small model, on the other hand GHS shows a slightly higher settlement compared to the HS small model.

Figure 29 shows the strut forces in the first and second row of struts with progressing excavation.

The strut forces capacity is changing by position, as a consequences the strut forces of the first row determined by using the GHS model is higher than the calculated using HS model and HS small model. In contrast the strut forces of the second row behave in a different way. For the second row, the force in the strut of our different models is highest for the HS model. The reason might be because of the influence of the wall deformation pattern as excavation progressed i.e., small wall deformation at the top.

Figure 29: Result deep excavation in Salzburg I: Strut forces [kNm/m]

In Figure 30 and Figure 31, the plastic point history for HS small as well as GHS user defined model are shown. As a consequence of utilizing the mean effective stresses, hence, the GHS – user defined model tends to show less failure points, in contrary to the HS small model.

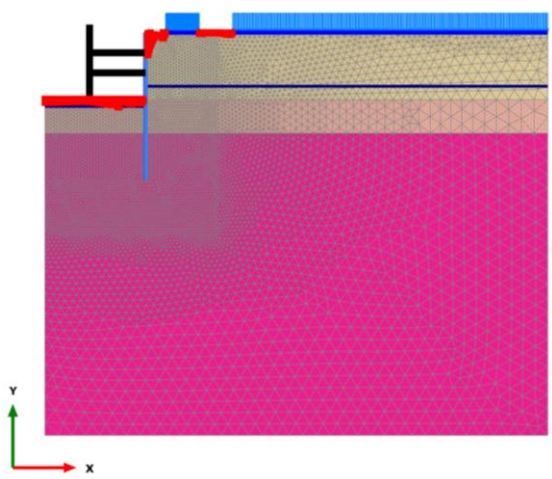

Figure 30: Result deep excavation in Salzburg I: Plastic point history for HS small

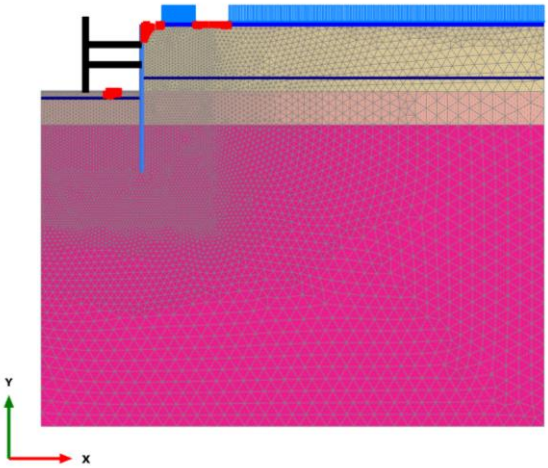

Figure 31: Result deep excavation in Salzburg I: Plastic point history for GHS - user defined model

Table 12: Result deep excavation in Salzburg I: Summary of the FE calculations

	Symbol	HS Model	HSS Model	GHS Model	Units
Maximum heave of the bottom of the excavation	Uy	24	6	5	mm
Maximum wall deflection	Ux	-8	-2	-2	mm
Maximum bending moment	M	252	130	138	kNm/m

7.4 Case study - Deep excavation in Salzburg II

The construction was carried out using 10 excavation stages with 2 level steel struts, and the maximum excavation depth was 9.73 m in the final excavation stage. The excavated pit was retained by a 0.65-m-thick and 20-m-deep diaphragm wall.

The basic geometry of the investigated deep excavation is depicted in Figure 32.

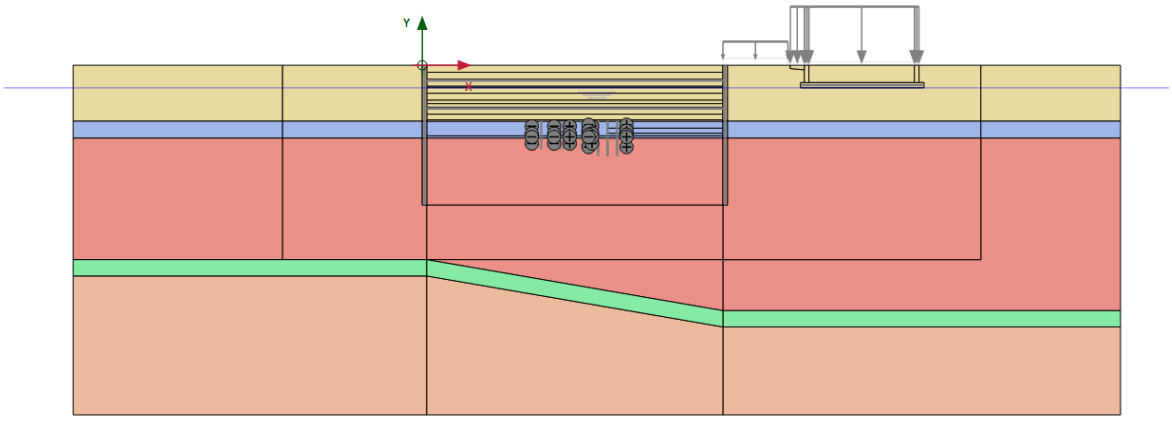

Figure 32: Deep excavation in Salzburg Ⅱ: Geometry

7.4.1 Material parameters

The soil properties for each model are presented in Table 13. Typically for the region of Salzburg is the “Seeton”. The upper 8 m of the subsoil conditions consists of gravel. Underneath, there is a thin layer of “Sandy Seeton” with a thickness of 2.4 m, followed by a thick layer of “Silty Seeton”. The “Seeton” is bedded on solid rock covered by a thin layer of Moraine. In addition, the ground water table is 3.20 m below the ground level.

Table 13: Deep excavation in Salzburg II: Material parameters

Symbol	Gravel	Seeton sandy	Seeton silty	Moraine	Solid rock	Unit
Model	HSS	HSS	HSS	HSS	HS	-
Type	drained	drained	drained	drained	drained	-
γ_{unsat}	21	20	19	21	25	$[kN/m^3]$
γ_{sat}	21	20	19	21	25	$[kN/m^3]$
E_{oed}	26680	30000	20990	21424	1090023	$[kN/m^2]$

Symbol	Gravel	Seeton sandy	Seeton silty	Moraine	Solid rock	Unit
E_{oed}^{ref}	30604	24701	12000	11514	497147	$[kN/m^2]$
E_{50}^{ref}	30604	24701	15000	11514	497147	$[kN/m^2]$
E_{ur}^{ref}	91812	74104	45000	34542	1491442	$[kN/m^2]$
E_{ur}	54011	55401	55277	47154	2135392	$[kN/m^2]$
c´	0	0	5	1.0	15	$[kN/m^2]$
φ´	33	30	25	27,5	35	[°]
ψ	2,5	0	0	0	0	[°]
ν_{ur}	0.2	0.2	0.2	0.2	0.2	[−]
p^{ref}	100	100	100	100	100	$[kN/m^2]$
m	0.5	0.7	0.7	0.5	0.5	[−]
K_0^{NC}	0.46	0.50	0.58	0.54	0.43	[−]
R_f	0.9	0.9	0.9	0.9	0.9	[−]
R_{inter}	0.75	0.75	0.75	0.75	-	[−]
$\gamma_{0.7}$	1.50E-04	2.00E-04	2.00E-04	1.50E-04	-	$[kN/m^2]$
k_x	8.64E+01	9.07E-02	4.75E-04	8.64E-03	-	$[m/d]$
k_y	6.48E+01	4.43E-02	8.64E-05	8.64E-03	-	$[m/d]$
G_{ur}^{ref}	38255	30877	18750	14392	621434	$[kN/m^2]$
G_0^{ref}	114765	92630	56250	43177	1864302	$[kN/m^2]$
OCR	3.0	3.0	3.0	3.0	3.0	[−]

Tables 14 and 15 list the input parameters of the diaphragm wall and struts used in the numerical analysis. The diaphragm wall was simulated by plate elements, while the steel struts were modelled by node-to-node anchor elements. The behaviour of both the plate elements and the node-to-node anchor elements were governed by the linear-elastic model, which requires two input parameters: Poisson's ratio and Young's modulus. Poisson's ratio of the structural elements was taken to be 0.2 for both the diaphragm wall and the foundation.

Table 14: Deep excavation in Salzburg II: Parameter for structural elements

Structural element	Model	Type	Isotropic	End bearing	EA kPa	EI kPa	w kN/m/m	ν
Sheet pile wall	plate	elastic	yes	no	8.00E7	1.5E6	8	0
Strut	Node-to-Node Anchor	elastic	-	-	1.74E7	$I_{SPACING}$ =5.0	-	

Table 15: Deep excavation in Salzburg II: FE Parameter diaphragm wall and foundation of building in vicinity

	Model	Type	γ kPa	E kPa	ν [-]
Concrete DW and foundation	Linear elastic	Non-porous	25	3.00E7	0.2

7.4.2 Mesh configuration

In the Mesh mode, the excavation pit and the surrounding zone are refined, and the Mesh option very Fine is used. The resulting refined mesh is shown in Figure 33.

The model is meshed with approximately 19834 elements and 159644 nodes.

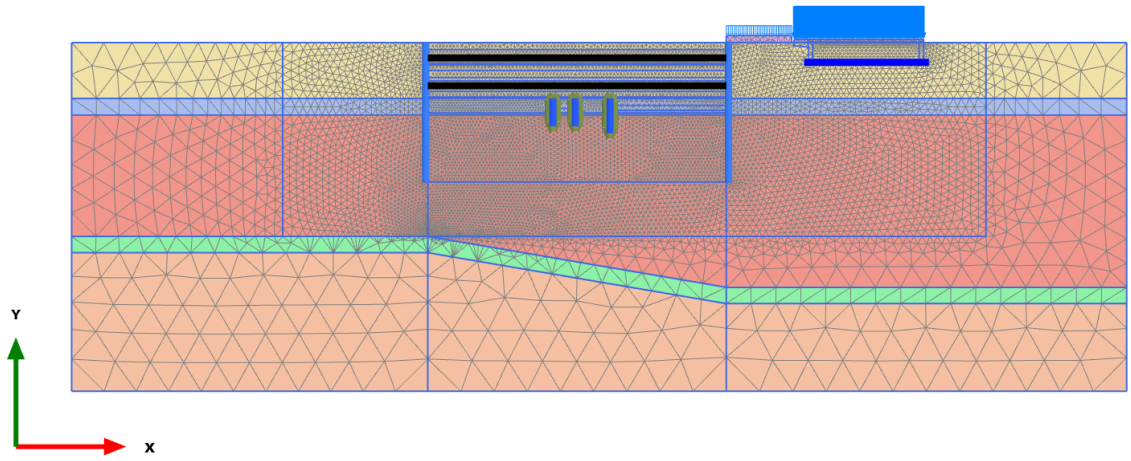

Figure 33: Deep excavation in Salzburg II: 2D mesh

7.4.3 Flow condition

For the given problem, the initial ground water table is located at 3.2 m below the ground surface. The excavation is planned to be conducted in different depths and so with this consideration, ground water lowering is done. In accordance with the excavation levels, 3 water levels were defined and renamed ‘GW_Level_’x’ m’.

To account for the difference of pore pressures, because when groundwater lowering is done inside the excavation pit, pore water pressure remains unchanged on the outer side, interpolation of pore pressures is done for all 3 defined water levels.

Note: However, the lowest final excavation depth is -9.73 m, due to construction reasons and practical considerations the final ground water level is defined at - 10.10 m.

In Figure 34, 35 and 36, the excavation phases and the ground water lowering are displayed. The excavation steps and ground water lowering are done in a 1 m interval in order to avoid excessive drawdown of the ground water resulting in excessive settlements in the surrounding building vicinities in the excavation process.

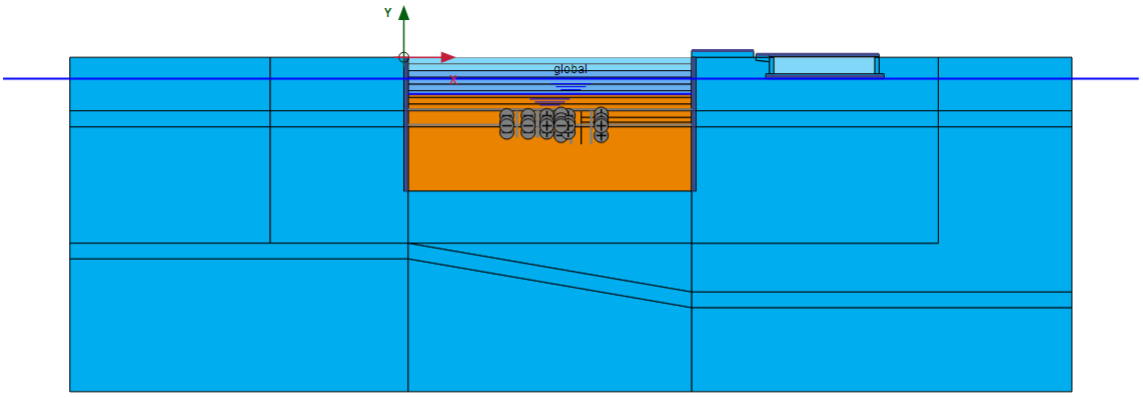

Figure 34: Deep excavation in Salzburg II: 1st GWT lowering

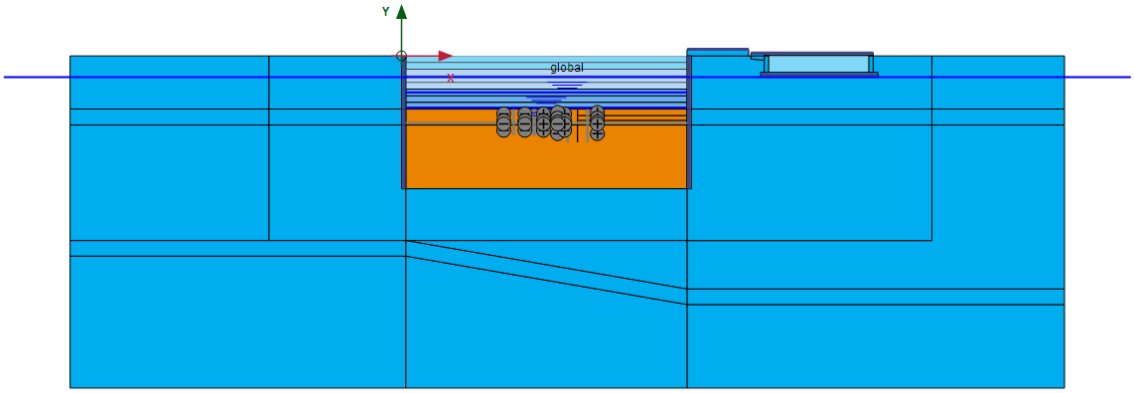

Figure 35: Deep excavation in Salzburg II: 2nd GWT lowering

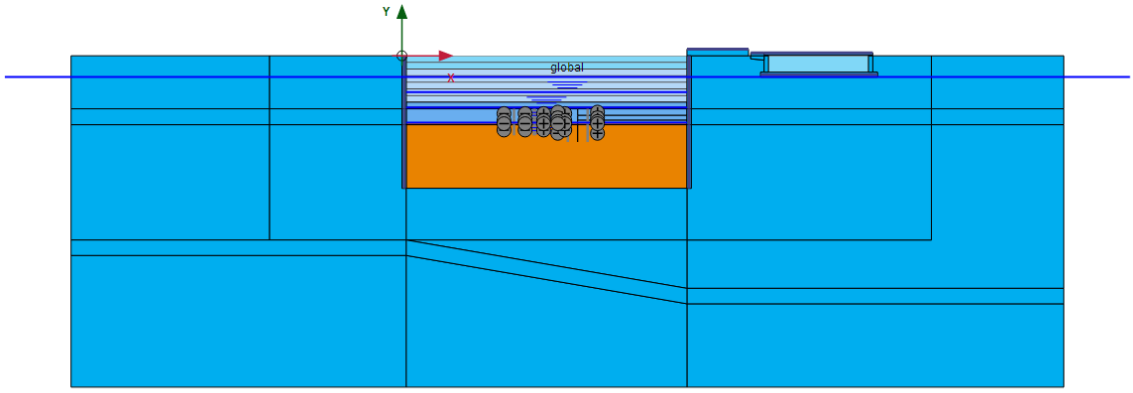

Figure 36: Deep excavation in Salzburg II: 3rd GWT lowering

7.4.4 Construction stages

In total 18 phases were used to simulate the deep excavation problem. The following calculation steps have been performed, but only results for the final stage are presented here:

1. Stage 0: initial phase “initial stress state”.
2. Stage 1: activation of the diaphragm wall.
3. Stage 2: nil step.
4. Stage 3: excavation (to level -1.0 m).
5. Stage 4: excavation (to level -2.0 m).
6. Stage 5: groundwater lowering to -5.5 m.
7. Stage 6: excavation (to level -3.0 m).
8. Stage 7: activation of strut 1 at level -2.2 m.
9. Stage 8: excavation (to level -4.0 m).

10. Stage 9: excavation (to level -5.0 m).
11. Stage 10: groundwater lowering to level -7.8.
12. Stage 11: excavation (to level -6.0 m).
13. Stage 12: excavation (to level -7.0).
14. Stage 13: activation of strut 2 at level -6.2 m.
15. Stage 14: groundwater lowering to -10.1 m.
16. Stage 15: excavation (to level -8.0 m).
17. Stage 16: installation of sheet pile wall for the small pit.
18. Stage 17: excavation (to level -9.0/9.45 m).
19. Stage 18: excavation (to level -9.73 m).

7.4.5 Results

Two cases were investigated using normally consolidated soils (NC) and over-consolidated soils (OC). For each case the soil was modelled using HS small model and GHS – user defined model. As a consequence, the following graphs present the numerical analysis results of the aforementioned cases.

Whereas:

$$OCR = 3.0$$

$$k_0 = 1.5$$

Numerical results of building and pavement displacements, bending moments and deflections of the diaphragm walls, forces in the struts and displacements at the bottom of the excavation are given in comparison with all two models and are presented in graphical form.

Note that, the following results are for the final excavation stage [Phase-18].

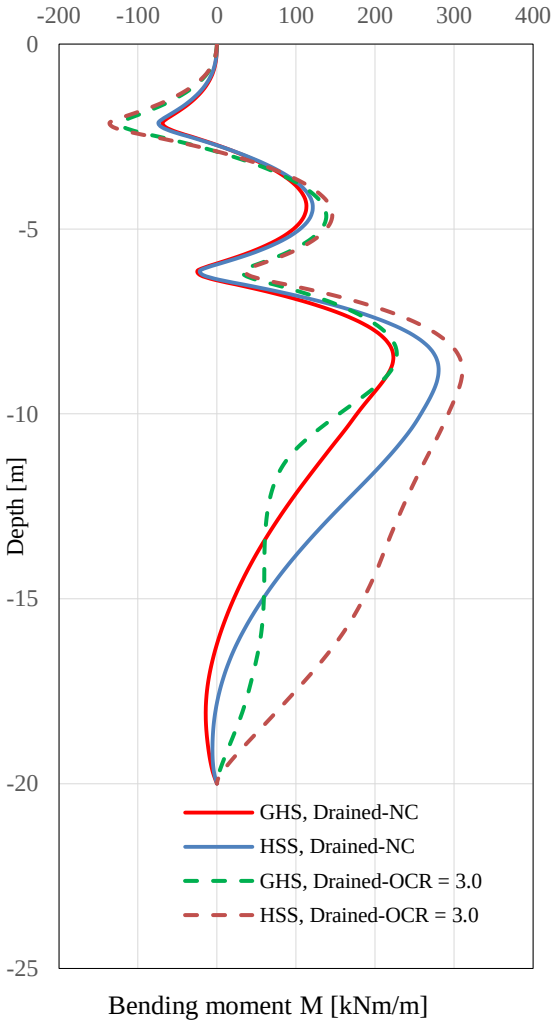

Figure 38: Result deep excavation in Salzburg II: Bending moment M of the left D wall

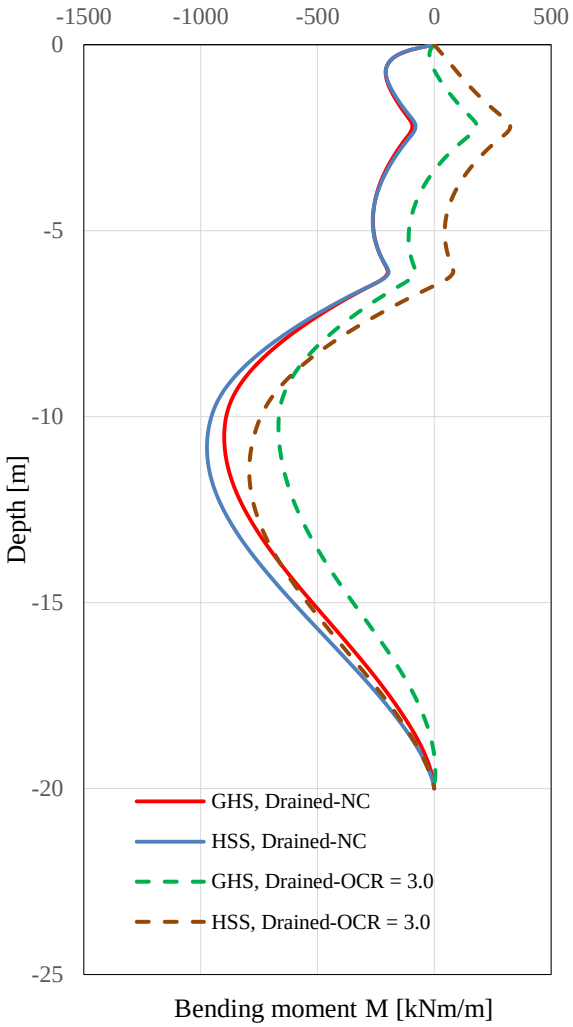

Figure 37: Result deep excavation in Salzburg II: Bending moment M of the right D wall

Maximum bending moments (Figure 37 and 38) calculated are similar although differences are observed at the middle part of the wall. This can be attributed to the fact that the ‘’stress-stiffness dependency’ is different in both models.

Figure 39 and 40 show the wall deflection for the final excavation stage for both analyses (GHS and HSS). It can be seen that the horizontal displacements are higher for the HS small model as compared to the Generalized Hardening Soil model. However the differences in values are not significant from a practical point of view.

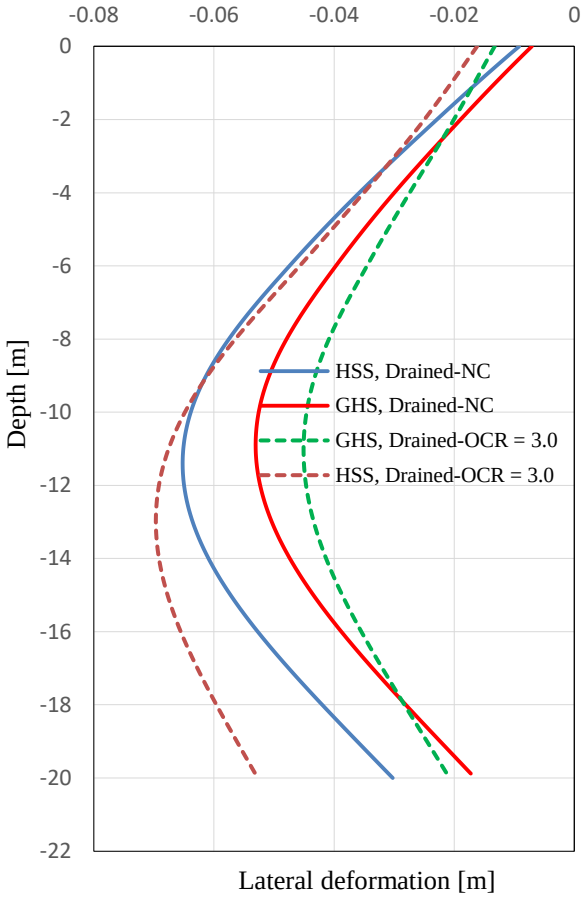

Figure 40: Result deep excavation in Salzburg II: Lateral deformation Ux of the right D wall

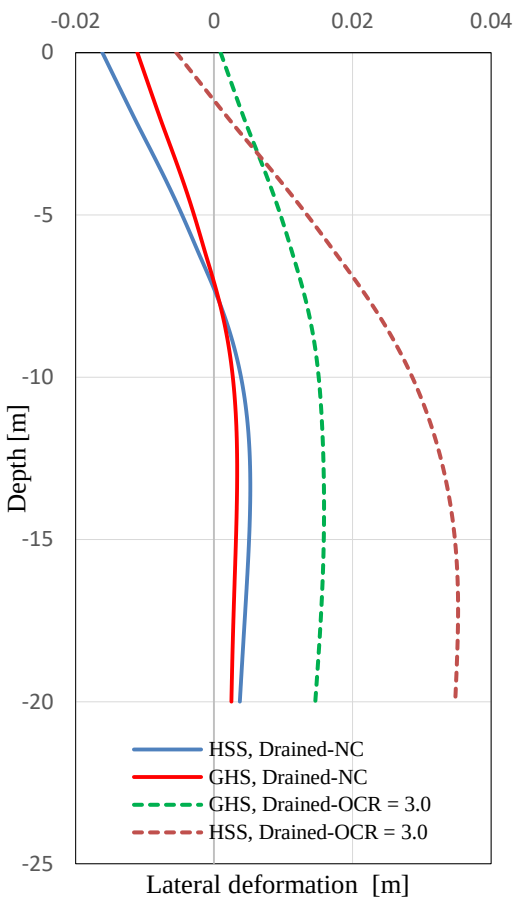

Figure 39: Result deep excavation in Salzburg II: Lateral deformation Ux of the left D wall

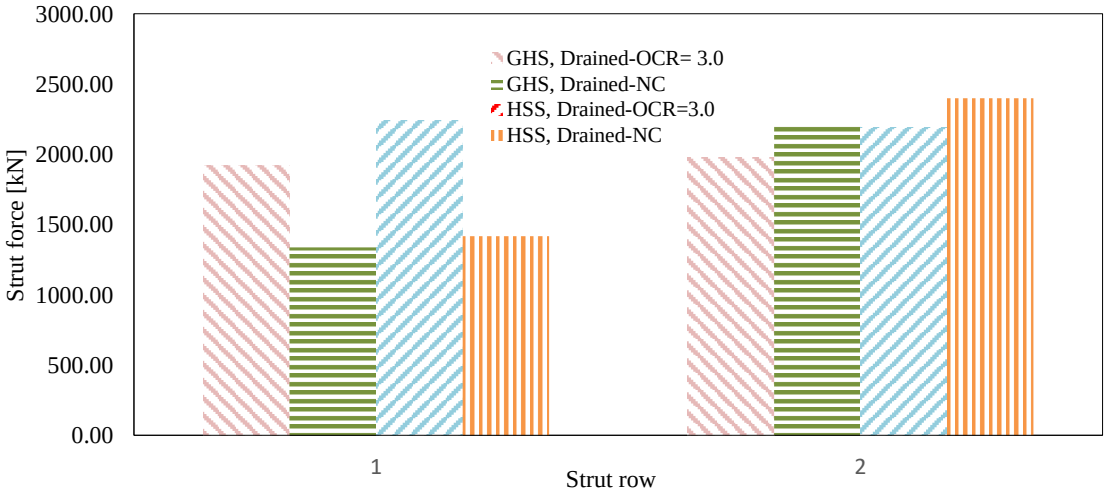

Figure 41: Result deep excavation in Salzburg II: Strut force

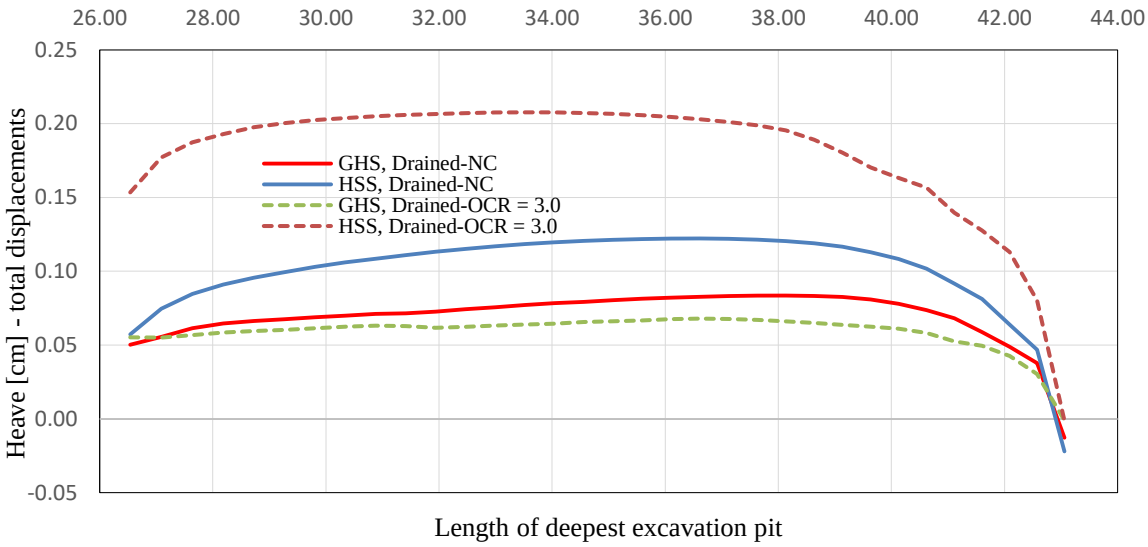

Figure 42: Result deep excavation in Salzburg II: Maximum heave at the excavation pit at depth of 9.73 m

Figure 42 shows the heave distribution for the NC and OC soils, using HSS model and GHS model. It can be seen that the HSS-model leads to higher deformations at the bottom of the excavation. For the case of the OC soil, this can be explained by the fact that the stress-dependency formulations in the HS small model does not account for the pre-consolidation stress. For the case of the NC soil, this might be explained by the fact that the stress dependency formulations do not consider for the mean effective stress.

When comparing the heave distribution along the excavation bottom for NC and OC soils using HS small model, a higher displacements for OC can be seen. This is due to the fact that the vertical stresses decreases during excavation, leading to a reduction of deviatoric stresses for NC-soils and an increase for OC-soils, consequently resulting in higher deformations for the OC-soils.

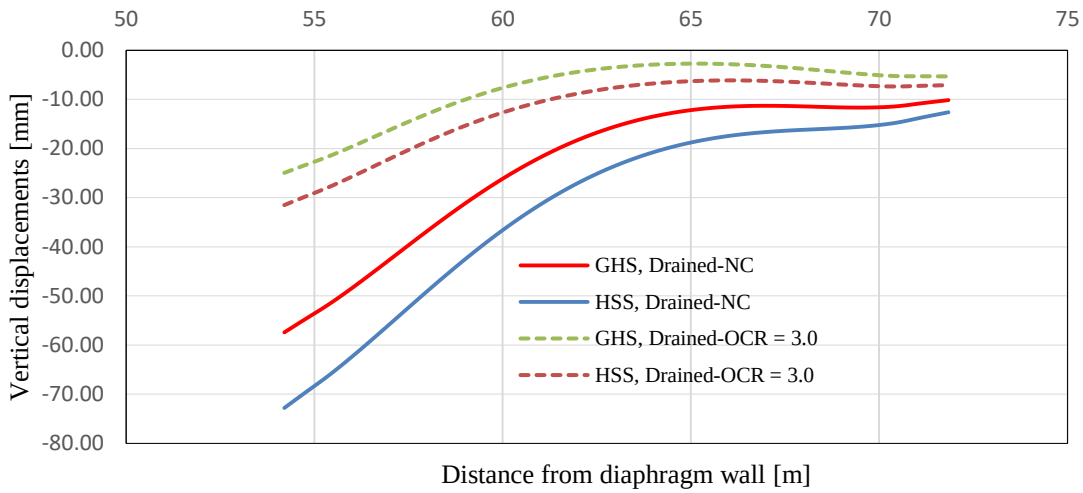

Figure 43: Result deep excavation in Salzburg II: Vertical displacements of the foundation

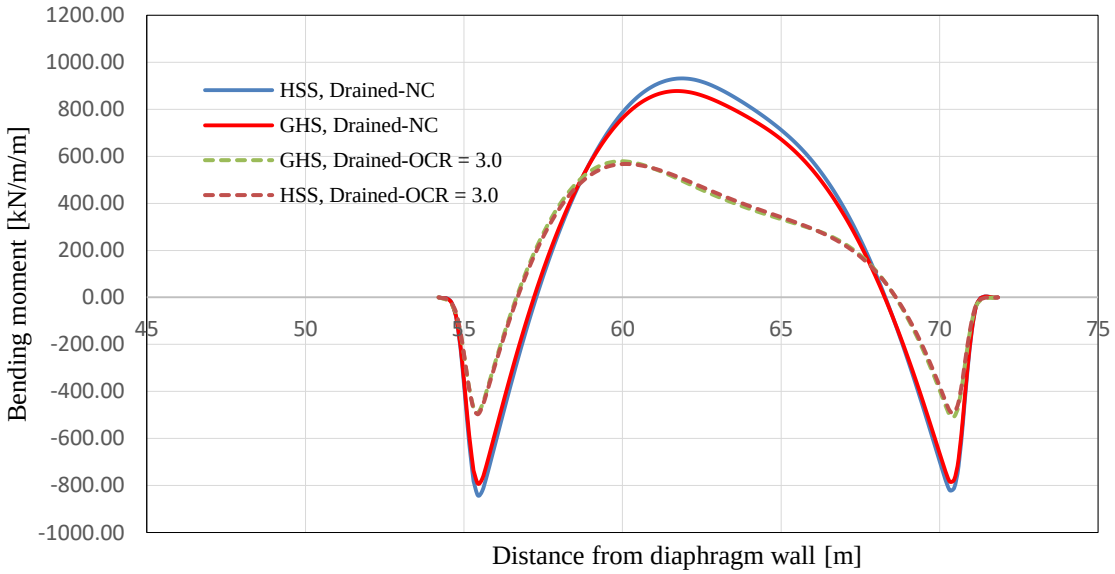

Figure 44: Result deep excavation in Salzburg II: Bending moment M of the foundation

In Figure 43 and 44, the vertical displacement and bending moment of the building are displayed. The HS small model overall gives a slight higher results. The GHS model improves results slightly.

The HS small model accumulates more settlement right next to the wall due to the small strain, in contrast, the GHS shows smaller settlement, whereas the settlement trough is similar (Figure 45). This is again related to the to the reduced excavation heave.

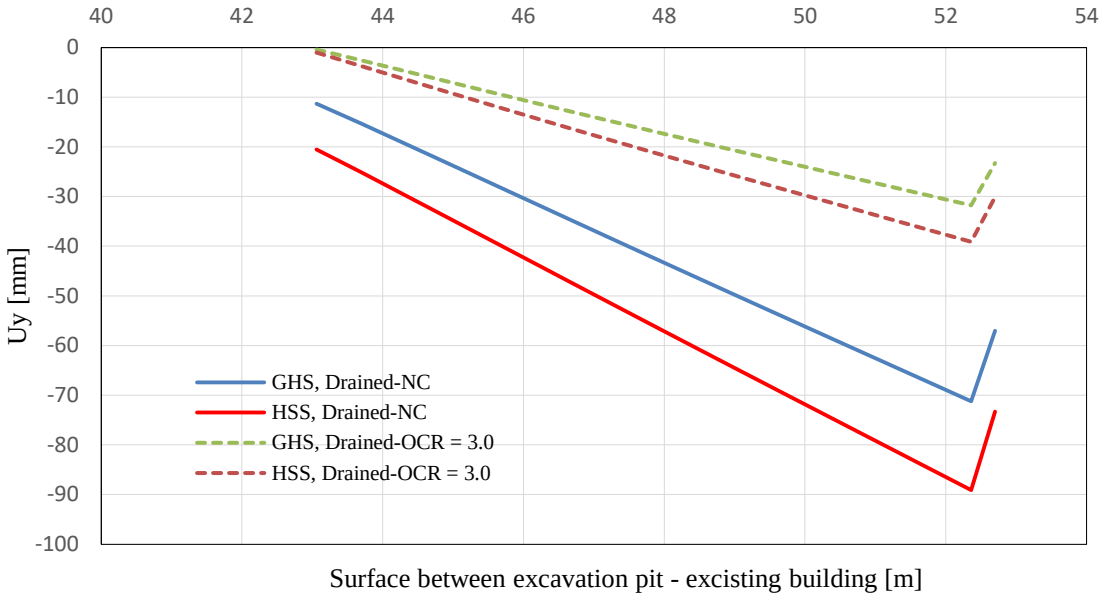

Figure 45: Result deep excavation in Salzburg II: surface settlement [mm]

In Figure 46, 47, 48 and 48, the plastic point history for HS and GHS models are shown.

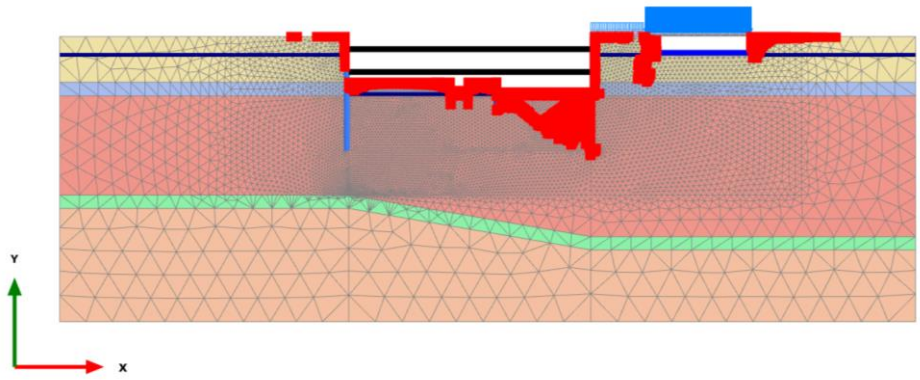

Figure 46: Result deep excavation in Salzburg II: Plastic point history failure for GHS – NC

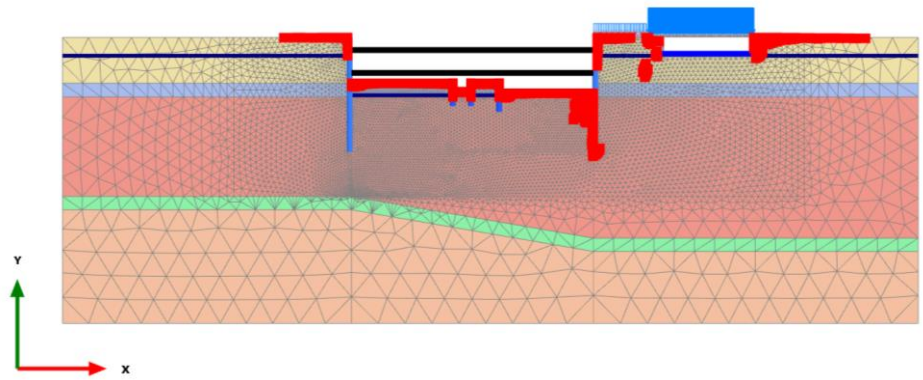

Figure 47: Result deep excavation in Salzburg II: Plastic point history failure for HSS - NC

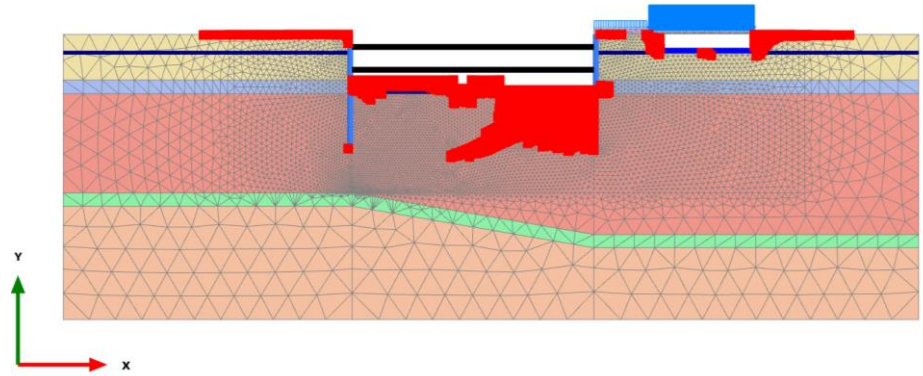

Figure 48: Result deep excavation in Salzburg II: Plastic point history failure for GHS - OC

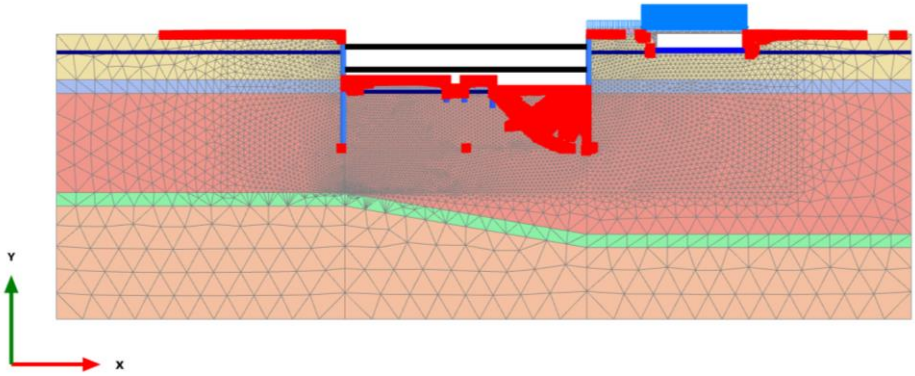

Figure 49: Result deep excavation in Salzburg II: Plastic point history failure for HSS - OC

7.4.6 Remarks

1- Figure 37 and 38 shows the comparison of the predicted wall bending moments with those using the $k_0 = 1.5$ for over-consolidated soil layers and those using NC soils. Over-consolidated soil "for GHS and HSS'' shows slightly lower bending moments results than the normally consolidated soil "for GHS and HSS'' of the right diaphragm wall. In contrast, the left diaphragm wall shows slight higher values for normally consolidated soil than over-consolidated soil.

2- In Figure 39 and 40, the horizontal displacements of the diaphragm walls are displayed. The maximum deflection of the right diaphragm wall is 7.0 cm (using HS small drained-OCR), which is located at the depth of approx. 13.0 m below the surface. While the maximum deflection of the left diaphragm wall is 3.0 cm (using HS small drained-OCR) at depth of approx. 15 m. therefore, the right-side wall is deformed more as compared to left-side wall. This occurred due to the additional surcharge on right side.

3- Calculated excavation heaves at the last excavation stage are shown in Figure 42. The heave using (HS small drained-OCR) shows very high values compared to the other calculated models (GHS drained-OCR, GHS drained-NC and HS small drained-NC).

4- The maximum strut load of the 1st level strut at the end of the excavation Figure 41 is considerably lower, which is likely due to the influence of the wall deformation pattern as excavation progress i.e., small wall deformation at the top.

5- One main tendency could be identified in this remarks section: a) The GHS model gives less excavation heave than the HS small model and hence, less deformation of the retaining structure and the adjoining soil.

7.5 Boston Trial Embankment

The study highlights the differences in prediction the final settlement of the embankment, by means of the HS, HS small as well as GHS model.

7.5.1 Problem definition

An 11 m high embankment was built on top of a 41 m thick over-consolidated clay. The embankment is 28 m wide and built on a 3.0 m thick sand layer. The ground water table is found at depth of 1.5 m below the ground surface.

The embankment problem is symmetrical, therefore only half of the embankment is modelled.

In Figure 50 the geometry of the embankment is presented.

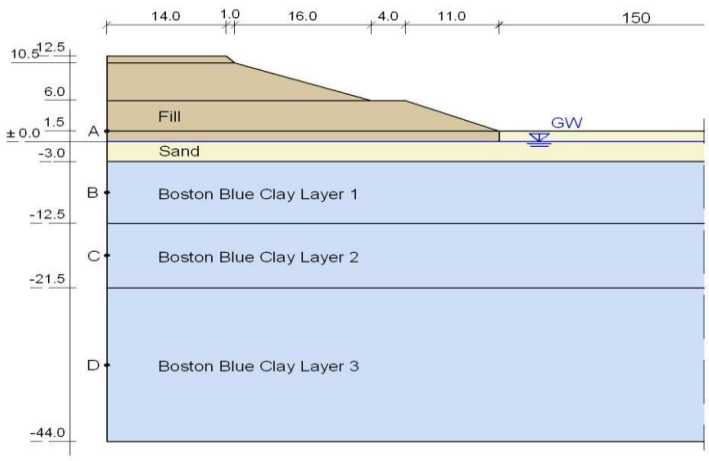

Figure 50: Cross section of the trail embankment

7.5.2 Material parameter

The fill material as well as the sand layers used for the embankment, are postulated to be drained; the “Boston Blue Clay Layers” behave undrained. The soil parameters are given in Table 16 and Table 17.

Table 16: Soil parameters of the fill, sand and the Boston clay layers (I).

		E_{50}^{ref} kPa	E_{oed}^{ref} kPa	E_{ur}^{ref} kPa	p^{ref} kPa	m	G_0^{ref} kPa	$\gamma_{0.7}$ -
Fill	Drained	40000	19000	120000	100	0.5	150000	2E-04
Sand	Drained	40000	18500	120000	100	0.5	150000	2E-04
Layer 1	Undrained	3400	1700	17000	100	1	35416.67	1.5E-04
Layer 2	Undrained	2000	1000	10000	100	1	20833.3	1.5E-04
Layer 3	Undrained	1200	600	6000	100	1	12500	1.5E-04

Table 17: Soil parameters of the fill, sand and the Boston clay layers (II).

	c' kPa	φ' [°]	OCR [-]	k_0^{OC}	Ψ [°]	R_f	v_{ur}	k_0^{NC}	k_x/k_y
Fill	5	35	-	-	0	0.9	0.2	0.35	0.1
Sand	1	37	-	-	0	0.9	0.2	0.35	0.1
Layer 1	1	33.4	4.04	1.26	0	0.9	0.2	0.5	1.13E-04
Layer 2	1	33.4	1.68	0.67	0	0.9	0.2	0.5	5.8E-04
Layer 3	1	33.4	1.1	0.525	0	0.9	0.2	0.5	5.8E-04

7.5.3 Mesh configuration

The model is meshed with approximately 6054 elements and 48985 nodes. The soil clusters of the embankment has a coarseness factor equal to 0.1768. The soil cluster beneath the embankment is subdivided into two zones. The first zone has a coarseness factor equal to 0.1768 and the second zone has coarseness factor equal to 0.25. In the Mesh mode the very fine option is used.

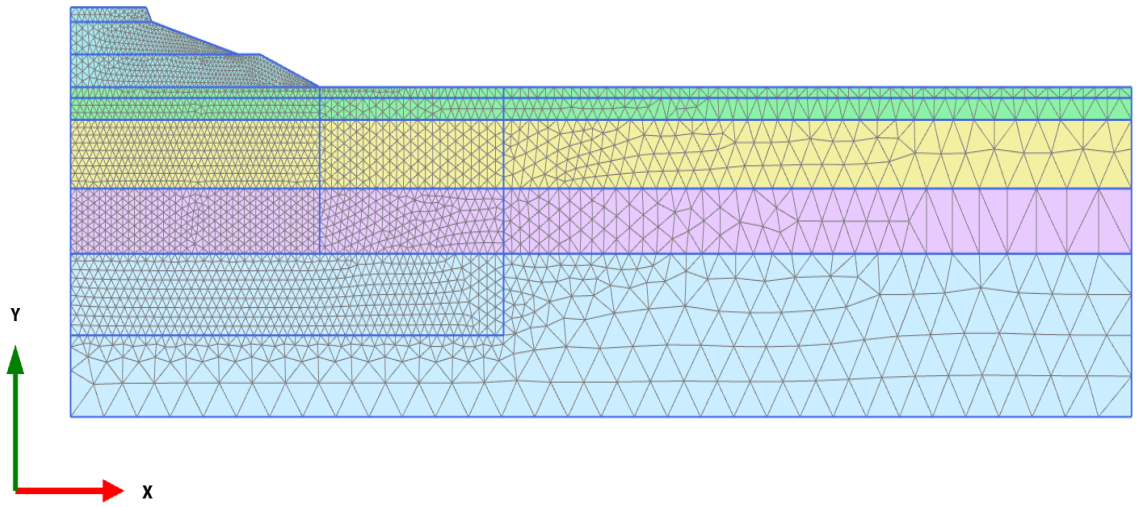

Figure 51: Boston trial embankment-Mesh configuration

7.5.4 Construction stages

1- Stage 0: Initial phase “K0-procedure”.
2- Stage 1: 1.5 meters of sand underneath the embankment is replaced by the fill material. The time interval is equal to 92 days.
3- Stage 2: the lowest 4.5 meters of the embankment are constructed in 31 days.
4- Stage 3: the embankment is left to consolidate for 175 days.
5- Stage 5: the main part of the embankment is built in 163 days.
6- Stage 6: the embankment is left to consolidate, consolidation time is equal to 137 days.
7- Stage 7: the top part of the embankment is built in 22 days.
8- Stage 8: consolidation for 1380 days.
9- Stage 9: end of primary consolidation (EOP), excess pore water pressure is less than 0.1 kPa

7.5.5 Flow condition

A hydrostatic water table is assumed at about 1.5 m below the ground surface. The calculation has been done with an opened consolidation boundary condition at the bottom of the model. The flow boundary conditions of a phase specified in the ‘GroundwaterFlow’ subtree under ‘Model conditions’ in the ‘Model explorer’.

7.5.6 Results

For the Boston trial embankment example, two cases were investigated using normally consolidated soils (NC) and over-consolidated soils (OC). For OC case the soil was modelled using HS, HS small model and GHS – user defined model. Whereas for NC case the soil was modelled using HS small and GHS model. Therefore, the following graphs represent the numerical analysis results for the both cases.

The following nodes A (0.0, 1.5); B (0.0, 7.5); C (0.0, -16.75) and D (0.0, -32.75) have been determined in Plaxis in order to plot the final consolidation results.

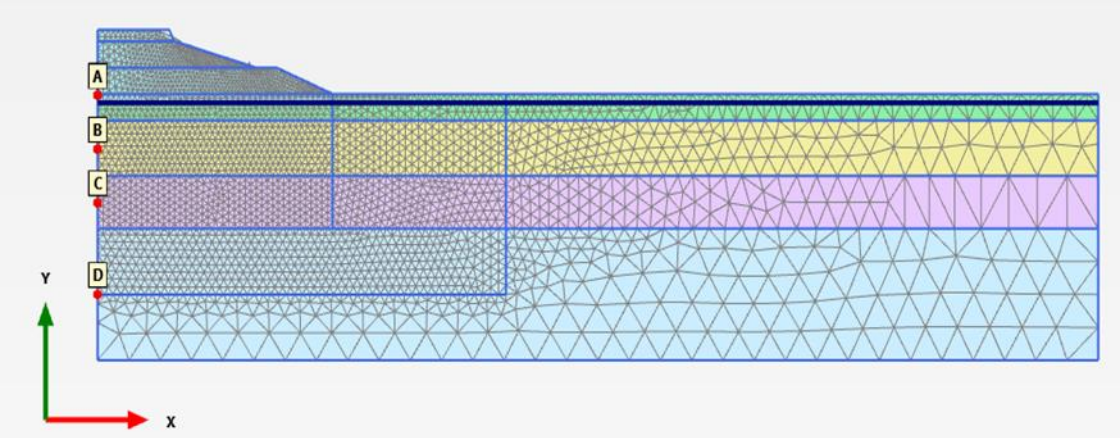

Figure 52: Boston trial embankment-illustration of the node points

The following figures show the displacement versus time for the NC and OC soils. It can be seen that the GHS-model gives a smaller displacement versus time, in contrast the HS and HS models show higher values. This can be explained by the fact that the stress-dependency formulations in the GHS small model accounts for the pre-consolidation stress and the mean effective stress.

i. Consolidation results (Reset all Boston layers to over-consolidated OC).

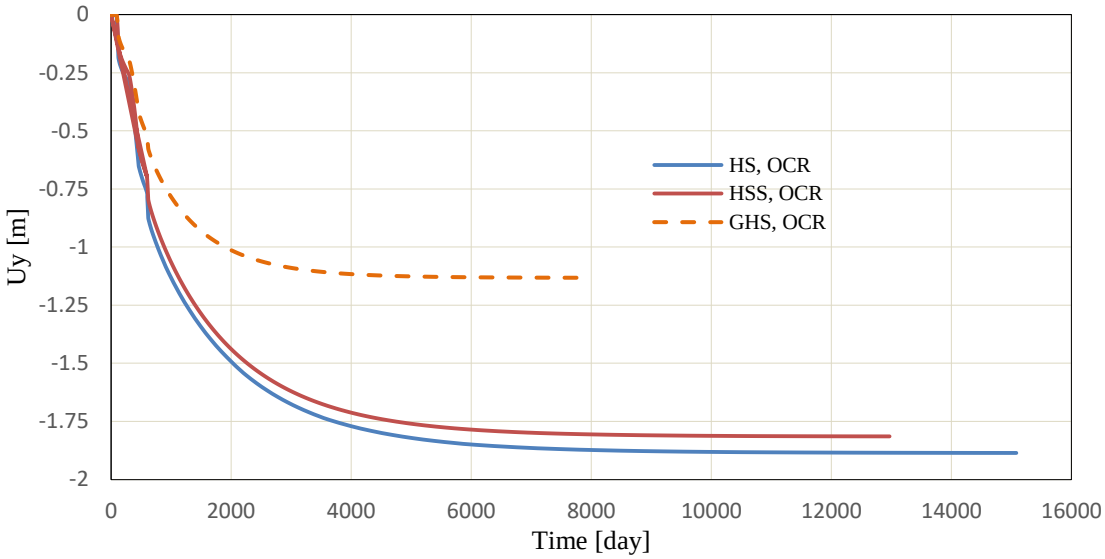

Figure 53: Result Boston trial embankment displacement versus time for point A (flow boundary at the bottom is open) for OC

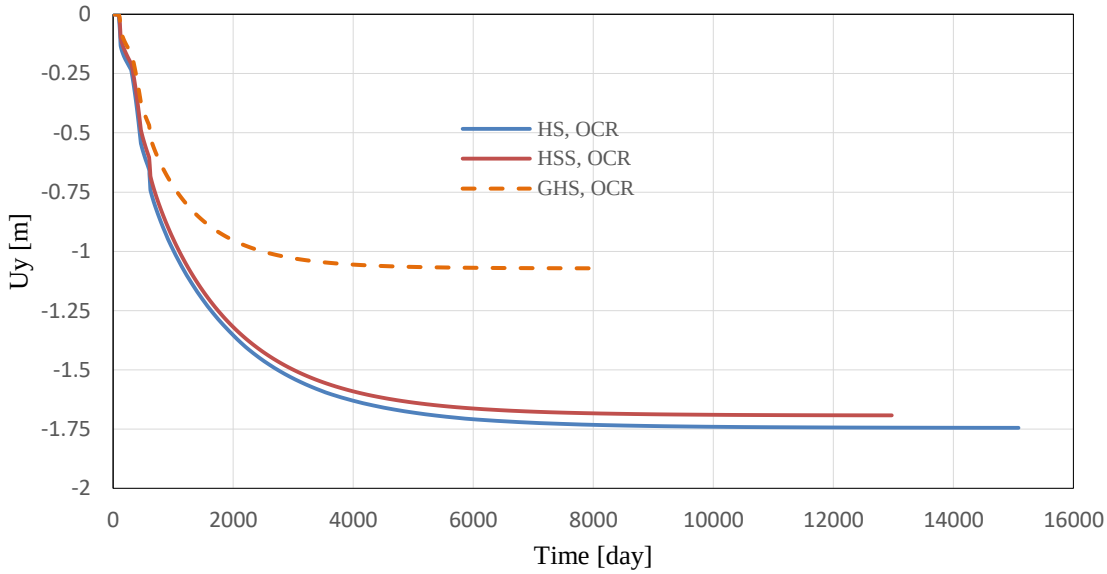

Figure 54: Result Boston trial embankment displacement versus time for point B (flow boundary at the bottom is open) for OC

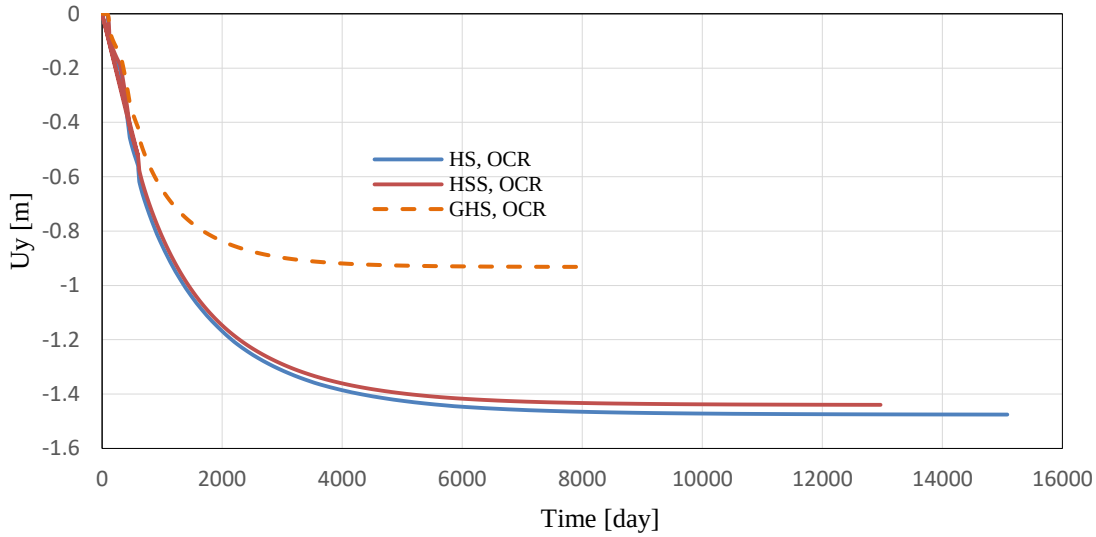

Figure 55: Result Boston trial embankment displacement versus time for point C (flow boundary at the bottom is open) for OC

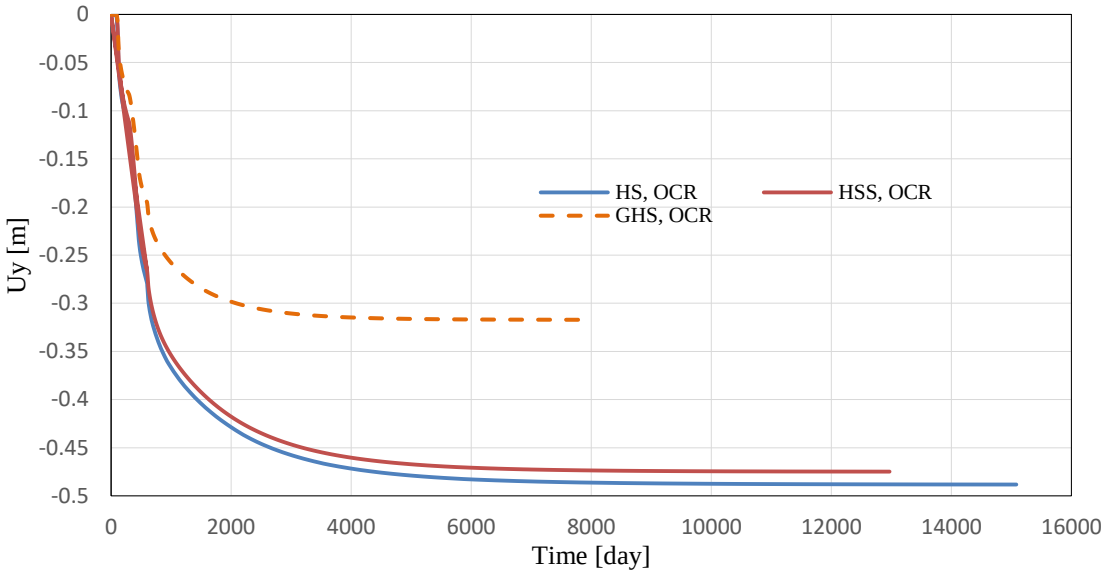

Figure 56: Result Boston trial embankment displacement versus time for point D (flow boundary at the bottom is open) for OC

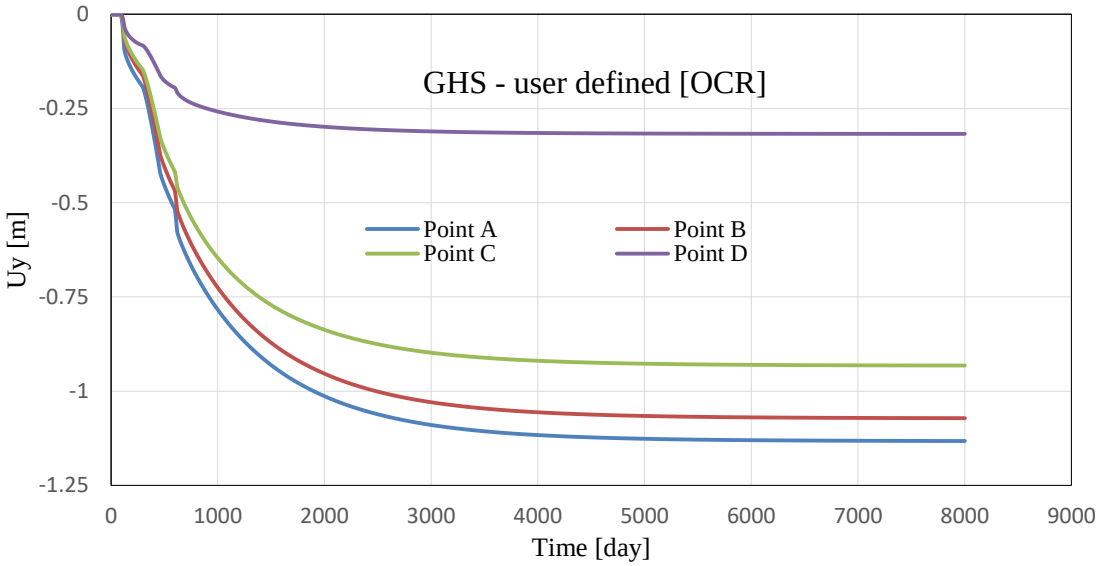

Figure 57: Result Boston trial embankment displacement versus time for point A, B, C and D (flow boundary at the bottom is open) using GHS – user defined model

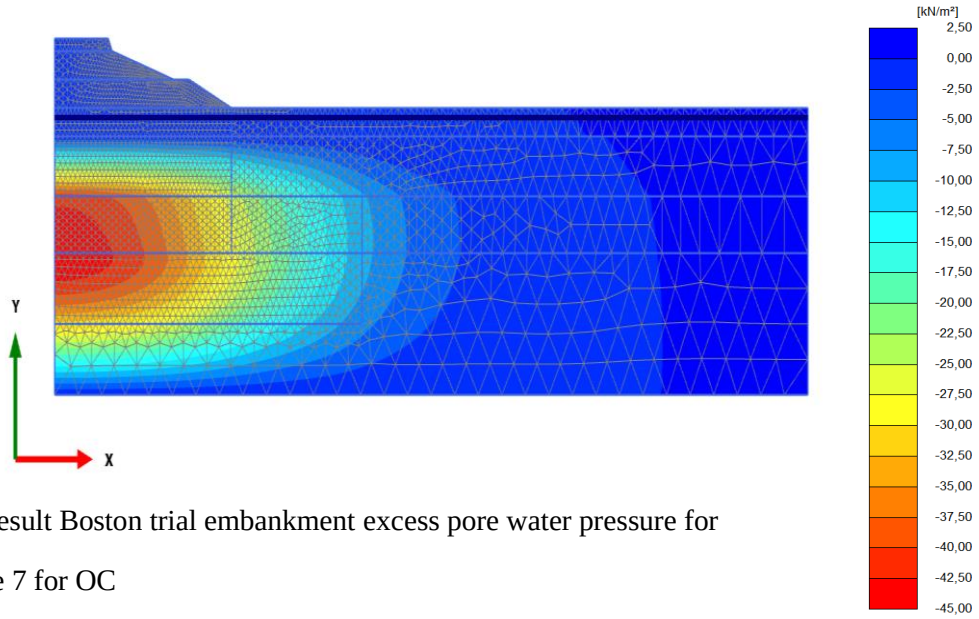

Figure 58: Result Boston trial embankment excess pore water pressure for HSS at phase 7 for OC

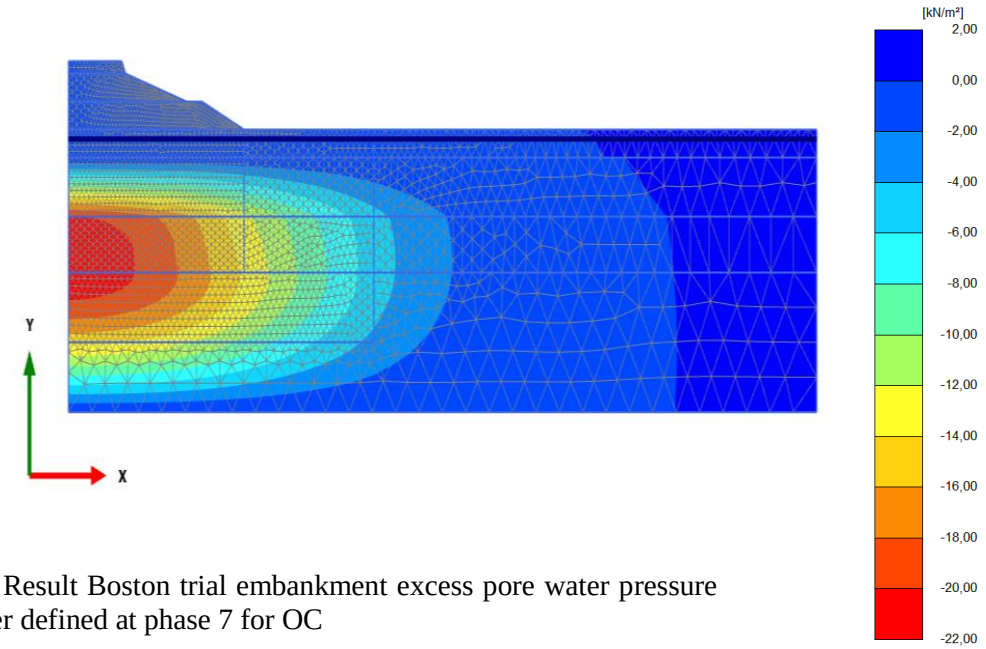

Figure 59: Result Boston trial embankment excess pore water pressure for GHS-user defined at phase 7 for OC

ii. Consolidation results (Reset all Boston layers to normally consolidated NC).

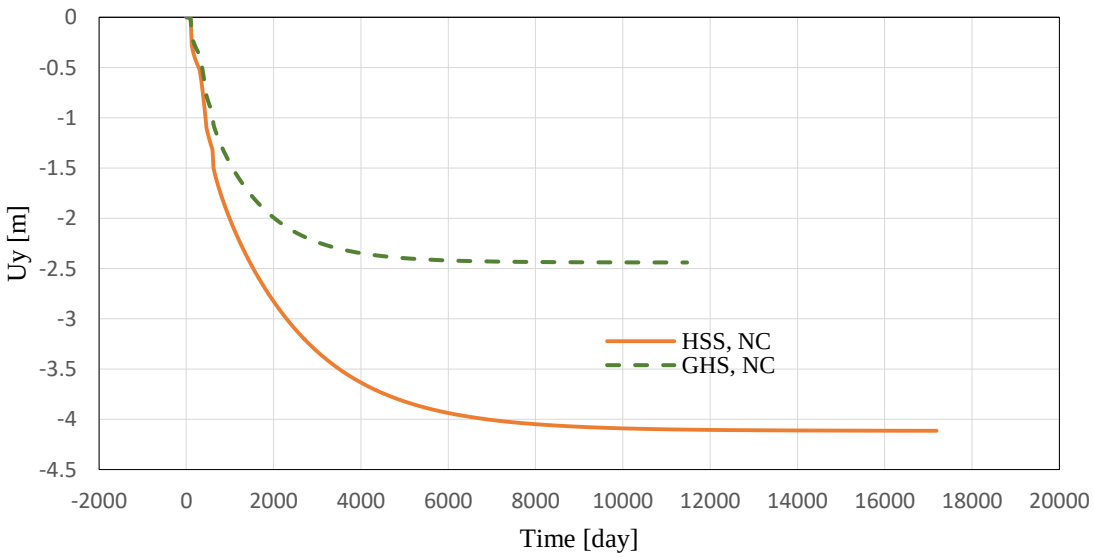

Figure 60: Result Boston trial embankment displacement versus time for point A for NC

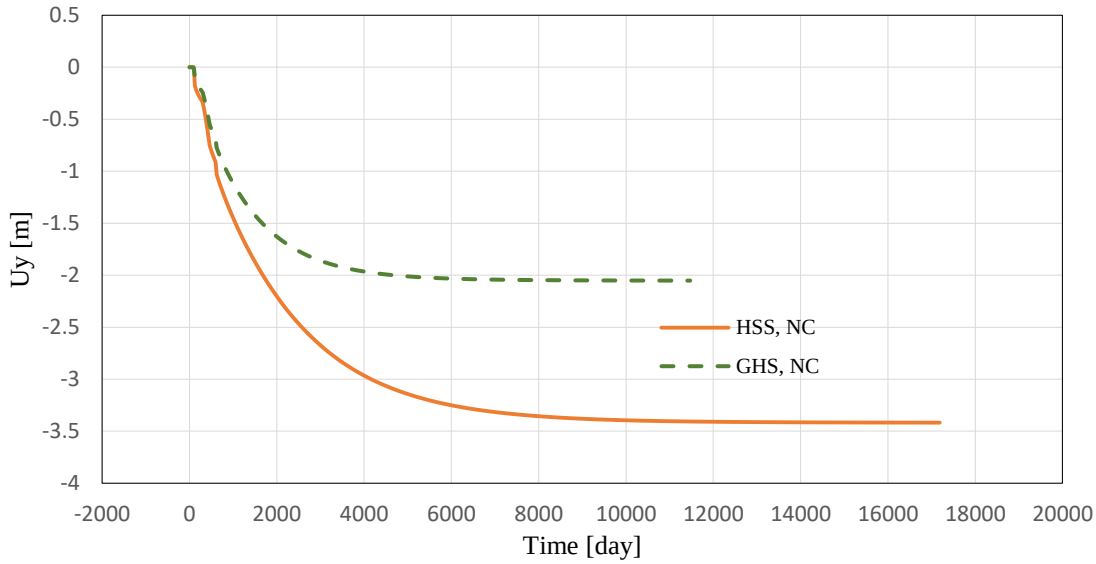

Figure 61: Result Boston trial embankment displacement versus time for point B for NC

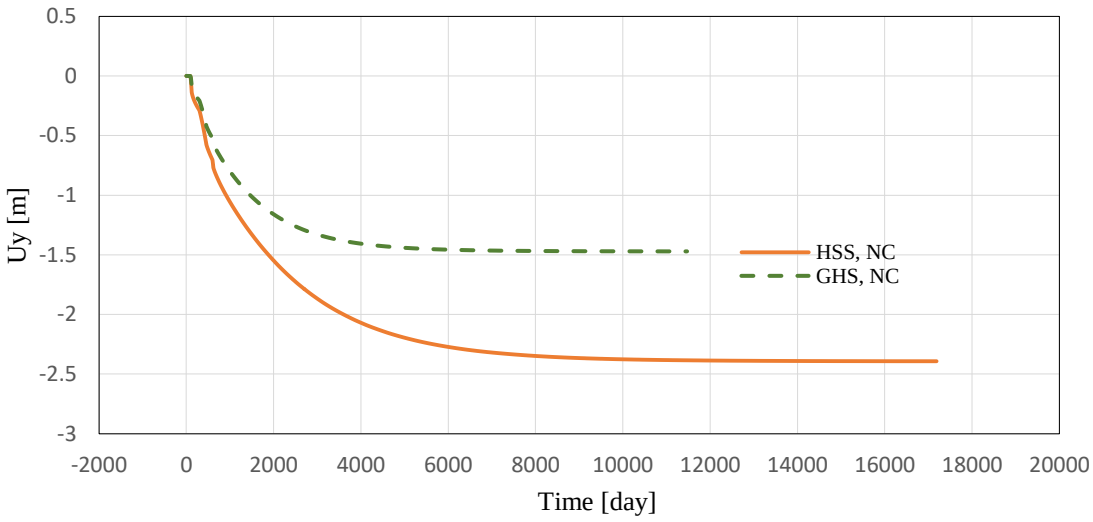

Figure 62: Result Boston trial embankment displacement versus time for point C for NC

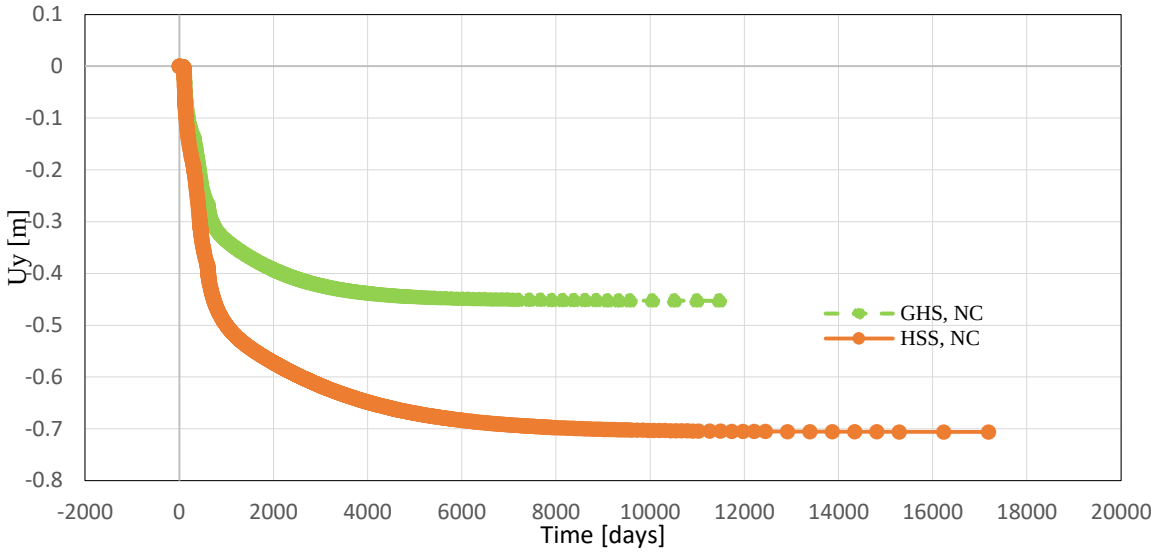

Figure 63: Result Boston trial embankment displacement versus time for point D for NC

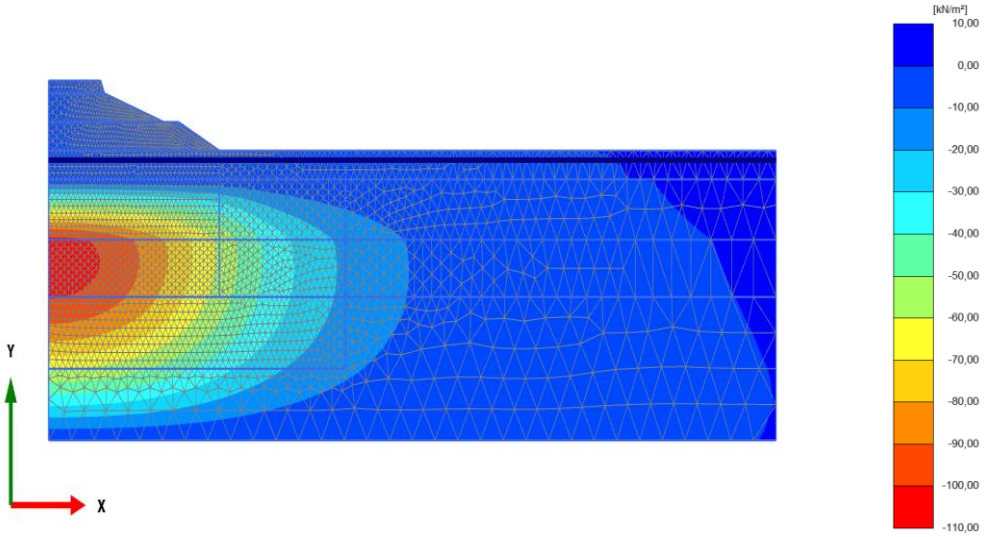

Figure 64: Result Boston trial embankment excess pore water pressure for HSS at phase 7 for NC

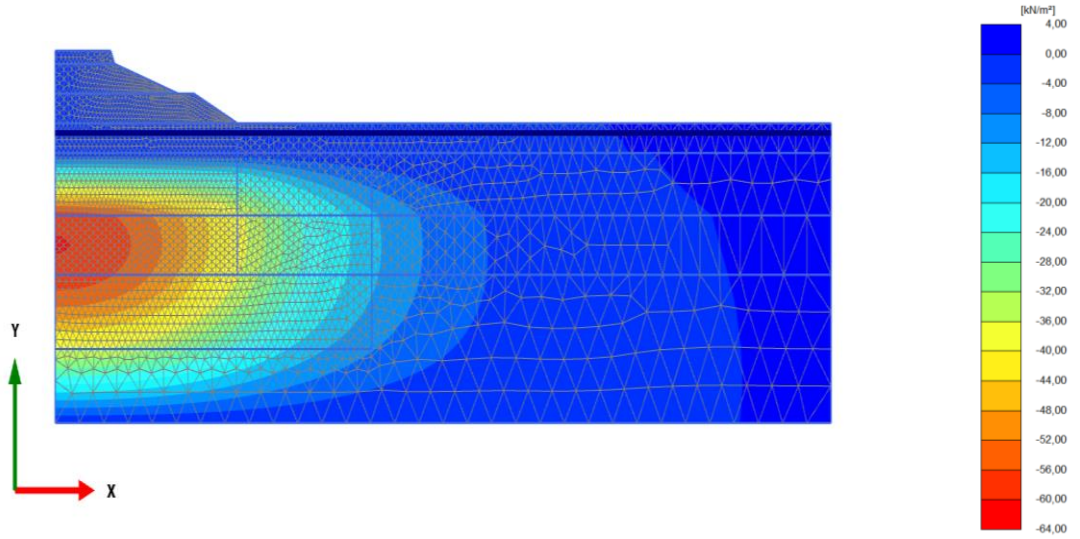

Figure 65: Result Boston trial embankment excess pore water pressure for GHS at phase 7 for NC

7.5.7 Remarks

1- The predicted vertical displacements versus time at points A, B, C and D, placed directly on the symmetry axis of the embankment, show that the differences between the GHS-user defined and HS small models are considerably higher after construction of the embankment.

2- Results for excess pore pressure displays that maximum excess pore water pressure occurs below the middle of the embankment “on the symmetry axis” and the values decreases with the distance from the centreline of the embankment.

3- The pore pressure dissipation is fast in case of GHS-user defined for the both NC and OC cases due to high effective mean stress compared to the HS small model (see Appendix).

8 Conclusion

The above study proves that the numerical analysis in geotechnical engineering can deliver valuable information for the design of deep excavations, embankment and tunnels. However, program like PLAXIS is just a tool in engineers' hands and must be used with care.

Three advanced constitutive models were studied in this thesis, namely Hardening Soil Model HS, Hardening Soil Small Model HSS and the Generalized Hardening Soil Model GHS. Various geotechnical problems, including deep excavation, embankment and tunnel were simulated, in order to evaluate the variations and the influence of the constitutive models on soil behaviour. The results were compared in terms of stresses and displacements in the soil itself and the effect on adjacent buildings and structures.
All discussed geotechnical models in this thesis are simulated in Plaxis 2D considering plane strain condition. The following conclusions can be drawn:

i. Deep excavations

The HS small model leads to lower displacement results compared to the HS-model, due to higher soil stiffness at small strains. The results of the computation confirm this statement. The GHS model has a major influence on the results. The displacements are significantly lower compared to the other two models.

The complete comparison between the results from the Hardening soil, the Hardening Soil small and Generalized Hardening soil models, produces some important differences:

1. The behaviour of GHS model is much stiffer in unloading/reloading than HS and HSS models, the reason is that the GHS model has a different stress dependency stiffness.

2. The inward movements of diaphragm walls are lower for the GHS model than for the HS and HSS models, the reason behind this is due to the differences of unloading/reloading behaviour of models. This is due to the fact that the vertical stresses decreases during excavation, leading to a reduction of deviatoric stresses.

3. For the HS and HSS model higher displacements are obtained at the surface behind the wall. This behaviour can be explained by the fact that the HS and the HSS models lead to higher displacements at the excavation bottom (due to the less stiff unloading/reloading behaviour), which consequently affects the vertical movement of the wall. And results in higher displacement behind the wall.

4. The strut forces are higher in the HS case than in the HSS and GHS cases. The reason for this can be because of the influence of the wall deformation pattern as excavation progressed i.e., small wall deformation at the top.

Simulated examples have proven that for different types of deep excavations, where the unloading/reloading behaviour of the soil is very important, the Generalized Hardening Soil (GHS) model gives smaller (and maybe accurate and realistic) results than the HS and HSS models.

ii. Tunnel

1- Regarding the surface settlement, the deepest and widest settlement trough is generated in the case of the HS model. The surface settlement trough from the GHS model is the narrowest, also this generally shows settlement troughs being more in agreement with expected behaviour. This behaviour can be referred to the fact that the dependency of the stiffness on the stress state is different in the investigated models.

2- The maximum normal forces, maximum shear force and maximum bending moments in the lining are compared for in the HS, HSS and GHS models. For the latter model the values are reduced significantly.

iii. Embankment

For the Boston embankment problem, the effects of the consolidation process on the displacements for over-consolidated and normally consolidated soils were investigated.

For the embankment, the effects of the mean effective stress, effective sigma 3 and the pore water pressure by using GHS model and HSS model were investigated along 5 sections.

The calculated vertical displacement versus time at points A, B, C and D, placed directly on the symmetry axis of the embankment, shows that the differences between the GHS user defined and HS small models are relatively large after construction of the embankment.

Finally, as the aim of the research presented here was to qualitatively emphasize the differences in results with respect to the constitutive models no quantitative comparison with in situ measurements of a real project has been presented.

References

[1] Plaxis, “Material Models Manual,” Plaxis, p. 202, 2016.

[2] A. Laera and R. B. J. Brinkgreve, “Site response analysis and liquefaction evaluation,” Plaxis bv, pp. 1–42, 2015.

[3] J.M. Duncan, & C.Y Chang, "Nonlinear analysis of stress and strain in soil," J.Soil Mech.Found. Div. ASCE 96, 1629-1653, 1970.

[4] T. Schanz, a Vermeer, and P. Bonnier, “The hardening soil model: formulation and verification,” Beyond 2000 Comput. Geotech. 10 years PLAXIS Int. Proc. Int. Symp. beyond 2000 Comput. Geotech. Amsterdam Netherlands 1820 March 1999, p. 281.

[5] T. Benz, " Small-Strain Stiffness of Soils and its Numerical Consequences". Ph.d. thesis. Universität Stuttgart, 2007.

[6] H.F.Schweiger, "Computational Geotechnics. Lecture WS 2016/17". Graz University of Technology, 2016.

[7] B. Hardin, and W. Black, "Closure to vibration modulus of normally consolidated clays". Proc.ASCE: Jounral of the Soils Mechanics and Foundation Division, 95(SM6),1531–1537, 1969.

[8] J.A. Santos, and A.G. Correia, "Reference threshold shear strain of soil: Its application to obtain a unique strain-dependent shear modulus curve for soil". Proceedings of the 15th International Conference on Soil Mechanics and Geotechnical Engineering, Vol. 1, Istanbul, A.A. Balkema, 267 – 270, 2001.

[9] B.O. Hardin, and V. P. Drnevich, " Shear modulus and damping in soils: design equations and curves". Journal of Soil Mechanics and Foundations Division – ASCE, Vol. 98(SM7), pp. 667 – 692, 1972.

[10] A. Truty, and R. F. Obrzud, "The hardening soil model-a practical guide book". Technical Report ZSoil.PC 100701, Zace Services Ltd , p. 216, 2018.

[11] Z. Y. Orazalin, " Three-Dimensional Finite Element Analysis of a Complex Excavation on the MIT campus, " 2012.

Appendix

For the Boston Embankment the influence of the mean effective stress, effective sigma 3 and the pore water pressure by using GHS model and HS small model was investigated along 5 sections (see Figure 66). The following figures show the results of the computations for [Phase-6].

Note that, the following graphs show only the numerical result for the over-consolidated OC condition. Normally consolidated soil shows similar behaviour to over-consolidated soil but associated with higher values.

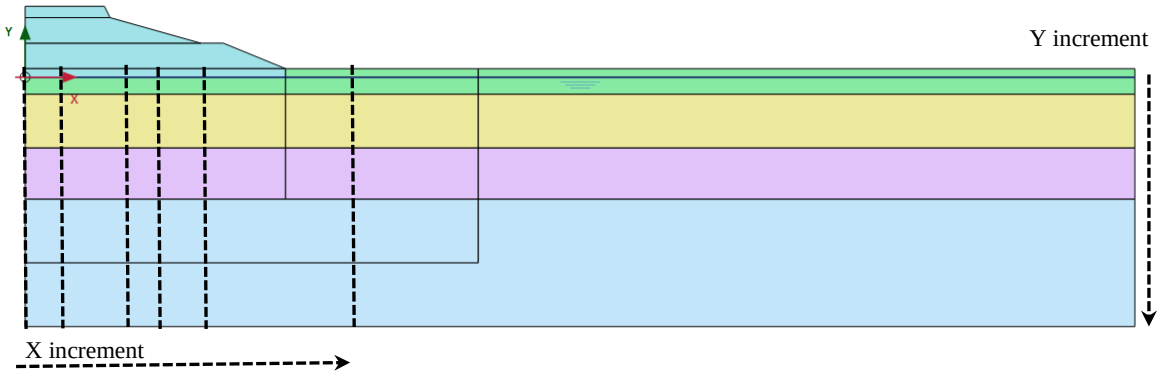

Figure 66: Boston trial embankment, selected cross sections for the evaluations of the stresses and pore pressures.

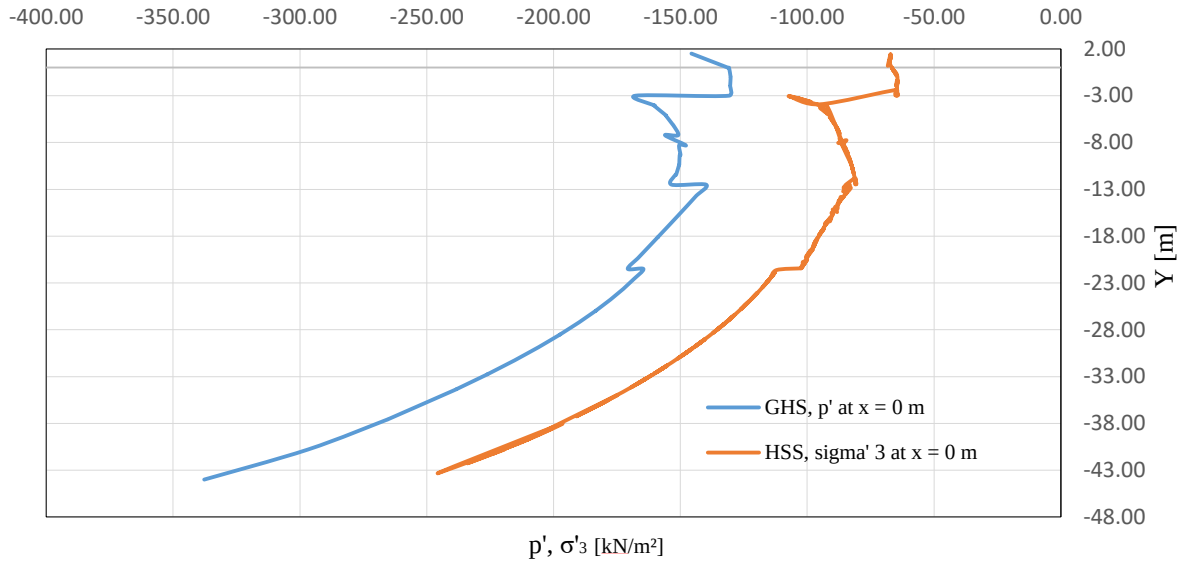

Figure 67: Result Boston trial embankment p', σ'3 at phase 6 for OC at x=0 m

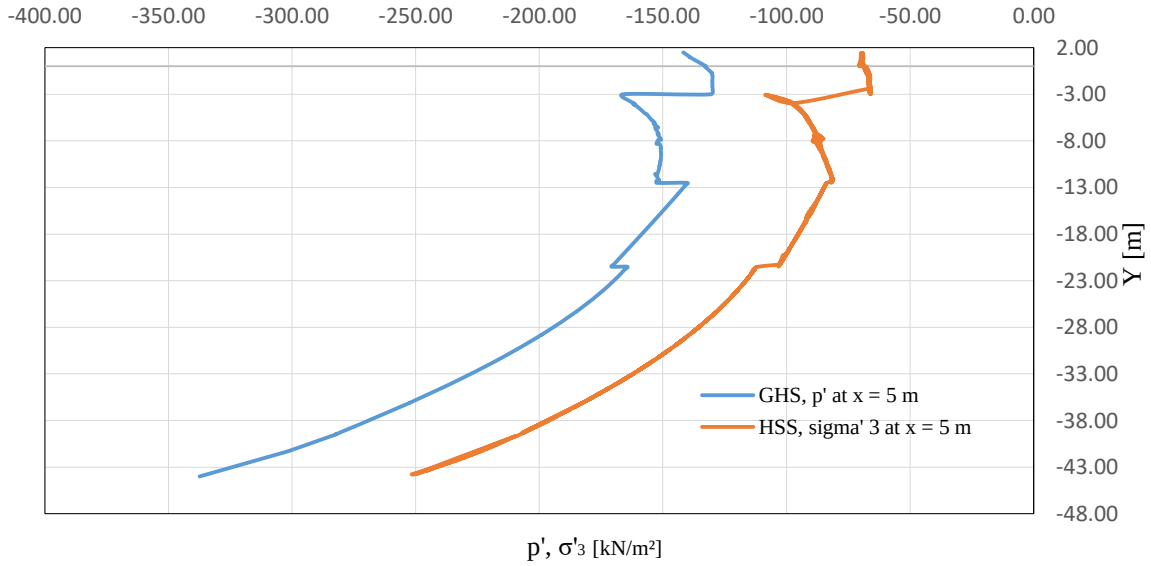

Figure 68: Result Boston trial embankment p', σ'3 at phase 6 for OC at x=5 m

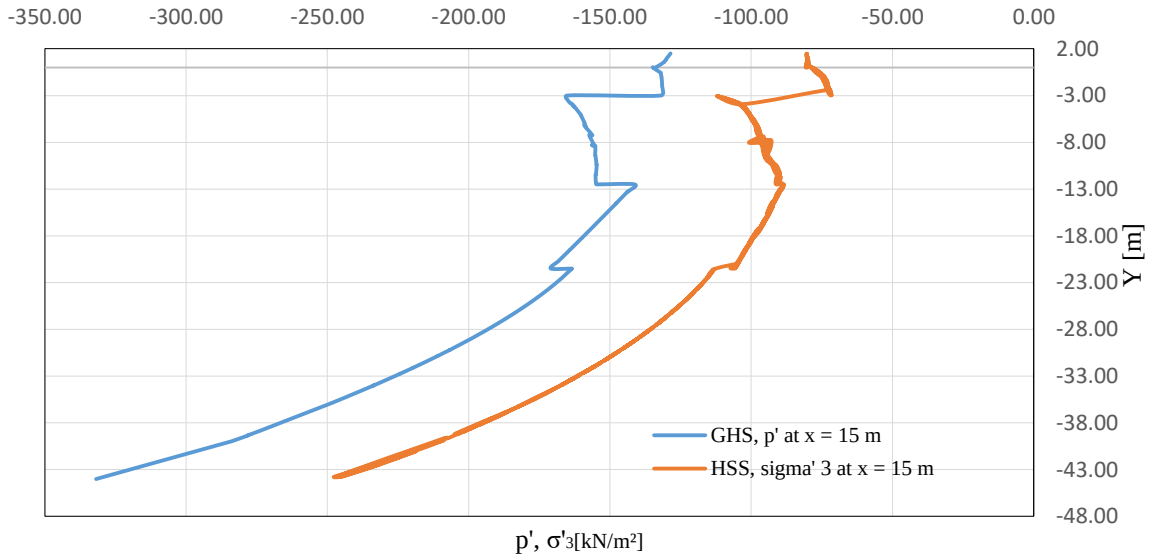

Figure 69: Result Boston trial embankment p', σ'3 at phase 6 for OC at x=15 m

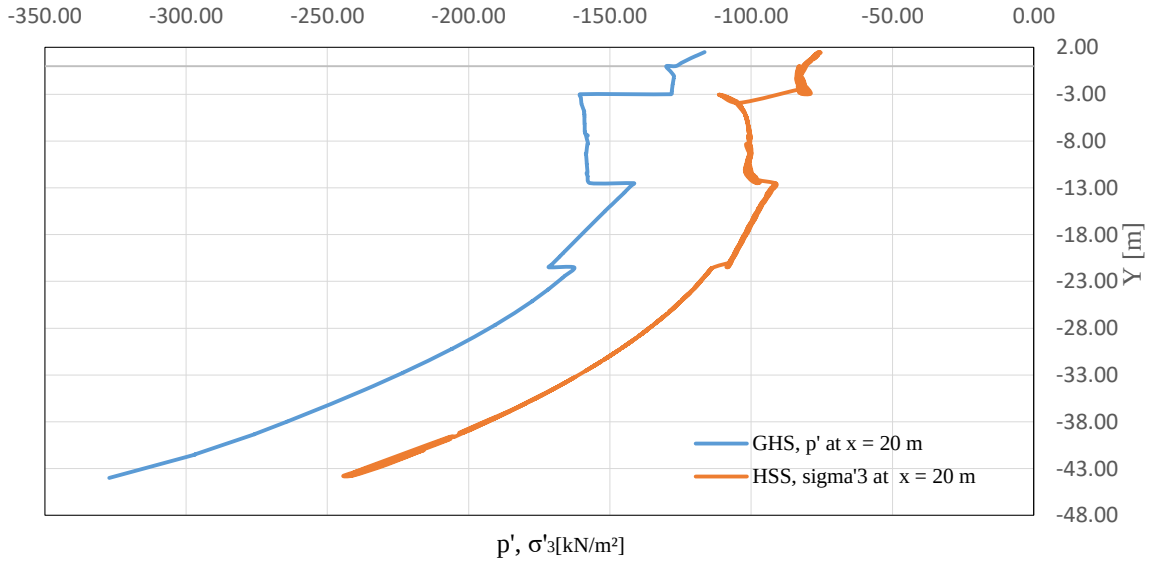

Figure 70: Result Boston trial embankment p', σ'3 at phase 6 for OC at x=20 m

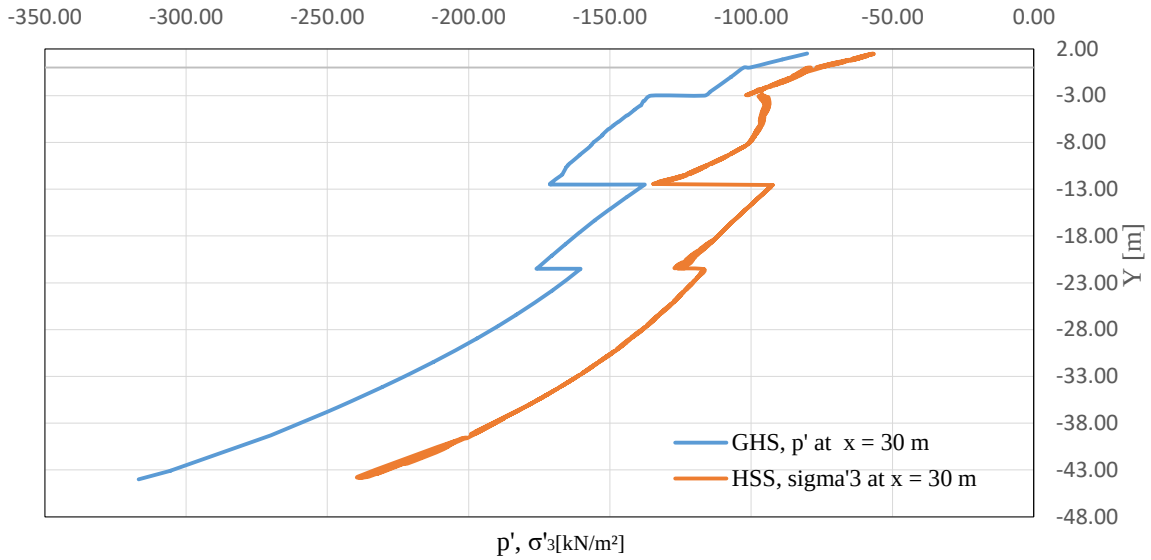

Figure 71: Result Boston trial embankment p', σ'3 at phase 6 for OC at x=30 m

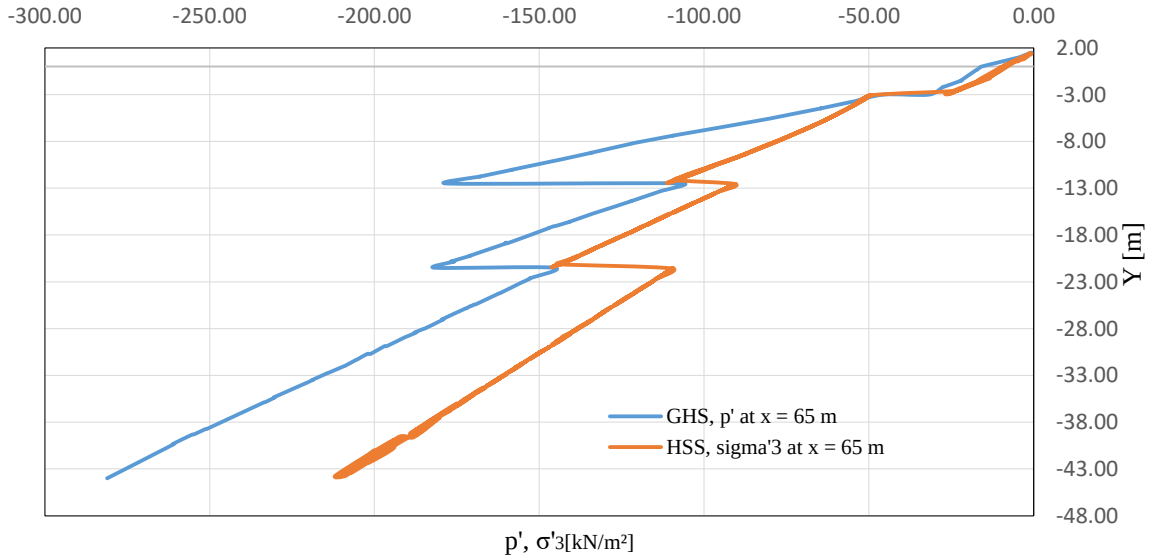

Figure 72: Result Boston trial embankment p', σ'3 at phase 6 for OC at x=65 m

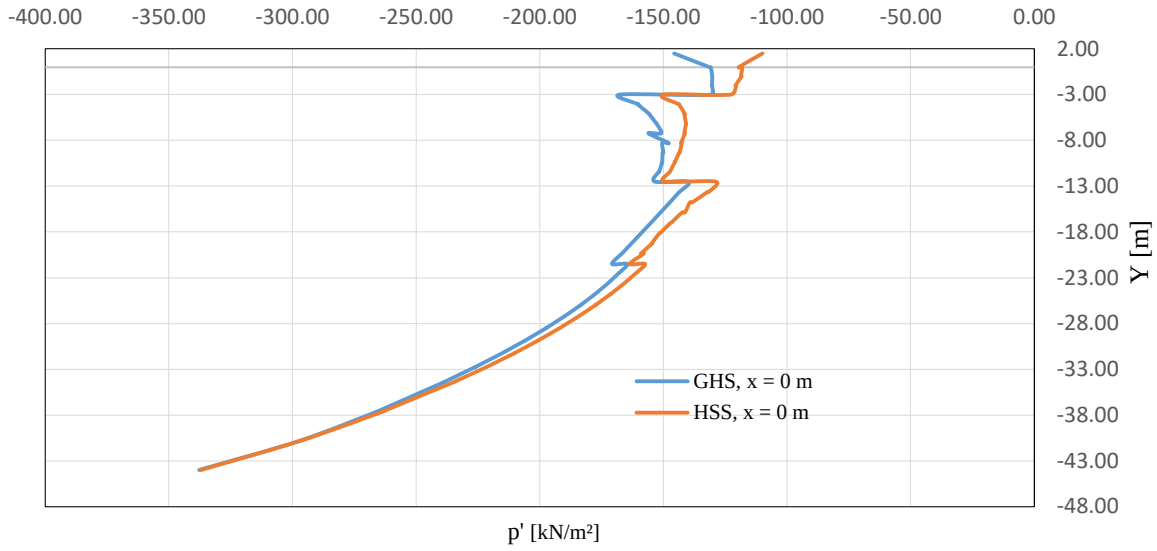

Figure 73: Result Boston trial embankment p' at phase 6 for OC at x=0 m

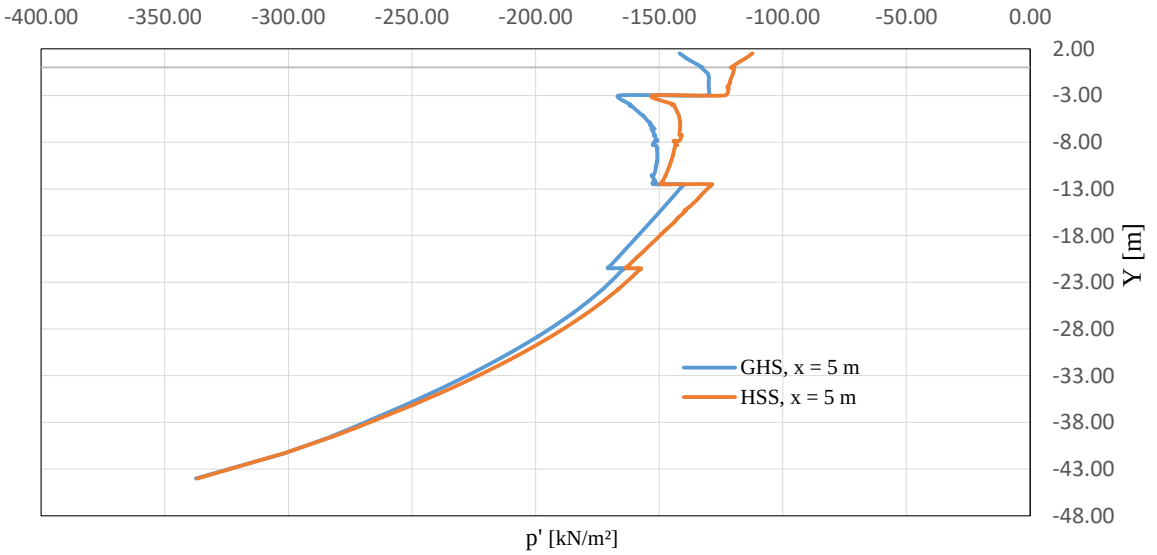

Figure 74: Result Boston trial embankment p' at phase 6 for OC at x=5 m

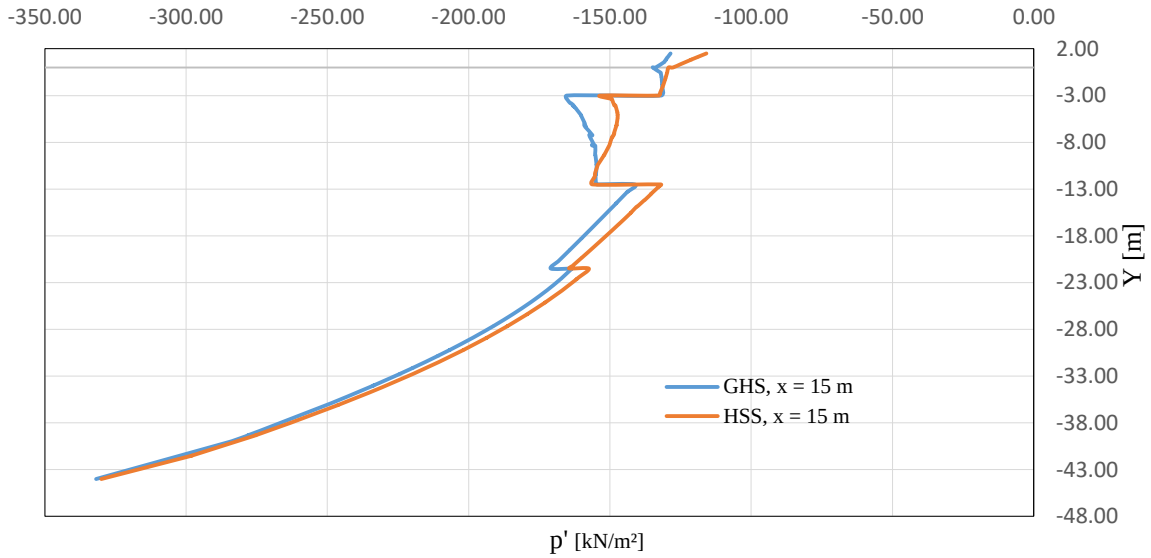

Figure 75: Result Boston trial embankment p' at phase 6 for OC at x=15 m

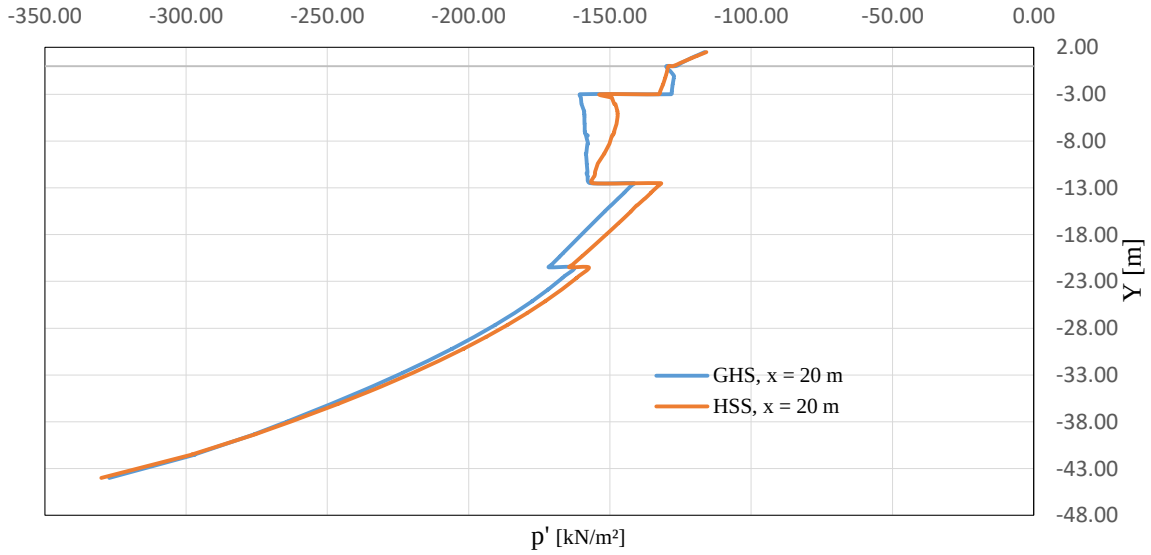

Figure 76: Result Boston trial embankment p' at phase 6 for OC at x=20 m

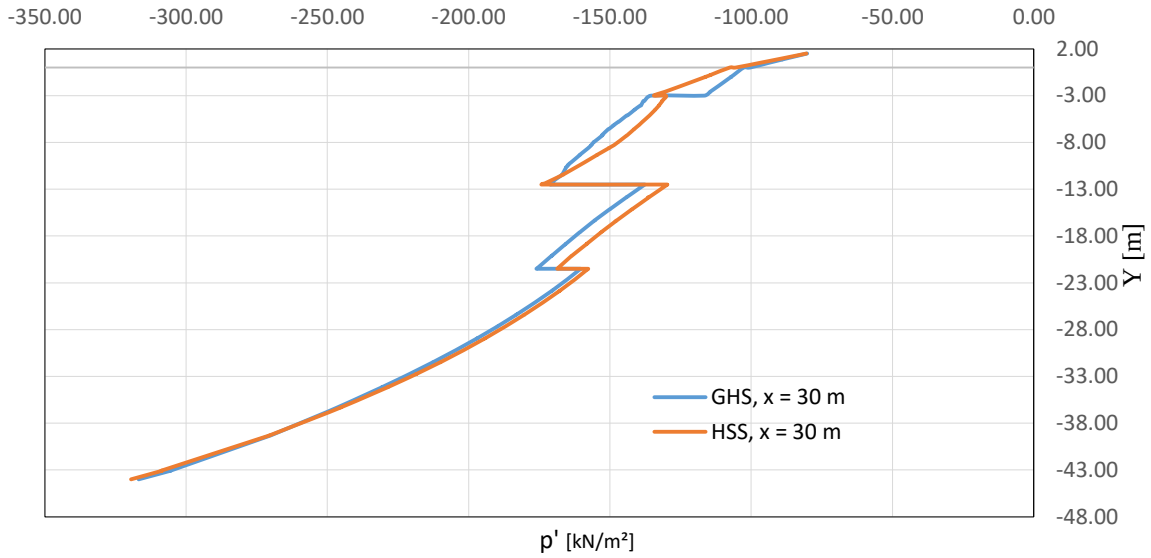

Figure 77: Result Boston trial embankment p' at phase 6 for OC at x=30 m

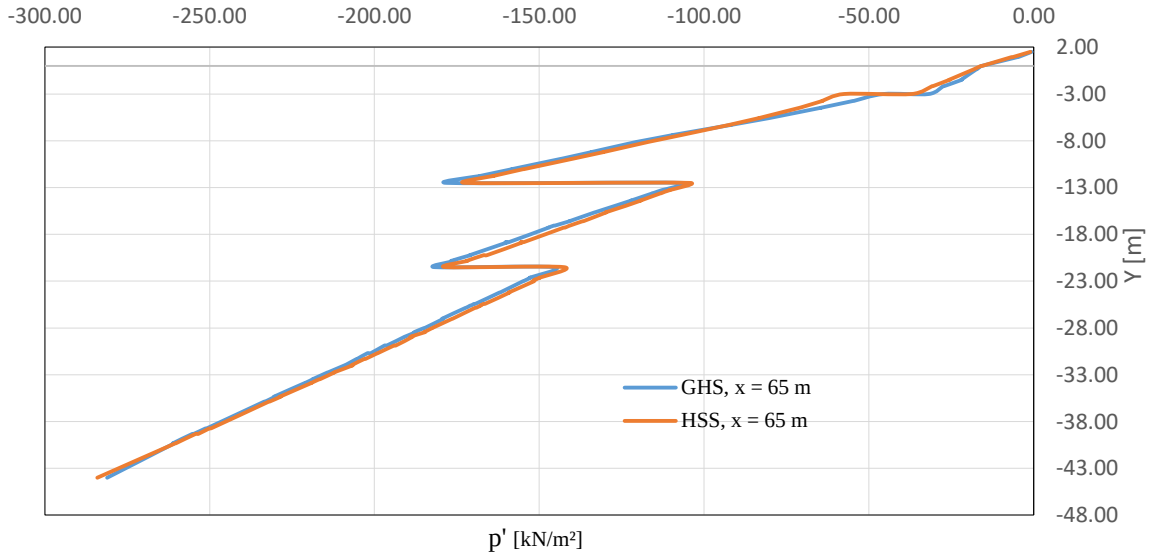

Figure 78: Result Boston trial embankment p' at phase 6 for OC at x=65 m

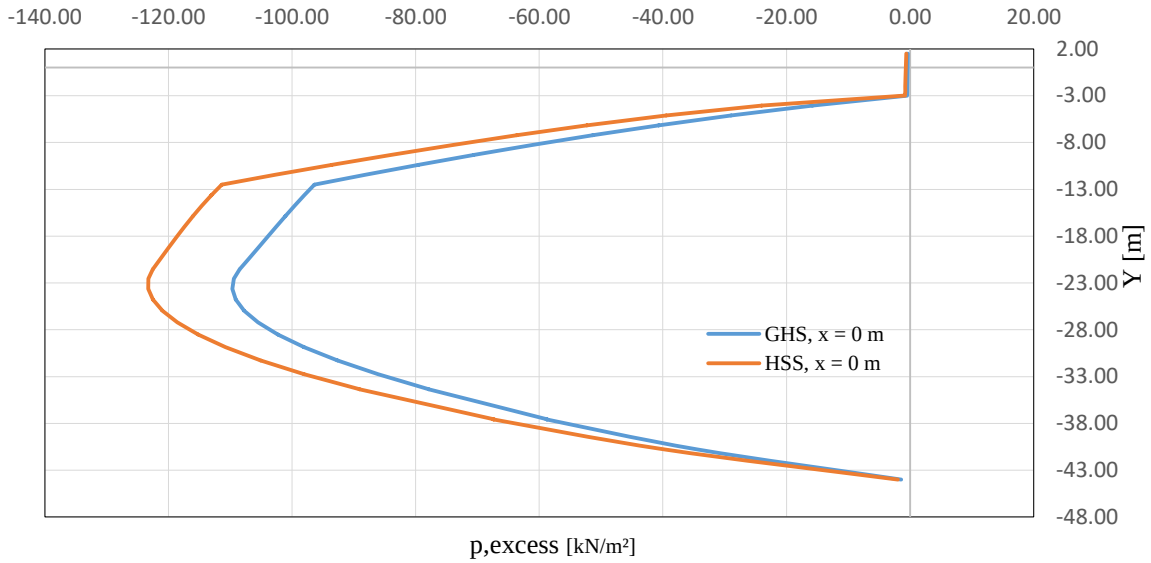

Figure 79: Result Boston trial embankment p, excess at phase 6 for OC at x=0 m

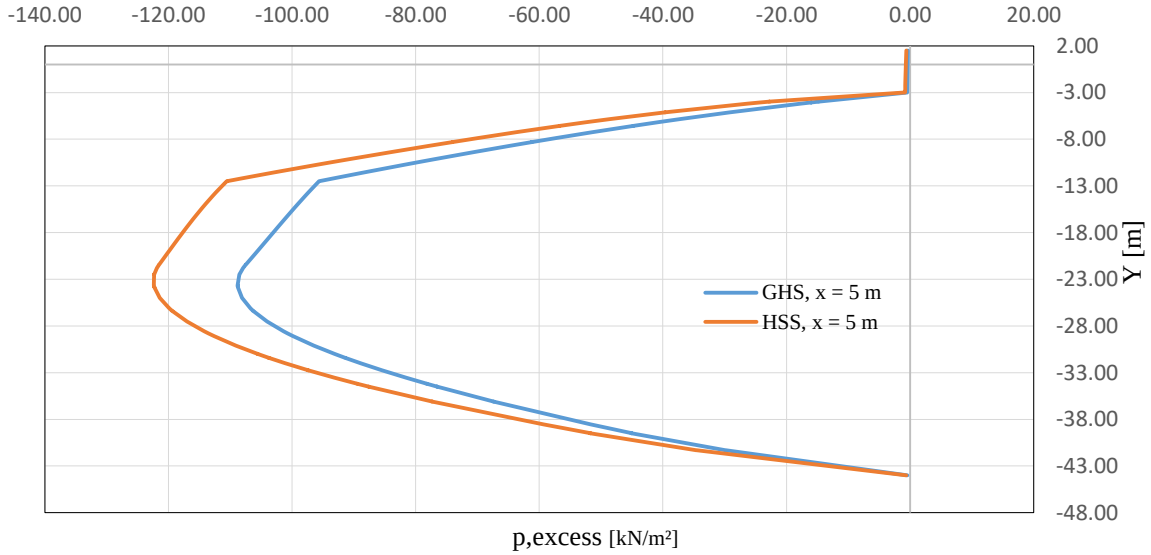

Figure 80: Result Boston trial embankment p, excess at phase 6 for OC at x=5 m

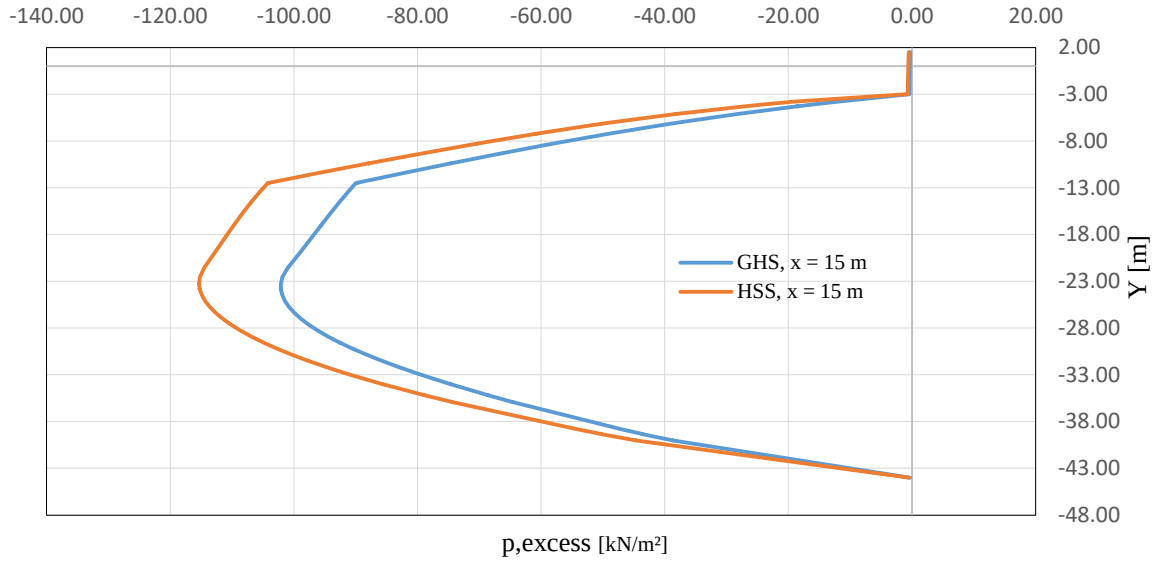

Figure 81: Result Boston trial embankment p, excess at phase 6 for OC at x=15 m

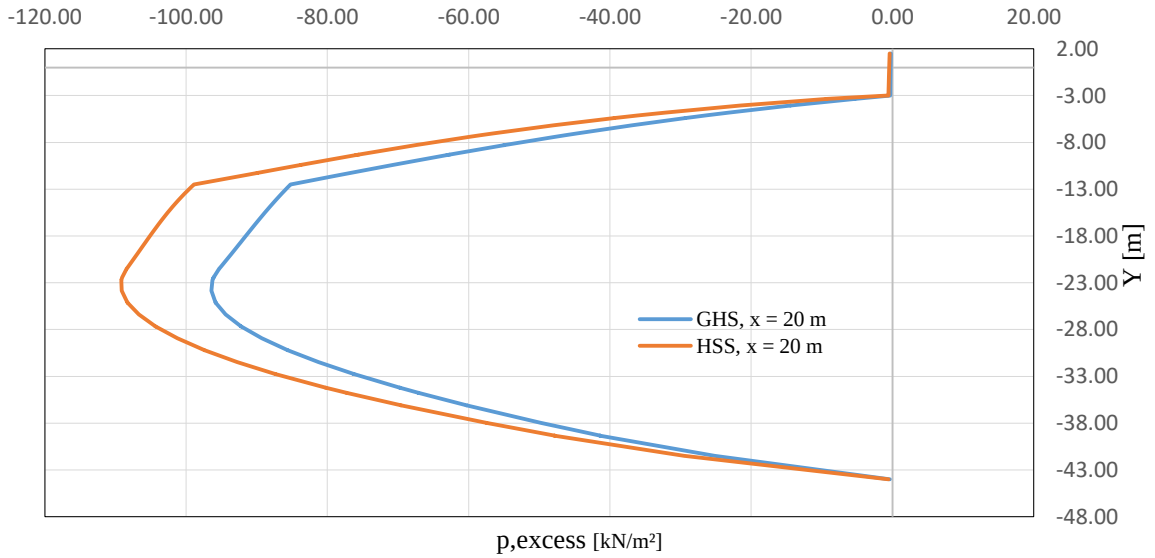

Figure 82: Result Boston trial embankment p, excess at phase 6 for OC at x=20 m

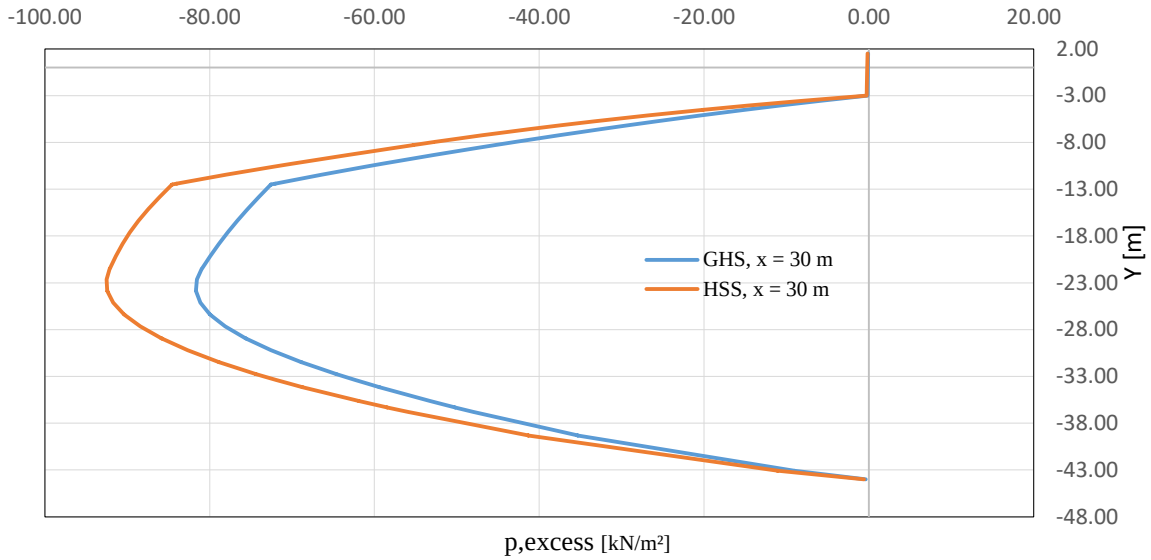

Figure 83: Result Boston trial embankment p, excess at phase 6 for OC at x=30 m

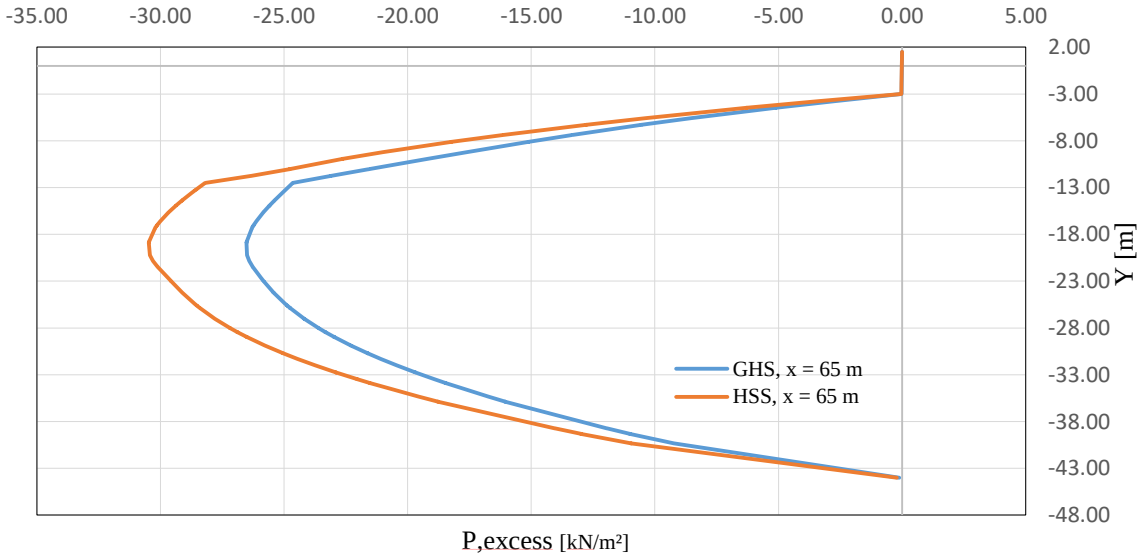

Figure 84: Result Boston trial embankment p, excess at phase 6 for OC at x=65 m

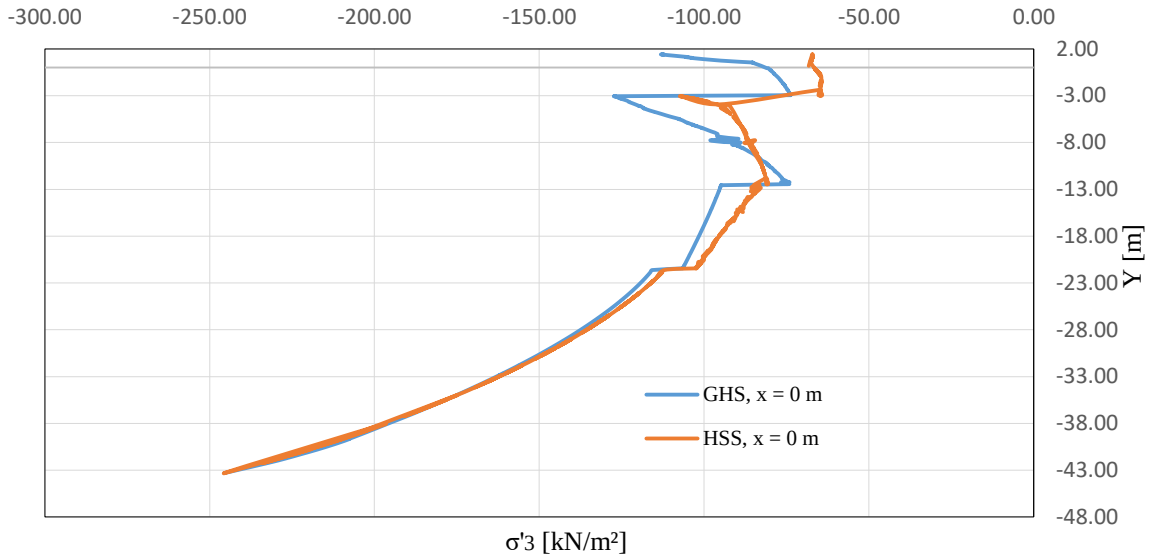

Figure 85: Result Boston trial embankment σ'3 at phase 6 for OC at x=0 m

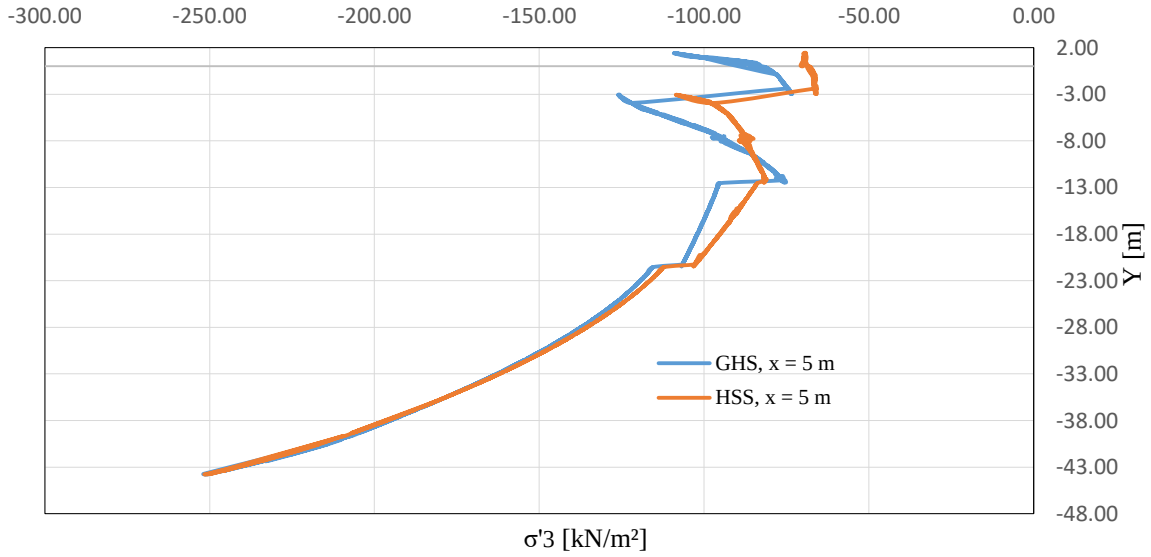

Figure 86: Result Boston trial embankment σ'3 at phase 6 for OC at x=5 m

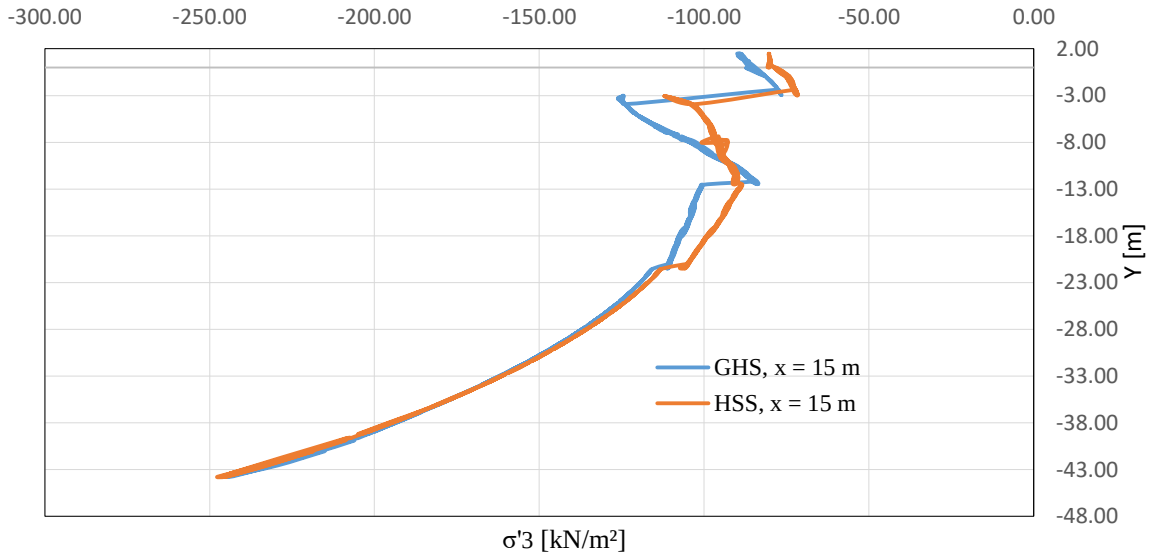

Figure 87: Result Boston trial embankment σ'3 at phase 6 for OC at x=15 m

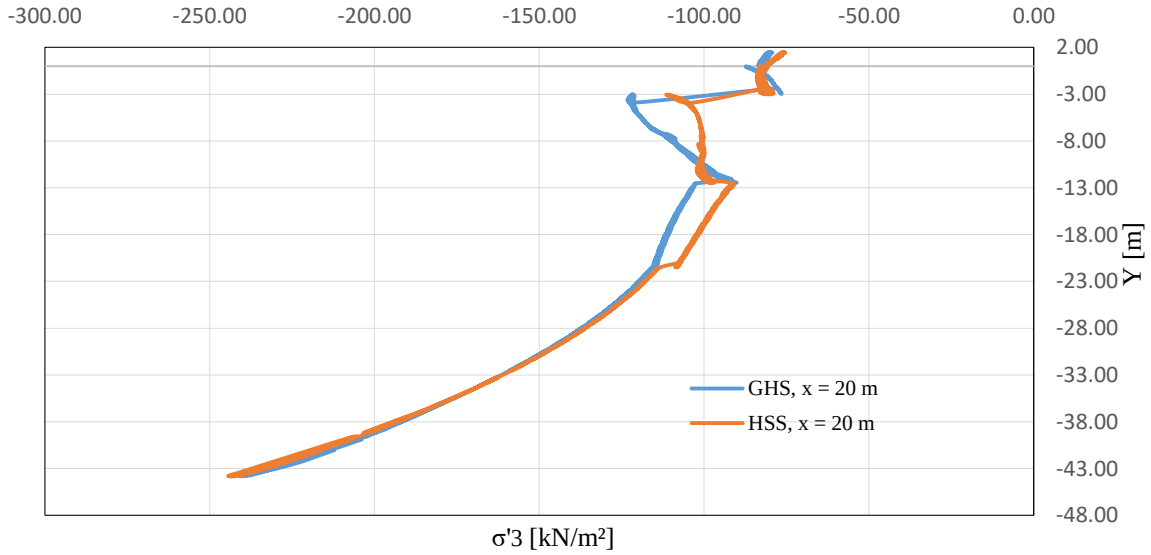

Figure 88: Result Boston trial embankment σ'3 at phase 6 for OC at x=20 m

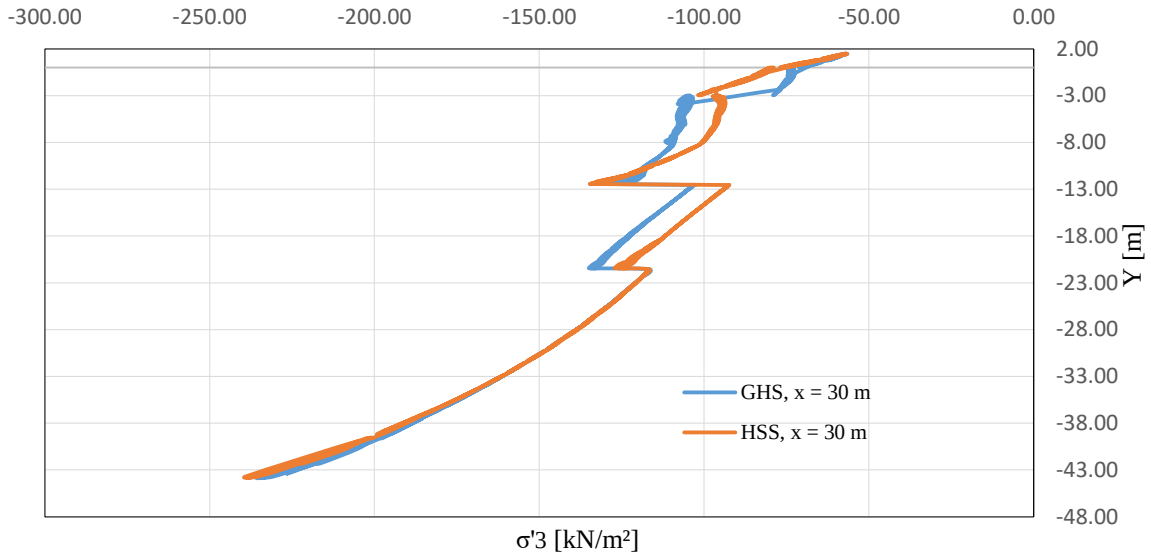

Figure 89: Result Boston trial embankment σ'3 at phase 6 for OC at x=30 m

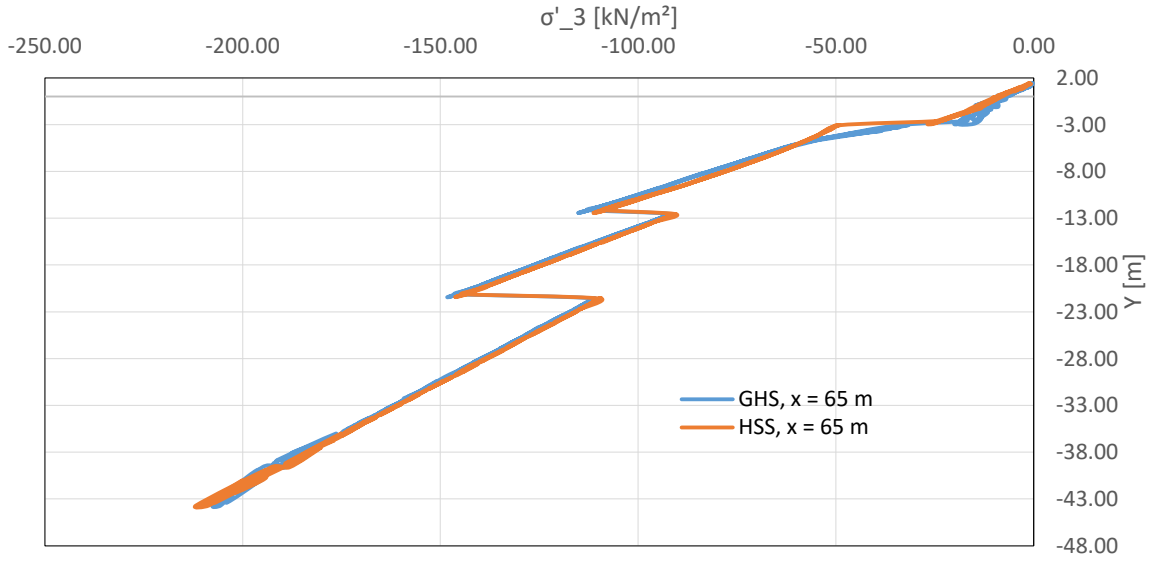

Figure 90: Result Boston trial embankment σ'3 at phase 6 for OC at x=65 m